Search for charginos and neutralinos in final states with two boosted hadronically decaying bosons and missing transverse momentum in *pp* collisions at $\sqrt{s} = 13$ TeV with the ATLAS detector

G. Aad *et al.*[*]
(ATLAS Collaboration)

(Received 18 August 2021; accepted 20 September 2021; published 27 December 2021)

A search for charginos and neutralinos at the Large Hadron Collider using fully hadronic final states and missing transverse momentum is reported. Pair-produced charginos or neutralinos are explored, each decaying into a high-p_{T} Standard Model weak boson. Fully hadronic final states are studied to exploit the advantage of the large branching ratio, and the efficient rejection of backgrounds by identifying the high-p_{T} bosons using large-radius jets and jet substructure information. An integrated luminosity of 139 fb^{-1} of proton-proton collision data collected by the ATLAS detector at a center-of-mass energy of 13 TeV is used. No significant excess is found beyond the Standard Model expectation. Exclusion limits at the 95% confidence level are set on wino or higgsino production with various assumptions about the decay branching ratios and the type of lightest supersymmetric particle. A wino (higgsino) mass up to 1060 (900) GeV is excluded when the lightest supersymmetry particle mass is below 400 (240) GeV and the mass splitting is larger than 400 (450) GeV. The sensitivity to high-mass winos and higgsinos is significantly extended relative to previous LHC searches using other final states.

DOI: 10.1103/PhysRevD.104.112010

I. INTRODUCTION

Supersymmetry (SUSY) [1–6] is a theoretical framework that extends the Standard Model (SM) by introducing new particles ("superpartners") that have the same quantum numbers as the SM particles except for their spins. In the Minimal Supersymmetric Standard Model (MSSM) [7,8], the bino ($\tilde{B}$), wino ($\tilde{W}$) and higgsino ($\tilde{H}$) are the superpartners of the $\mathrm{U}(1)_{\mathrm{Y}}$ and SU(2) gauge fields and the Higgs field, respectively. These are collectively referred to as "electroweakinos" and form the chargino ($\tilde{\chi}_1^{\pm}, \tilde{\chi}_2^{\pm}$) and neutralino ($\tilde{\chi}_1^0, \tilde{\chi}_2^0, \tilde{\chi}_3^0, \tilde{\chi}_4^0$) mass eigenstates through mixing, with the subscripts indicating increasing mass. The lightest neutralino ($\tilde{\chi}_1^0$) is often considered to be the lightest SUSY particle (LSP), since it is then a viable candidate for weakly interacting massive particle dark matter [9,10] when R-parity conservation is assumed [11]. Depending on the signal model, the superpartner of the graviton (gravitino, $\tilde{G}$) and the axion (axino, $\tilde{a}$) are alternatively considered to be the LSP and dark matter candidate in this search.

Electroweakinos with masses of the order of 0.1–1 TeV are motivated by various phenomenological arguments: (1) the mass of the neutralino LSP dark matter candidate is constrained to be less than a few TeV by the observed relic density [12,13]; (2) the higgsino mass is also motivated to be of the same order as the Z boson mass by naturalness arguments [14–17]; (3) the MSSM parameter space explaining the discrepancy between the measured muon anomalous magnetic moment [18] and its SM predictions [19] tends to include electroweakinos with masses from 200 GeV to 1 TeV [20–22].

This search targets the pair production of electroweakinos ($\tilde{\chi}_{\mathrm{heavy}}$), where each of them decays into a lighter one ($\tilde{\chi}_{\mathrm{light}}$) and an on-shell W, Z or SM Higgs boson (h). A mass splitting $\Delta m(\tilde{\chi}_{\mathrm{heavy}}, \tilde{\chi}_{\mathrm{light}})$ greater than 400 GeV is considered in the search. The $\tilde{\chi}_{\mathrm{heavy}}$ can be either wino- or higgsinolike, and $\tilde{\chi}_{\mathrm{light}}$ can be a bino-, wino-, higgsinolike chargino/neutralino, gravitino, or axino as discussed more in Sec. II. Cases where both $\tilde{\chi}_{\mathrm{heavy}}$ and $\tilde{\chi}_{\mathrm{light}}$ are wino- or higgsinolike are not considered as they lead to very small $\Delta m(\tilde{\chi}_{\mathrm{heavy}}, \tilde{\chi}_{\mathrm{light}})$. The $\tilde{\chi}_{\mathrm{light}}$ is either the LSP or an electroweakino nearly degenerate with it, leading to missing transverse momentum ($\mathbf{p}_{\mathrm{T}}^{\mathrm{miss}}$, with magnitude $E_{\mathrm{T}}^{\mathrm{miss}}$) in the decay signature.[1]

[*]Full author list given at the end of the article.

[1]In the regime of large mass splitting, the effect of chargino/neutralino mixing is highly suppressed so that the gauge eigenstates (e.g., bino) and the mass eigenstates (e.g., binolike $\tilde{\chi}_1^0$) can be regarded as almost identical. Therefore, this paper does not make the distinction and "electroweakinos" are defined to represent both unless explicitly stated otherwise.

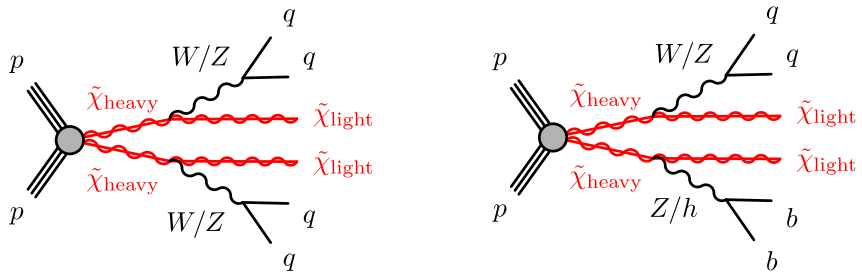

(a) $qqqq$ final state (b) $bbqq$ final state

FIG. 1. Diagrams for the targeted signatures and final states.

The analysis focuses on the hadronic decay modes of the W, Z, and h bosons, namely $W \to q\bar{q}$, $Z \to q\bar{q}/b\bar{b}$ and $h \to b\bar{b}$, where q ($\bar{q}$) represents light-flavor (anti)quarks u, d, s, c ($\bar{u}, \bar{d}, \bar{s}, \bar{c}$).[2] Two fully hadronic final states are considered: the $qqqq$ final state which involves two W/Z bosons decaying into two light-flavor (anti)quarks, and the $bbqq$ final state where a W/Z boson decays into two light-flavor (anti)quarks and a Z/h boson decays into $b\bar{b}$, as illustrated by the diagrams in Fig. 1. While the ATLAS and CMS experiments have typically searched for pair production of electroweakinos using leptonic decay modes [23–36], the fully hadronic final states are used here to take advantage of the larger W, Z, and h hadronic branching ratios, and thereby provide sensitivity to the production of heavier electroweakinos, despite their smaller production cross sections. Final states with four b quarks are not considered in this search;[3] however, they are targeted by dedicated searches [37,38] complementing the sensitivity.

The multijet background is highly suppressed by requiring large $E_{\text{T}}^{\text{miss}}$, and the dominant backgrounds in the analysis are $Z(\to \nu\nu) + \text{jets}$, $W(\to \ell\nu) + \text{jets}$, and diboson production. These can be effectively suppressed when targeting large mass splittings between the produced electroweakinos and the LSP by selecting high-p_{T} kinematics and explicitly reconstructing the two boosted SM bosons. The "boson tagging" technique developed by the ATLAS and CMS experiments [39–42] is employed, where a single large-radius jet is used to capture the two collimated energetic jets from each boosted SM boson decay. Analysis of the jet substructure helps to identify the hadronic decays of W, Z, and h. The introduction of this technique significantly improves upon the previous fully hadronic final-state analysis in ATLAS targeting the $bbqq$ final state [27], and establishes the sensitivity of the $qqqq$ final state for the first time at the Large Hadron Collider (LHC), achieving unprecedented search sensitivity to electroweakinos as heavy as 1 TeV.

This search uses proton-proton collision data collected by the ATLAS detector in the years 2015–2018 at a center-of-mass energy of $\sqrt{s} = 13$ TeV, corresponding to an integrated luminosity of 139 fb^{-1}. The results are interpreted in terms of various models with different electroweakino types for ($\tilde{\chi}_{\text{heavy}}$, $\tilde{\chi}_{\text{light}}$) and their branching ratio assumptions. While each model predicts different electroweakino branching ratios into W, Z, or h, the search combines the dedicated event selections for each decay to achieve only a small model dependency.

II. TARGET PHYSICS SCENARIOS AND THE SIGNAL MODELS

Three physics scenarios are considered in the analysis:

(i) a baseline MSSM scenario where bino, wino and higgsino are considered as $\tilde{\chi}_{\text{heavy}}$ or $\tilde{\chi}_{\text{light}}$;

(ii) a scenario with a gravitino LSP and light higgsinos inspired by the general gauge mediation (GGM) [43–47] models and naturalness;

(iii) a scenario with an axino LSP assuming the SM extension with a QCD axion and light higgsinos driven by naturalness.

The signal models considered in the analysis, derived from each physics scenario, are described in the following subsections. Each model is labeled as (A, B), where A and B represent the dominant component of $\tilde{\chi}_{\text{heavy}}$ and $\tilde{\chi}_{\text{light}}$, respectively. All the SUSY particles other than $\tilde{\chi}_{\text{heavy}}$ and $\tilde{\chi}_{\text{light}}$ are assumed to be decoupled in mass [48,49]. The production modes, final states, and the branching ratio assumptions for $\tilde{\chi}_{\text{heavy}}$ are summarized in Table I.

The winolike states form a doublet consisting of one chargino and one neutralino, while the higgsinolike triplet includes an additional neutralino. The mass degeneracy within these wino/higgsino multiplets is dictated by the extent of mixing with the other electroweakino states, which is characterized by $\Delta m(\tilde{\chi}_{\text{heavy}}, \tilde{\chi}_{\text{light}})$. With $\Delta m(\tilde{\chi}_{\text{heavy}}, \tilde{\chi}_{\text{light}}) > 400$ GeV, the mass splittings within

[2]In this paper the symbols q (b) represent both (bottom) quarks and (bottom) antiquarks unless explicitly stated otherwise, since they are not distinguished in the search. In addition, charm quarks and antiquarks are treated as light-flavor quarks and antiquarks in the analysis.

[3]The contributions from signals with two h bosons are included in the signal models although not targeted. Likewise, all the decays of W, Z, and h are taken into account for the signals.

TABLE I. Summary of the production modes, final states, and signal regions (SRs) used for the hypothesis tests, and the branching ratio assumptions for the signal models targeted in the search. The notation and definition of the SRs are described in Sec. VI B. The $(\tilde{W},\tilde{B})$ and $(\tilde{H},\tilde{G})$ models are used to optimize the selection, and the rest are considered in the interpretation. The $(\tilde{W},\tilde{B})$ simplified models ($(\tilde{W},\tilde{B})$-SIM) discussed in Sec. IV B 2 are also interpreted in order to allow comparisons with the ATLAS electroweakino search results [23–25,29,68].

Model	Production	Final states	SRs simultaneously fitted	Branching ratio
$(\tilde{W},\tilde{B})$	$\tilde{\chi}_1^\pm\tilde{\chi}_1^\mp$, $\tilde{\chi}_1^\pm\tilde{\chi}_2^0$	WW, WZ, Wh	4Q-VV, 2B2Q-WZ, 2B2Q-Wh	$\mathcal{B}(\tilde{\chi}_1^\pm \to W\tilde{\chi}_1^0) = 1$ $\mathcal{B}(\tilde{\chi}_2^0 \to Z\tilde{\chi}_1^0)$ scanned
$(\tilde{H},\tilde{B})$	$\tilde{\chi}_1^\pm\tilde{\chi}_1^\mp$, $\tilde{\chi}_1^\pm\tilde{\chi}_2^0$, $\tilde{\chi}_1^\pm\tilde{\chi}_3^0$, $\tilde{\chi}_2^0\tilde{\chi}_3^0$	WW, WZ, Wh, ZZ, Zh, hh	4Q-VV, 2B2Q-VZ, 2B2Q-Vh	$\mathcal{B}(\tilde{\chi}_1^\pm \to W\tilde{\chi}_1^0) = 1$ $\mathcal{B}(\tilde{\chi}_2^0 \to Z\tilde{\chi}_1^0)$ scanned $\mathcal{B}(\tilde{\chi}_3^0 \to Z\tilde{\chi}_1^0) = 1 - \mathcal{B}(\tilde{\chi}_2^0 \to Z\tilde{\chi}_1^0)$
$(\tilde{W},\tilde{H})$	$\tilde{\chi}_2^\pm\tilde{\chi}_2^\mp$, $\tilde{\chi}_2^\pm\tilde{\chi}_3^0$	WW, WZ, Wh, ZZ, Zh, hh	4Q-VV, 2B2Q-VZ, 2B2Q-Vh	Determined from $(M_2, \mu, \tan\beta)$
$(\tilde{H},\tilde{W})$	$\tilde{\chi}_2^\pm\tilde{\chi}_2^\mp$, $\tilde{\chi}_2^\pm\tilde{\chi}_2^0$, $\tilde{\chi}_2^\pm\tilde{\chi}_3^0$, $\tilde{\chi}_2^0\tilde{\chi}_3^0$	WW, WZ, Wh, ZZ, Zh, hh	4Q-VV, 2B2Q-VZ, 2B2Q-Vh	Determined from $(M_2, \mu, \tan\beta)$
$(\tilde{H},\tilde{G})$	$\tilde{\chi}_1^\pm\tilde{\chi}_1^\mp$, $\tilde{\chi}_1^\pm\tilde{\chi}_1^0$, $\tilde{\chi}_1^\pm\tilde{\chi}_2^0$, $\tilde{\chi}_1^0\tilde{\chi}_2^0$	ZZ, Zh, hh	4Q-ZZ, 2B2Q-ZZ, 2B2Q-Zh	$\mathcal{B}(\tilde{\chi}_1^0 \to Z\tilde{G})$ scanned
$(\tilde{H},\tilde{a})$	$\tilde{\chi}_1^\pm\tilde{\chi}_1^\mp$, $\tilde{\chi}_1^\pm\tilde{\chi}_1^0$, $\tilde{\chi}_1^\pm\tilde{\chi}_2^0$, $\tilde{\chi}_1^0\tilde{\chi}_2^0$	ZZ, Zh, hh	4Q-ZZ, 2B2Q-ZZ, 2B2Q-Zh	$\mathcal{B}(\tilde{\chi}_1^0 \to Z\tilde{a})$ scanned
		$(\tilde{W},\tilde{B})$ simplified models: $(\tilde{W},\tilde{B})$-SIM		
C1C1-WW	$\tilde{\chi}_1^\pm\tilde{\chi}_1^\mp$	WW	4Q-WW	$\mathcal{B}(\tilde{\chi}_1^\pm \to W\tilde{\chi}_1^0) = 1$
C1N2-WZ	$\tilde{\chi}_1^\pm\tilde{\chi}_2^0$	WZ	4Q-WZ, 2B2Q-WZ	$\mathcal{B}(\tilde{\chi}_1^\pm \to W\tilde{\chi}_1^0) = \mathcal{B}(\tilde{\chi}_2^0 \to Z\tilde{\chi}_1^0) = 1$
C1N2-Wh	$\tilde{\chi}_1^\pm\tilde{\chi}_2^0$	Wh	2B2Q-Wh	$\mathcal{B}(\tilde{\chi}_1^\pm \to W\tilde{\chi}_1^0) = \mathcal{B}(\tilde{\chi}_2^0 \to h\tilde{\chi}_1^0) = 1$

the wino/higgsino multiplets are typically small (<10 GeV), such that the decay products are almost never reconstructed in this analysis. Therefore, these multiplets are treated as approximately degenerate; the masses of the winolike chargino and winolike neutralino are treated as identical; and the masses of the higgsinolike chargino and the heavier higgsinolike neutralino are set 1 GeV heavier than the lighter higgsinolike neutralino.[4] Particles originating from decays within the wino doublet or higgsino triplet are ignored so that only the decays of the form $\tilde{\chi}_{\text{heavy}} \to \tilde{\chi}_{\text{light}} + W/Z/h$ are taken into account in the signature.

A. Bino/wino/higgsino LSP models: $(\tilde{W},\tilde{B})$, $(\tilde{W},\tilde{H})$, $(\tilde{H},\tilde{B})$, $(\tilde{H},\tilde{W})$

Two of $\tilde{B}$, $\tilde{W}$, and $\tilde{H}$ are assumed to be light enough to be produced at the LHC while the others are decoupled. Four mass hierarchies are experimentally explorable under this regime: $(\tilde{W},\tilde{B}), (\tilde{W},\tilde{H}), (\tilde{H},\tilde{B}), (\tilde{H},\tilde{W})$. A bino is not considered as $\tilde{\chi}_{\text{heavy}}$ here because the production cross section is negligible when sfermions and the non-SM Higgs bosons are decoupled.

The $(\tilde{W},\tilde{H})$, $(\tilde{H},\tilde{B})$, and $(\tilde{H},\tilde{W})$ hierarchies are typically predicted by the MSSM parameter space that explains the muon $g-2$ anomaly with loop contributions including a wino and/or higgsino.[5] The $(\tilde{H},\tilde{B})$ hierarchy is additionally motivated when the mass of a binolike LSP is half of the Z or h boson mass, where the LSP dark matter can annihilate via the Z/h resonance ("Z/h-funnel" dark matter). This is a special case of *well-tempered neutralino dark matter* where a large higgsino-bino mass splitting is favored in order to realize the observed relic density [50–58].

A signal model is defined for each of the four hierarchies with a set of assumptions described below. The mass spectra, corresponding mass eigenstates, and the decays considered are illustrated for each model in Fig. 2. A W boson is generated when a chargino decays into a neutralino or vice versa; a Z or h boson is emitted when a chargino decays into a chargino, or a neutralino decays into a neutralino.

The production modes considered in each model are shown in Table I. Processes involving chargino-chargino or chargino-neutralino pair production are taken into account in the wino production models: $(\tilde{W},\tilde{B})$ and $(\tilde{W},\tilde{H})$; and

[4] A mass splitting of 1 GeV is used to avoid potential technical issues when setting it exactly to zero. This choice is arbitrary and has no impact on the analysis.

[5] In this case, smuons and muon sneutralinos need to be only mildly decoupled in mass.

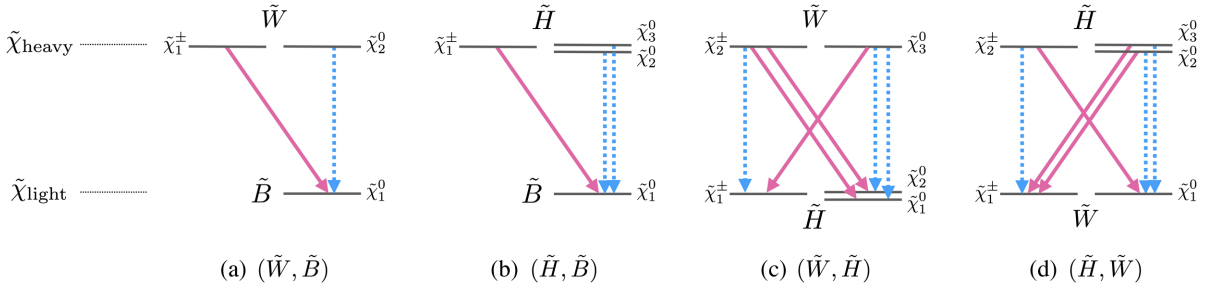

FIG. 2. The electroweakino mass spectra and corresponding mass eigenstates in each model in the bino/wino/higgsino LSP scenario. The solid (dashed) arrows represent the decay modes emitting a W (Z or h) boson. A W boson is generated when a chargino decays into a neutralino or vice versa; a Z or h boson is emitted when a chargino decays into a chargino or a neutralino decays into a neutralino.

neutralino-neutralino production is additionally included for the higgsino production models: $(\tilde{H},\tilde{B})$ and $(\tilde{H},\tilde{W})$. It should be noted that neutral wino pairs can only be produced via a t-channel exchange of squarks, which is prohibited when squarks are assumed to be decoupled.

The branching ratios of $\tilde{\chi}_{\text{heavy}}$ are treated as follows. In the $(\tilde{W},\tilde{B})$ and $(\tilde{H},\tilde{B})$ models, the produced chargino $(\tilde{\chi}_1^{\pm})$ decays with 100% probability into the bino LSP $(\tilde{\chi}_1^0)$ and a W boson. Meanwhile, the produced neutralino(s) can decay either into Z or into h.[6] Given the complicated model dependency, the branching ratio of the second lightest neutralino $(\tilde{\chi}_2^0)$ is treated as a free parameter,[7] and $\mathcal{B}(\tilde{\chi}_2^0 \to Z\tilde{\chi}_1^0)(= 1 - \mathcal{B}(\tilde{\chi}_2^0 \to h\tilde{\chi}_1^0))$ is scanned over 0, 25, 50, 75, and 100% in both models. For the $(\tilde{H},\tilde{B})$ model, the branching ratios of the heavy neutral higgsino $(\tilde{\chi}_3^0)$ are fixed relative to those of the light neutral higgsino $(\tilde{\chi}_2^0)$ via

(i) $\mathcal{B}(\tilde{\chi}_2^0 \to Z\tilde{\chi}_1^0) + \mathcal{B}(\tilde{\chi}_3^0 \to Z\tilde{\chi}_1^0) = 1$,
(ii) $\mathcal{B}(\tilde{\chi}_2^0 \to h\tilde{\chi}_1^0) + \mathcal{B}(\tilde{\chi}_3^0 \to h\tilde{\chi}_1^0) = 1$.

These provide a good approximation when $\Delta m(\tilde{\chi}_{\text{heavy}}, \tilde{\chi}_{\text{light}})$ is significantly larger than m_h [59].

In $(\tilde{W},\tilde{H})$ and $(\tilde{H},\tilde{W})$ models, however, the branching ratios of the produced chargino and neutralino(s) are largely dictated by the three MSSM parameters: the wino mass parameter M_2, the higgsino mass parameter μ, and the ratio of vacuum expectation values of the two Higgs fields, $\tan\beta$. For a given set of $(M_2,\mu,\tan\beta)$ the branching ratios are coherently derived using SOFTSUSY 4.1.7 [60,61], with all the SUSY mass parameters except for M_2 and μ being set as decoupled. The signal models are tested using various combinations of $(M_2,\mu,\tan\beta)$ where $M_2 \in [0, 1.2]$ TeV, $\mu \in [-1.2, 1.2]$ TeV, and $\tan\beta = 2$, 5, 10, 30 are considered.

[6]Produced heavier higgsinos are assumed to decay 100% directly into bino rather than the lighter higgsino, which is reasonable given the much smaller higgsino mass splitting compared with the higgsino-bino mass splitting.

[7]Particularly for $(\tilde{W},\tilde{B})$, the branching ratio strongly depends on the higgsino mass as the decay has to rely on the small higgsino component, even though it is assumed to be decoupled.

The vast majority of the previous electroweakino searches at the LHC have targeted the simplified $(\tilde{W},\tilde{B})$ model, where only a specific production channel and decay mode are considered (detailed in Sec. IV B 2). For $\tilde{\chi}_1^{\pm}\tilde{\chi}_1^{\mp}$ production with decays into WW, $m(\tilde{\chi}_1^{\pm}) < 400$ GeV is excluded for $m(\tilde{\chi}_1^0) < 200$ GeV [23,31]. For $\tilde{\chi}_1^{\pm}\tilde{\chi}_2^0$ production, $m(\tilde{\chi}_1^{\pm}/\tilde{\chi}_2^0) < 640$ GeV is excluded for $m(\tilde{\chi}_1^0) < 300$ GeV when the $\tilde{\chi}_2^0$ is assumed to decay into Z and $\tilde{\chi}_1^0$ with 100% probability [24–26,32,33]. Alternatively, $m(\tilde{\chi}_1^{\pm}/\tilde{\chi}_2^0) < 740$ GeV is excluded for $m(\tilde{\chi}_1^0) < 250$ GeV [27–29,34–36] when the $\tilde{\chi}_2^0$ decays solely into h and $\tilde{\chi}_1^0$.

B. GGM/naturalness-driven gravitino LSP model: $(\tilde{H},\tilde{G})$

GGM, a class of SUSY-breaking scenarios characterized by a messenger sector to which only SM gauge bosons can couple, typically predicts a nearly massless gravitino $(\tilde{G})$ as the LSP. Motivated also by the naturalness argument, the production of a relatively light higgsino triplet $(\tilde{\chi}_1^{\pm}, \tilde{\chi}_2^0, \tilde{\chi}_1^0)$ decaying into a gravitino LSP has been explored at ATLAS [30,37] and CMS [33], as illustrated in Fig. 3(a). All of the four production modes are considered together: $\tilde{\chi}_1^{\pm}\tilde{\chi}_1^{\mp}$, $\tilde{\chi}_1^{\pm}\tilde{\chi}_1^0$, $\tilde{\chi}_1^{\pm}\tilde{\chi}_2^0$, $\tilde{\chi}_1^0\tilde{\chi}_2^0$. A moderately small higgsino-gravitino coupling is considered in this analysis, where the produced heavy higgsinos $(\tilde{\chi}_1^{\pm}/\tilde{\chi}_2^0)$ always decay into a gravitino via

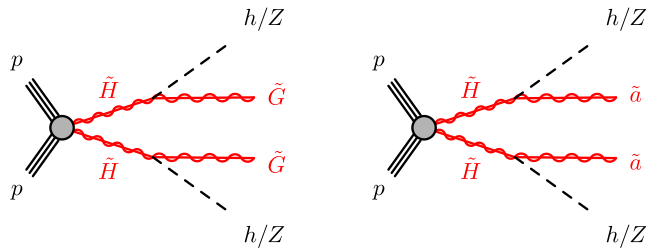

FIG. 3. Diagrams of signals considered in the (a) $(\tilde{H},\tilde{G})$ model and (b) $(\tilde{H},\tilde{a})$ model. In the $(\tilde{H},\tilde{G})$ and $(\tilde{H},\tilde{a})$ models, the higgsino triplets $(\tilde{\chi}_1^{\pm},\tilde{\chi}_2^0,\tilde{\chi}_1^0)$ are collectively represented by $\tilde{H}$.

the lightest neutral higgsino ($\tilde{\chi}_1^0$), while the $\tilde{\chi}_1^0$ still has a short enough lifetime to be regarded as decaying promptly. In this model, the $\tilde{\chi}_1^0$ decays into a gravitino and either a Z or h boson, where the branching ratio $\mathcal{B}(\tilde{\chi}_1^0 \to Z\tilde{G})(=1-\mathcal{B}(\tilde{\chi}_1^0 \to h\tilde{G}))$ is treated as a free parameter and scanned in the limit setting. The previous searches have excluded masses of $\tilde{\chi}_1^0$ lighter than 650–880 GeV depending on the branching ratio [30,33,37].

C. Naturalness-driven axino LSP model: $(\tilde{H}, \tilde{a})$

While the QCD Lagrangian generally allows for CP violation, the absence of such observation suggests a highly unnatural tuning of the parameters in the theory, referred to as the "strong CP problem." The Peccei-Quinn mechanism aims to solve this problem by introducing an additional chiral U(1) symmetry [62]. Through its spontaneous symmetry breaking, the CP-violating term vanishes dynamically, leaving a Nambu-Goldstone boson known as the axion [63,64]. In the SUSY extension, the axino is introduced as the superpartner of the axion. A model including a light higgsino triplet ($\tilde{\chi}_1^{\pm}$, $\tilde{\chi}_2^0$, $\tilde{\chi}_1^0$) decaying into an axino LSP [65] is proposed in the spirit of pursuing naturalness as well as axion/axino dark matter [66,67] under R-parity conservation.

A diagram of the model is shown in Fig. 3(b). Higgsinos are produced by each of the four modes: $\tilde{\chi}_1^{\pm}\tilde{\chi}_1^{\mp}$, $\tilde{\chi}_1^{\pm}\tilde{\chi}_1^0$, $\tilde{\chi}_1^{\pm}\tilde{\chi}_2^0$, $\tilde{\chi}_1^0\tilde{\chi}_2^0$. The produced heavier higgsinos ($\tilde{\chi}_1^{\pm}/\tilde{\chi}_2^0$) are assumed to always decay into the axino via the lightest natural higgsino ($\tilde{\chi}_1^0$). This is typically valid when the wino and bino are reasonably decoupled so as to maintain approximate mass degeneracy of the higgsino triplet, and when the conventionally motivated range of the axion coupling constant is assumed [65]. A prompt $\tilde{\chi}_1^0$ decay into an axino and a Z or h boson is considered in the search. The value of the branching ratio $\mathcal{B}(\tilde{\chi}_1^0 \to Z\tilde{a})(=1-\mathcal{B}(\tilde{\chi}_1^0 \to h\tilde{a}))$ is scanned over 25, 50, 75, and 100% in the interpretation. The model is similar to $(\tilde{H}, \tilde{G})$, except that the LSP can be massive.

III. ATLAS DETECTOR

The ATLAS experiment [69,70] is a multipurpose detector with a forward-backward symmetric cylindrical geometry and nearly 4π coverage in solid angle.[8] It consists of an inner tracking detector surrounded by a thin superconducting solenoid providing a 2-T axial magnetic field, electromagnetic and hadron calorimeters, and a muon spectrometer.

The inner detector (ID) consists of pixel and microstrip silicon detectors covering the pseudorapidity range $|\eta| < 2.5$ and a transition radiation tracker covering $|\eta| < 2.0$. Outside the ID, a lead/liquid-argon (LAr) electromagnetic calorimeter (ECAL) and a steel/scintillator-tile hadronic calorimeter cover the $|\eta| < 3.2$ and $|\eta| < 1.7$ ranges, respectively. In the forward regions, a copper/LAr endcap calorimeter extends the coverage of hadronic measurements to $1.7 < |\eta| < 3.2$, while copper/LAr and tungsten/LAr forward calorimeters are employed for electromagnetic and hadronic measurements in the $3.1 < |\eta| < 4.9$ region. The muon spectrometer (MS) surrounds the calorimeters and comprises three layers of trigger and high-precision tracking chambers spanning $|\eta| < 2.4$ and $|\eta| < 2.7$, respectively. A magnetic field is provided by a system of three superconducting air-core toroidal magnets with eight coils each. The field integral of the toroids ranges between 2.0 and 6.0 Tm across most of the detector.

Events of interest are selected and collected by the ATLAS trigger system [71], consisting of a hardware-based first-level trigger (L1) and a software-based high-level trigger (HLT). The L1 trigger is designed to accept events from the 40-MHz bunch crossings at a rate below 100 kHz, and the HLT reduces this to about 1 kHz, the rate at which events are recorded to disk. An extensive software suite [72] is used for real and simulated data reconstruction and analysis, for operation and in the trigger and data acquisition systems of the experiment.

IV. DATA AND MONTE CARLO SIMULATION

A. Data sample

The data events used in the analysis are from proton-proton collisions at $\sqrt{s} = 13$ TeV, recorded during stable beam conditions at the LHC during 2015–2018. The collected dataset corresponds to an integrated luminosity of 139 fb^{-1} after applying the data quality criteria [73]. The primary dataset was collected by triggers targeting large missing transverse momentum [74]. Events were accepted when the $E_{\mathrm{T}}^{\mathrm{miss}}$ calculated at trigger level was greater than 70–110 GeV, with the threshold rising with the increased instantaneous luminosity during the data-taking period. The efficiency reaches approximately 100% for events reconstructed offline with $E_{\mathrm{T}}^{\mathrm{miss}} > 200$ GeV, which is generally required in the search. Auxiliary data samples used to validate the background estimation were selected using triggers requiring at least one isolated electron, muon or photon [75,76]. The thresholds were $p_{\mathrm{T}} = 24(26)$ GeV for electrons, $p_{\mathrm{T}} = 20(26)$ GeV for muons, and $p_{\mathrm{T}} = 120(140)$ GeV for photons in data taken in 2015 (2016–2018).

[8] ATLAS uses a right-handed coordinate system with its origin at the nominal interaction point (IP) in the center of the detector and the z axis along the beam pipe. The x axis points from the IP to the center of the LHC ring, and the y axis points upwards. Cylindrical coordinates (r, ϕ) are used in the transverse plane, ϕ being the azimuthal angle around the z axis. The pseudorapidity is defined in terms of the polar angle θ as $\eta = -\ln\tan(\theta/2)$. Angular distance is measured in units of $\Delta R \equiv \sqrt{(\Delta\eta)^2 + (\Delta\phi)^2}$.

B. Monte Carlo simulation

Monte Carlo (MC) simulations are used to estimate the SM backgrounds and the signals contributing to the analysis regions. All of the generated events were propagated through the ATLAS detector simulation [77] based on GEANT4 [78]. Multiple proton-proton collisions in the same and neighboring bunch crossings (pileup) were modeled by overlaying the hard-scatter events with minimum-bias events simulated by PYTHIA 8.186 [79] with a set of tuned parameters called the A3 tune [80] and NNPDF2.3LO parton distribution function (PDF) set [81].

The simulated events are processed with the same trigger and reconstruction algorithms as the data. The lepton and photon trigger efficiencies in the simulation are corrected to match those in data using scale factors that depend on the p_{T} and η of the leptons and photons, as derived from control samples [75,76].

1. Standard Model backgrounds

Events with a leptonically decaying W or Z boson associated with hadron jets were simulated using the SHERPA 2.2.1 [82] generator. The matrix elements were calculated for up to two partons at next-to-leading-order (NLO) accuracy and up to four jets at leading-order (LO) accuracy using the Comix [83] and OpenLoops [84,85] generators. The NLO matrix elements for a given jet multiplicity were matched to the parton shower using a color-exact variant of the MC@NLO algorithm [86]. Different jet multiplicities were then merged into an inclusive sample using an improved Catani-Krauss-Kuhn-Webber (CKKW) matching procedure [87,88] which is extended to NLO accuracy using the MEPS@NLO prescription [89]. The NNPDF3.0NNLO PDF sets [90] were used. Prompt single-photon production, denoted by $\gamma+$ jets, was simulated using the same configuration except that the generator version is SHERPA 2.2.2. The photons must be isolated according to a smooth-cone isolation criterion [91].

Samples of $t\bar{t}$ and single-top-quark ($t+X$) events were generated with POWHEGBOX v2 [92–95] at NLO with the NNPDF3.0NLO PDF sets. The top-quark mass was set to 172.5 GeV. For the $t\bar{t}$ generation, the h_{damp} parameter, which controls the p_{T} of the first additional emission beyond the Born configuration in POWHEG, was set to 1.5 times the top-quark mass. This is to regulate the high-p_{T} emission recoiling against the $t\bar{t}$ system so as to reproduce the data [96]. The parton shower, fragmentation, and underlying event were simulated using PYTHIA 8.230 with the NNPDF2.3LO PDF set and the A14 tune [97]. The decays of bottom and charm hadrons were performed by EvtGen 1.6.0 [98]. The diagram removal scheme [99] was employed to account for the interference between $t\bar{t}$ and single-top Wt production.

Events containing $t\bar{t}$ with additional heavy particles, such as $t\bar{t}+W/Z/h$, $t\bar{t}+WW$, $t\bar{t}t$ and $t\bar{t}t\bar{t}$, are collectively referred to as $t\bar{t}+X$ in this paper. The $t\bar{t}+W/Z$ events were modeled by MadGraph5_aMC@NLO2.3.3 [100] at NLO accuracy with the NNPDF3.0NLO PDF [90] set, while $t\bar{t}+h$ events were modeled by POWHEGBOX 2.2. Both were interfaced with PYTHIA 8.230 for parton showering. The $t\bar{t}+h$ events were generated using the same setup as for $t\bar{t}$ described above, with the h mass set to 125 GeV. The $t\bar{t}+WW$, $t\bar{t}t$, and $t\bar{t}t\bar{t}$ events were generated with MadGraph5_aMC@NLO2.2.2, interfaced to PYTHIA 8.210 using the A14 tune and the NNPDF2.3LO PDF set. The decays of bottom and charm hadrons were simulated using EvtGen 1.2.0.

Diboson production, including WW, WZ and ZZ, is collectively denoted here by VV. Events with semileptonic VV decays ($\ell\nu qq$, $\ell\ell qq$ and $\nu\nu qq$) were simulated with SHERPA 2.2.1 using matrix elements with up to one additional parton at NLO accuracy in QCD and up to three additional parton emissions at LO accuracy. Events with fully leptonic VV decays were simulated with SHERPA 2.2.1 ($ZZ\to\nu\nu\nu\nu$) or SHERPA 2.2.2 ($\ell\ell\ell\ell$, $\ell\ell\ell\nu$, $\ell\ell\nu\nu$ and $\ell\nu\nu\nu$), where all the processes at orders of $(\alpha_{\mathrm{EW}}^4,\alpha_{\mathrm{s}}^0)$ and $(\alpha_{\mathrm{EW}}^6,\alpha_{\mathrm{s}}^0)$ are taken into account, including the off-shell contributions and those mediated by Higgs bosons. The NNPDF3.0NNLO PDF set is used.

The production of Wh and Zh (collectively denoted by Vh) was modeled by POWHEGBOX 2.2 interfaced with PYTHIA 8.186. The h mass was set to 125 GeV. The NNPDF3 PDF set and the AZNLO tune were used.

Triboson production, including WWW, WWZ, WZZ and ZZZ, are collectively denoted by VVV. The $V(\to\ell\ell/\ell\nu/\nu\nu)V(\to qq)V(\to qq)$ processes were generated using MadGraph5_aMC@NLO2.6.6 at LO, interfaced to PYTHIA 8.243 for modeling of parton showers and hadronization using the A14 tune. The NNPDF3.0LO PDF set was used.

Theoretical cross sections are used to normalize the generated background samples. The $t\bar{t}$ sample is normalized to the cross section predicted at NNLO in QCD, including the resummation of next-to-next-to-leading-logarithmic (NNLL) soft-gluon terms calculated using Top++ 2.0 [101–107]. The cross sections of single-top-quark t- and s-channel production are calculated using the HATHOR 2.1 program [108,109], while the Wt-channel calculation followed the prescriptions from Refs. [110,111]. The VV and $t\bar{t}+W/Z$ samples are normalized to the cross sections calculated at NLO [112–114]. The cross sections for the $V+$ jets and $\gamma+$ jets samples are calculated at NNLO [115]. The remaining samples, including the production of Vh, $V\gamma$, VVV, $t\bar{t}+WW$, tWZ, $t\bar{t}+h$, $t\bar{t}t$, and $t\bar{t}t\bar{t}$, are normalized to the cross sections calculated at LO by the generators.

2. Signals

The $(\tilde{W},\tilde{B})$, $(\tilde{H},\tilde{B})$, $(\tilde{W},\tilde{H})$, $(\tilde{H},\tilde{W})$, and $(\tilde{H},\tilde{a})$ models discussed in Sec. II were simulated by combining the "simplified model" signals in which a fixed production mode and decay chain are considered. Six sets of simplified

model samples, derived as variants of the $(\tilde{W},\tilde{B})$ and $(\tilde{H},\tilde{B})$ models, were generated to cover the different final states:

(i) wino pair production, with each decaying into a bino LSP (referred to as $(\tilde{W},\tilde{B})$ simplified models, or $(\tilde{W},\tilde{B})$-SIM):

$$\textbf{C1C1-WW}: \tilde{\chi}_1^{\pm}\tilde{\chi}_1^{\pm} \to WW\tilde{\chi}_1^0\tilde{\chi}_1^0(\mathcal{B}(\tilde{\chi}_1^{\pm} \to W\tilde{\chi}_1^0) = 100\%)$$
$$\textbf{C1N2-WZ}: \tilde{\chi}_1^{\pm}\tilde{\chi}_2^0 \to WZ\tilde{\chi}_1^0\tilde{\chi}_1^0(\mathcal{B}(\tilde{\chi}_1^{\pm} \to W\tilde{\chi}_1^0) = \mathcal{B}(\tilde{\chi}_2^0 \to Z\tilde{\chi}_1^0) = 100\%)$$
$$\textbf{C1N2-Wh}: \tilde{\chi}_1^{\pm}\tilde{\chi}_2^0 \to Wh\tilde{\chi}_1^0\tilde{\chi}_1^0(\mathcal{B}(\tilde{\chi}_1^{\pm} \to W\tilde{\chi}_1^0) = \mathcal{B}(\tilde{\chi}_2^0 \to h\tilde{\chi}_1^0) = 100\%),$$

(ii) neutral higgsino pair production, with each decaying into a bino LSP (denoted by $(\tilde{H},\tilde{B})$-SIM):

$$\textbf{N2N3-ZZ}: \tilde{\chi}_2^0\tilde{\chi}_3^0 \to ZZ\tilde{\chi}_1^0\tilde{\chi}_1^0(\mathcal{B}(\tilde{\chi}_2^0 \to Z\tilde{\chi}_1^0) = \mathcal{B}(\tilde{\chi}_3^0 \to Z\tilde{\chi}_1^0) = 100\%)$$
$$\textbf{N2N3-Zh}: \tilde{\chi}_2^0\tilde{\chi}_3^0 \to Zh\tilde{\chi}_1^0\tilde{\chi}_1^0(\mathcal{B}(\tilde{\chi}_2^0 \to Z\tilde{\chi}_1^0) = \mathcal{B}(\tilde{\chi}_3^0 \to h\tilde{\chi}_1^0) = 100\%)$$
$$\textbf{N2N3-hh}: \tilde{\chi}_2^0\tilde{\chi}_3^0 \to hh\tilde{\chi}_1^0\tilde{\chi}_1^0(\mathcal{B}(\tilde{\chi}_2^0 \to h\tilde{\chi}_1^0) = \mathcal{B}(\tilde{\chi}_3^0 \to h\tilde{\chi}_1^0) = 100\%).$$

The symbols C1, N2 and N3 in the model names represent $\tilde{\chi}_1^{\pm}$, $\tilde{\chi}_2^0$ and $\tilde{\chi}_3^0$, respectively. These samples are used to model event kinematics for each final state; the $(\tilde{W},\tilde{B})$-SIM samples are used for events containing WW, WZ or Wh, while $(\tilde{H},\tilde{B})$-SIM samples are employed to model events with ZZ, Zh or hh. The events are reweighted to account for the production cross section and the $\tilde{\chi}_{\text{heavy}}$ branching ratios considered in the model. The underlying assumption for the method is that the event kinematics depend only on $m(\tilde{\chi}_{\text{light}})$ and $m(\tilde{\chi}_{\text{heavy}})$, and not on the production mode, type of LSP, or other MSSM variables such as $\tan\beta$. This is validated in the phase space considered in the analysis by using generator-level samples.

The $(\tilde{W},\tilde{B})$-SIM models are also considered in the limit interpretation in order to allow comparisons with previous ATLAS searches, as these models were the most commonly studied [23,25–29,31–36]. For the $(\tilde{H},\tilde{G})$ model, a dedicated sample was generated with all of the production modes $(\tilde{\chi}_1^{\pm}\tilde{\chi}_1^{\mp}, \tilde{\chi}_1^{\pm}\tilde{\chi}_1^0, \tilde{\chi}_1^{\pm}\tilde{\chi}_2^0, \tilde{\chi}_1^0\tilde{\chi}_2^0)$ included.

The $(\tilde{W},\tilde{B})$-SIM and $(\tilde{H},\tilde{G})$ signal samples were simulated using LO matrix elements with up to two extra partons in MadGraph5_aMC@NLO2.6.2. The events were subsequently interfaced to PYTHIA 8.230 [116] together with the A14 tune and NNPDF2.3LO PDF set for simulation of parton showering and hadronization. For $(\tilde{H},\tilde{B})$-SIM, MadGraph5_aMC@NLO2.6.7 and PYTHIA 8.244 were used. The mass of the SM Higgs boson was set to 125 GeV.

Decays of the produced electroweakinos are simulated using PYTHIA. As the performance of the boosted W/Z boson tagging is known to be sensitive to the boson polarization [39], W/Z bosons from the electroweakino decays were carefully modeled either by using MADSPIN 2.7.3 [117,118] or by reweighting the helicity angle distribution such that the overall cross section remains unchanged. The W/Z bosons are typically longitudinally polarized when $\Delta m(\tilde{\chi}_{\text{heavy}},\tilde{\chi}_{\text{light}}) > 400$ GeV is considered. The decays of bottom and charm hadrons were performed by EVTGEN 1.2.0.

The signal cross sections are computed at NLO in the strong coupling constant, adding the resummation of soft-gluon emission at next-to-leading-logarithm (NLL) accuracy [119–124]. The PDF4LHC15_MC PDF set is used following the recommendations in Ref. [125]. Assuming a mass of 800 GeV, the calculated cross section for winolike (higgsinolike) chargino pair production is 2.21 (0.63) fb, and 4.76 (1.12) fb for winolike (higgsinolike) chargino-neutralino production. For neutral higgsino pair production, the corresponding cross section is 0.59 fb.

V. EVENT RECONSTRUCTION

The primary reconstructed objects used in the analysis are large-radius (large-R) jets, denoted by J. These are reconstructed from locally calibrated topo-clusters [126] using the anti-k_t algorithm [127] implemented in the FASTJET package [128] with a radius parameter $R = 1.0$. A trimming algorithm [129] is applied to mitigate the effects of pileup and soft radiation. The constituents of each jet are reclustered with the k_t algorithm [130] into $R = 0.2$ subjets, and the subjets are removed if $p_{\text{T}}^{\text{subjet}}/p_{\text{T},J} < 0.05$, where $p_{\text{T}}^{\text{subjet}}$ and $p_{\text{T},J}$ are the transverse momenta of the subjet and the large-R jet, respectively. The jet mass, m_J, is calculated according to the combined mass prescription [131] in order to achieve the best mass resolution, which is given by the weighted sum of masses computed using only the calorimeter information and with tracking information included. The p_{T} and mass scales are calibrated using simulation, followed by an *in situ* calibration [132] to correct for residual differences between

data and MC simulation. Large-R jets used in the analysis are selected with $p_{\mathrm{T}} > 200$ GeV, $|\eta| < 2.0$, and $m_J > 40$ GeV.

Track jets are used to identify large-R-jet subjets that contain b hadrons. They are reconstructed from ID tracks by using the anti-k_t algorithm with a sliding radius parameter $R = 30\ \mathrm{GeV}/p_{\mathrm{T}}$ truncated at 0.02 and 0.4 [133]. The MV2c10 b-tagging algorithm [134] is applied to track jets satisfying $p_{\mathrm{T}} > 20$ GeV and $|\eta| < 2.5$. This algorithm is a multivariate discriminator that utilizes track impact parameters, the presence of secondary vertices, and the trajectories of b- and c hadrons inside the jet. A working point is chosen such that b jets from simulated $t\bar{t}$ events are identified with 85% efficiency, with rejection factors of 3 against c jets and 33 against jets originating from other light-flavor quarks or gluons [134]. Efficiency correction factors are applied to simulated samples to account for the efficiency difference observed between MC and data events in dedicated measurement regions in which $t\bar{t}$ samples [134,135] are used for b jets and mistagged c jets, and $Z+$jets samples are used for the light-flavor mistagged jets [136].

The b-jet multiplicity of each large-R jet is defined by the number of b-tagged track jets it contains. A b-tagged track jet is contained in a large-R jet if the two jet axes have an angular separation $\Delta R < 1.0$.

Two types of boosted boson tagging are employed for the preselected large-R jets to identify the SM boson decays: $W_{qq}(Z_{qq})$-tagging targeting $W(Z) \to qq$, and $Z_{bb}(h_{bb})$-tagging targeting $Z(h) \to bb$. The $W_{qq}(Z_{qq})$ tagging utilizes cuts on m_J, the energy correlation function D_2, and the track multiplicity n_{track} [39,137]. In order to maintain orthogonality with the $Z_{bb}(h_{bb})$ tagging, the b-jet multiplicity of the large-R jet is required to be less than two. The D_2 variable is defined as a ratio of three-point to two-point energy correlation functions [138,139] based on the energies and pairwise angular separations of particles within a jet, and n_{track} is the number of tracks matched to the large-R jet by ghost association [140] before trimming is applied. While the upper bound on n_{track} is fixed, the cut values applied to m_J and D_2 are shifted smoothly as a function of p_{T} to maximize the rejection for typical single-parton initiated jets, maintaining a constant efficiency for signal jets that contain the decay products of $W(Z) \to qq$. The selections are optimized separately for targeting W and Z, and V_{qq} tagging is defined by a selection satisfying either the W_{qq}- or Z_{qq} tagging. The cut values applied to m_J and D_2 are the same as for the "50% efficiency W/Z tagger" in Ref. [137]; however, a loosened n_{track} cut, from ≤ 26 to $\leq 32(34)$ for the $W_{qq}(Z_{qq})$ tagging, is applied to achieve the optimum sensitivity for the analysis and better modeling in MC simulation. The efficiency correction factors are rederived according to this refinement, using a methodology similar to that described in Ref. [137]. A correction factor of 0.85–1.05 is typically obtained. The performance of the W_{qq}-and Z_{qq} tagging is summarized in Figs. 4(a) and 4(b). For a sample of preselected large-R jets ($p_{\mathrm{T}} > 200$ GeV, $|\eta| < 2.0$, $m_J > 40$ GeV), the tagging efficiency is about 50% for the signal jets originating from electroweakino decays,[9] while the background rejection is typically about 10 (40) at $p_{\mathrm{T}} = 200(1000)$ GeV per jet in $Z(\to \nu\nu) +$ jets events.

The $Z_{bb}(h_{bb})$ tagging is applied to large-R jets containing exactly two b jets (denoted by J_{bb}) by applying a jet mass window cut that selects the peak consistent with $Z(h)$ bosons. The jet mass is corrected by adding the momentum of the highest-p_{T} muon identified inside the large-R jet in order to improve the resolution of the mass peak. The $Z_{bb}(h_{bb})$ tagging requires the jet mass to satisfy $70(100)\ \mathrm{GeV} < m_J < 100(135)\ \mathrm{GeV}$. The performance of the Z_{bb}-and h_{bb} tagging is summarized in Figs. 4(c) and 4(d).

The analysis also uses reconstructed electrons and muons (collectively referred to as "leptons"), as well as photons and small-radius (small-R) jets, for kinematic selection, validation of the background estimation, and the $E_{\mathrm{T}}^{\mathrm{miss}}$ computation. Electron candidates are reconstructed from energy clusters that are consistent with electromagnetic showers in the ECAL and are matched to tracks in the ID, which are calibrated *in situ* using $Z \to ee$ samples [141]. Muon candidates in the detector are typically reconstructed by matching tracks in the MS to tracks in the ID, and they are calibrated *in situ* using $Z \to \mu\mu$ and $J/\psi \to \mu\mu$ samples [142]. Small-R jet candidates are reconstructed from particle-flow objects [143] calibrated at the electromagnetic scale using the anti-k_t algorithm with a radius parameter of $R = 0.4$. After subtracting the expected energy contribution from pileup using the jet area technique [144], the jet energy scale and resolution are corrected to particle level using MC simulation as well as by *in situ* calibration using $Z+$jets, $\gamma+$jets, and multijet events [145]. Photon candidates are reconstructed either as electromagnetic clusters with no matching ID track or as e^+e^- pairs from photon conversions in the ID material [141].

Reconstructed electrons, muons, small-R jets, and photons are subject to two sets of identification criteria: the looser "baseline" criteria and the tighter "signal" criteria. The baseline objects are used for the $E_{\mathrm{T}}^{\mathrm{miss}}$ computation, event cleaning, and the overlap removal procedure that resolves ambiguities between reconstructed objects as described below. Baseline electrons are required to have $p_{\mathrm{T}} > 4.5$ GeV and $|\eta| < 2.47$, and meet the *Loose* criteria of the likelihood-based identification [141]. Baseline muons are required to have $p_{\mathrm{T}} > 3$ GeV and $|\eta| < 2.7$, and to meet the *Medium* identification criteria defined in Ref. [142]. To suppress the contributions from pileup, baseline leptons

[9]The corresponding efficiency for the nominal working point (50% efficiency W/Z tagger in Ref. [137]) is 35–40% for this particular set of preselected jets.

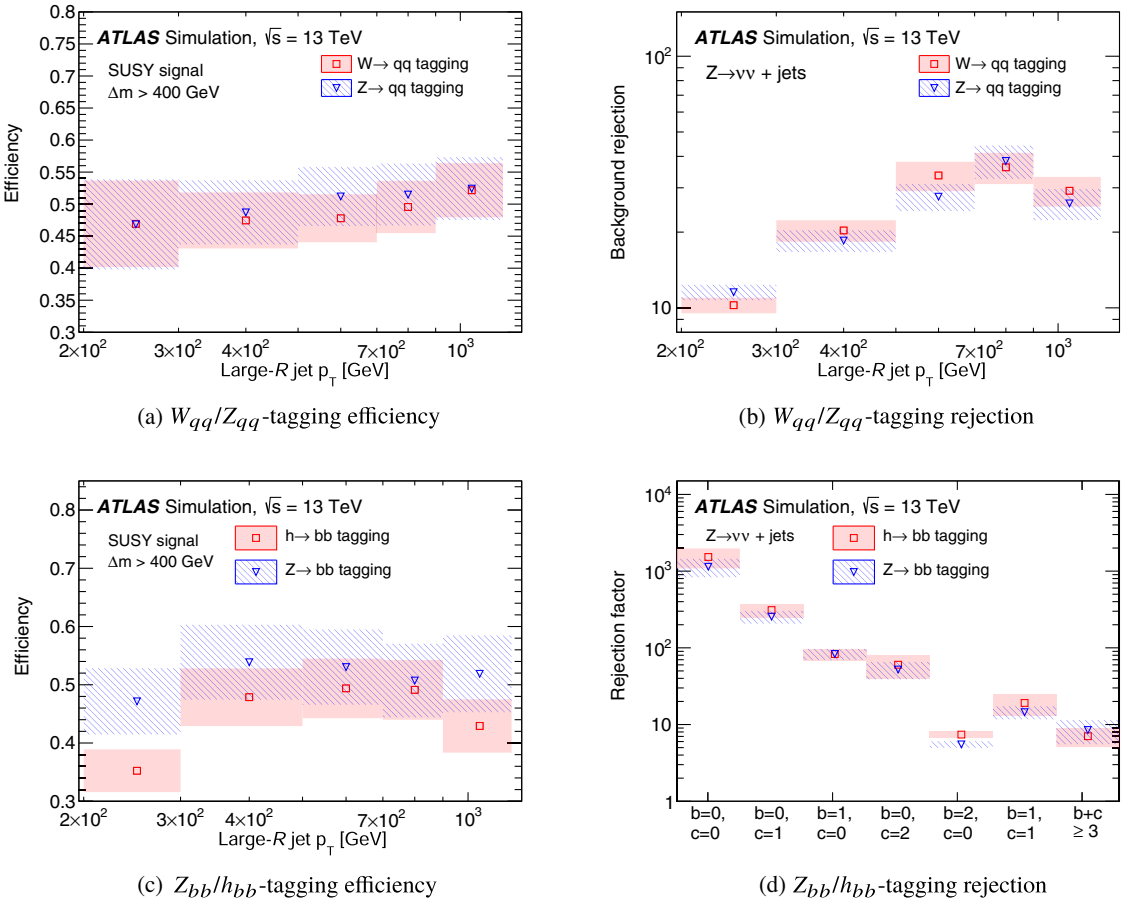

(a) W_{qq}/Z_{qq}-tagging efficiency

(b) W_{qq}/Z_{qq}-tagging rejection

(c) Z_{bb}/h_{bb}-tagging efficiency

(d) Z_{bb}/h_{bb}-tagging rejection

FIG. 4. (a), (c) The boson-tagging efficiency for jets arising from $W/Z/h$ bosons decaying into $q\bar{q}$ or $b\bar{b}$ (signal jets) and (b), (d) the rejection factor (inverse of the efficiency) for jets that have other origins (background jets) are shown. The signal jet efficiency of W_{qq}/Z_{qq} tagging (Z_{bb}/h_{bb} tagging) is evaluated using a sample of preselected large-R jets ($p_{\mathrm{T}} > 200$ GeV, $|\eta| < 2.0$, $m_J > 40$ GeV) in the simulated $(\tilde{W}, \tilde{B})$-SIM signal events with $\Delta m(\tilde{\chi}_{\mathrm{heavy}}, \tilde{\chi}_{\mathrm{light}}) \geq 400$ GeV. The jets are matched with generator-level W/Z (Z/h) bosons within $\Delta R < 1.0$ which decay into $q\bar{q}$ ($b\bar{b}$). The background jet rejection factor is calculated using preselected large-R jets in the sample of simulated $Z(\rightarrow \nu\nu) +$ jets events, dominated by initial-state radiation jets. As in the Z_{bb}/h_{bb} tagging, the rejection factor is shown as a function of the number of b- or c quarks contained in the large-R jet within $\Delta R < 1.0$. The efficiency correction factors are applied to the signal efficiency and background rejection for the W_{qq}/Z_{qq} tagging. The uncertainty is represented by the hashed bands, which includes the MC statistical uncertainty and the systematic uncertainties discussed in Sec. VIII A.

are also required to have a trajectory consistent with the primary vertex, i.e., $|z_0 \sin\theta| < 0.5$ mm.[10] Baseline small-R jets must have $p_{\mathrm{T}} > 30$ GeV and $|\eta| < 4.5$. Baseline photons must meet the *Tight* identification criteria [141] in addition to satisfying $p_{\mathrm{T}} > 50$ GeV and $|\eta| < 2.4$.

To prevent the reconstruction of a single particle as multiple objects, an overlap removal procedure is applied to the baseline leptons, photons, and jets in the following order. Any electron sharing an ID track with a muon or other electrons is removed, such that only the highest-p_{T} electron is kept when multiple electrons share the same ID track. Photons around the remaining electrons and muons are removed if the photon-lepton separation is $\Delta R < 0.4$. Next, small-R jets are removed if they are $\Delta R < 0.2$ from a remaining electron or photon, or are $\Delta R < 0.4$ from a muon and the jet has fewer than three associated tracks with $p_{\mathrm{T}} > 500$ MeV. Leptons (photons) are removed if they are separated from a remaining small-R jet by $\Delta R < \min(0.4, 0.04 + 10\ \mathrm{GeV}/p_{\mathrm{T},\ell})$ ($\Delta R < 0.4$). Finally, large-R jets are removed if they are separated by $\Delta R < 1.0$ from any remaining electrons.

The missing transverse momentum, with magnitude $E_{\mathrm{T}}^{\mathrm{miss}}$, is calculated as the negative vectorial sum of the transverse momenta of all baseline leptons, photons and small-R jets calibrated to their respective energy scales, and an additional

[10]The transverse impact parameter, d_0, is defined as the distance of closest approach in the transverse plane between a track and the beam line. The longitudinal impact parameter, z_0, corresponds to the z-coordinate distance between the point along the track at which the transverse impact parameter is defined and the primary vertex.

"soft term" constructed from tracks originating from the primary vertex but not associated with any of the baseline objects [146].

Signal objects are defined by applying additional stringent criteria in event selections to ensure a high selection purity. Signal leptons and photons are used only for validating the background estimation. Signal electrons and muons must satisfy $p_{\mathrm{T}} > 10$ GeV. Additionally, the *Tight* identification criteria are imposed for signal electrons. To reduce the contribution from nonprompt decays of heavy-flavor hadrons, the significance of the transverse impact parameter is required to satisfy $|d_0/\sigma(d_0)| < 5(3)$ for signal electrons (muons). An isolation selection is imposed to further suppress the residual misidentified leptons originating from jets. The *Tight* (*HighPtCaloOnly*) working point defined in Ref. [141] is used for signal electrons with $p_{\mathrm{T}} <$ 200 GeV ($p_{\mathrm{T}} > 200$ GeV), and the *Tight* working point defined in Ref. [142] is applied for signal muons. Signal small-R jets are selected within $|\eta| < 2.8$, and those with $p_{\mathrm{T}} < 120$ GeV and $|\eta| < 2.5$ must satisfy the *Tight* quality criteria of the track-based jet vertex tagger [144,147] in order to suppress jets originating from pileup. Signal photons are defined as baseline photons with $p_{\mathrm{T}} > 200$ GeV.

VI. EVENT SELECTION

A. Common preselection

As described below, a common preselection is used when defining the signal regions (SRs), as well as the control regions (CRs) and validation regions (VRs) used for background estimation.

After the trigger requirement discussed in Sec. IV A, both the data and MC events are required to have at least one reconstructed vertex that is associated with two or more tracks with $p_{\mathrm{T}} > 500$ MeV. The primary vertex of each event is selected as the vertex with the largest $\sum p_{\mathrm{T}}^2$ of associated tracks [148].

A set of event cleaning criteria are applied to ensure the quality of the measurements as well as to veto noncollision backgrounds. Events with baseline muons consistent with cosmic muons ($|z_0| > 1$ mm or $|d_0| > 0.2$ mm) are removed. To avoid pathological $E_{\mathrm{T}}^{\mathrm{miss}}$ reconstruction, events are also vetoed if any baseline jet points to a module of the tile hadronic calorimeter that was not operational during the data taking, or if any baseline muon suffers from a poor momentum measurement [$\sigma(q/p)/(q/p) > 0.4$ where q/p is the measured charge divided by momentum and $\sigma(q/p)$ is its uncertainty]. Track jets can overlap due to their p_{T}-dependent variable radius. To avoid the ambiguous cases of concentric jets, events with a track jet overlapping with another track jet are removed. An overlap is defined by $\Delta R < R_{\mathrm{min}}$ where ΔR is the angular distance between a given pair of track jets and R_{min} is the smaller of their radii.

Beam-induced background is one of the major noncollision backgrounds. Particles (typically muons) generated by interactions between the beam and the upstream collimators may directly hit the detector material. Particular care is needed for this background since it can cause high-energy jetlike signatures and, correspondingly, large spurious $E_{\mathrm{T}}^{\mathrm{miss}}$ [149]. Events with baseline jets failing the *Loose* cleaning [150] are removed. Further cleaning is applied to events with no baseline leptons and photons by requiring consistency between the $E_{\mathrm{T}}^{\mathrm{miss}}$ and the alternative $E_{T,\mathrm{track}}^{\mathrm{miss}}$, which is computed using only the good-quality ID tracks associated with the primary vertex. While those events satisfy $E_{\mathrm{T}}^{\mathrm{miss}} >$ 200 GeV due to the trigger requirements, $E_{T,\mathrm{track}}^{\mathrm{miss}} > 75$ GeV and $\Delta\phi(E_{\mathrm{T}}^{\mathrm{miss}}, E_{T,\mathrm{track}}^{\mathrm{miss}}) < 2.0$ are required in the cleaning procedure.

Finally, events are required to contain at least two large-R jets. Events with three or more large-R jets are not vetoed in the analysis, in order to be as inclusive as possible in model coverage; however, the applied event selection is always based on the two highest-p_{T} large-R jets.

B. Signal region selection

After the preselection, events with no baseline leptons are selected. Two orthogonal signal region categories, 4Q and 2B2Q, based on the absence or presence of a large-R jet containing exactly two b-tagged track jets (J_{bb}) are defined in order to target the $qqqq$ and $bbqq$ final states, respectively.

Boson tagging is required for the two leading large-R jets. The two leading large-R jets must pass the V_{qq} tagging ($n(V_{qq}) = 2$) in SR-4Q. On the other hand, SR-2B2Q requires J_{bb} to satisfy the Z_{bb}- or h_{bb} tagging, while the other jet (denoted by J_{qq}) must satisfy the V_{qq}-tagging criteria. Multiple SRs are defined in each SR category to target the different final states of the signal processes.

TABLE II. Definition of each SR in the 4Q and 2B2Q categories, where $n(W_{qq})$, $n(Z_{qq})$, $n(V_{qq})$, $n(Z_{bb})$, and $n(h_{bb})$ are, respectively, the number of large-R jets passing the W_{qq}-, Z_{qq}-, V_{qq}-, Z_{bb}-, and h_{bb} tagging of the two leading large-R jets. SR-4Q-WZ requires $n(W_{qq}), n(Z_{qq}) \geq 1$ instead of $n(W_{qq}) = n(Z_{qq}) = 1$ because the selections in W_{qq}-and Z_{qq} tagging are not exclusive. The overlap and the segmentation between the SRs are illustrated in Fig. 5.

	$n(W_{qq})$	$n(Z_{qq})$	$n(V_{qq})$	$n(Z_{bb})$	$n(h_{bb})$
4Q-WW	$= 2$	$\cdots$	$= 2$	$= 0$	$= 0$
4Q-WZ	≥ 1	≥ 1	$= 2$	$= 0$	$= 0$
4Q-ZZ	$\cdots$	$= 2$	$= 2$	$= 0$	$= 0$
4Q-VV	$\cdots$	$\cdots$	$= 2$	$= 0$	$= 0$
2B2Q-WZ	$= 1$	$\cdots$	$= 1$	$= 1$	$= 0$
2B2Q-ZZ	$\cdots$	$= 1$	$= 1$	$= 1$	$= 0$
2B2Q-Wh	$= 1$	$\cdots$	$= 1$	$= 0$	$= 1$
2B2Q-Zh	$\cdots$	$= 1$	$= 1$	$= 0$	$= 1$
2B2Q-VZ	$\cdots$	$\cdots$	$= 1$	$= 1$	$= 0$
2B2Q-Vh	$\cdots$	$\cdots$	$= 1$	$= 0$	$= 1$

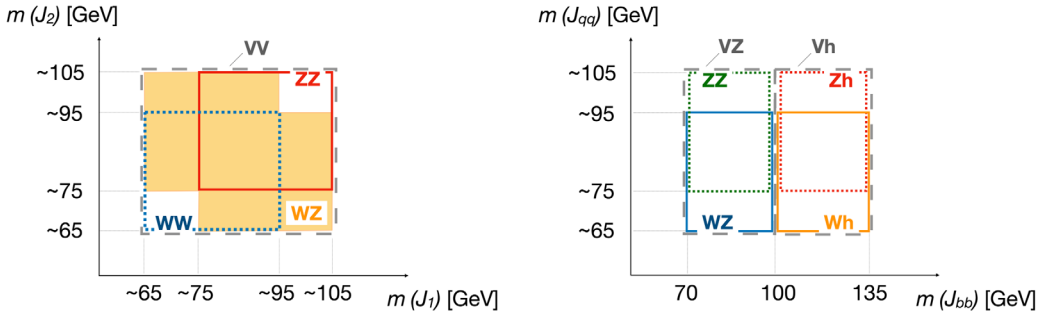

(a) SR-4Q (b) SR-2B2Q

FIG. 5. The SR segmentation illustrated as a function of the masses of the two leading large-R jets. (a) In SR-4Q, both jets are required to pass the W_{qq}-or Z_{qq} tagging. (b) In SR-2B2Q, one of the two jets is required to contain exactly two b-tagged track jets (J_{bb}) while the other (J_{qq}) has at most one. The mass of J_{bb} is required to be consistent with a Z boson (70–100 GeV) or an h boson (100–135 GeV), while J_{qq} is required to pass the W_{qq}-or Z_{qq} tagging. The mass window cuts of the W_{qq}/Z_{qq} tagging shown in the plot only indicate the typical values, while variable cut values along p_{T} are applied in the analysis. The inclusive SRs, defined by the logical union of a few mutually overlapping SRs, are indicated by the gray dashed lines.

The WW(ZZ) region in SR-4Q requires both leading large-R jets to pass the $W_{qq}(Z_{qq})$ tagging, while the WZ region is defined to contain events with at least one W_{qq}-tagged jet and at least one Z_{qq}-tagged jet. The inclusive bin VV, the logical union of WW, WZ, and ZZ, is designed to cover the signals that can have various $\tilde{\chi}_{\mathrm{heavy}}$ branching ratios into W relative to Z. Similarly, the 2B2Q category accommodates the WZ/ZZ/Wh/Zh region, which varies by W_{qq}-versus Z_{qq} tagging or Z_{bb}-versus h_{bb} tagging. The VZ (Vh) region serves as the inclusive SR defined by the logical union of WZ and ZZ (Wh and Zh). The SR segmentation is summarized in Table II and illustrated schematically in Fig. 5. In total, four and six SRs are defined in SR-4Q and SR-2B2Q, respectively. SR-4QXX, SR-2B2QXZ, and SR-2B2QXh (where X = W/Z/V) are mutually orthogonal, and are statistically combined according to the models considered in Table I.

Finally, a series of background rejection cuts are applied to further suppress the main SM backgrounds at this stage: $Z(\to\nu\nu)+\mathrm{jets}$, $W(\to\ell\nu)+\mathrm{jets}$, and $t\bar{t}$. To reject backgrounds including top quarks, the b jets that do not originate from boosted boson candidates are vetoed. This is done by requiring $n_{b\text{-jet}}^{\mathrm{unmatched}}=0$, where $n_{b\text{-jet}}^{\mathrm{unmatched}}$ denotes the number of b-tagged track jets that are not matched with any of the two leading large-R jets by the $\Delta R<1.0$ criterion. For the 4Q category, the total number of b-tagged track jets in the event ($n_{b\text{-jet}}$) must be less than two in order to further suppress the $t\bar{t}$ background. The effective mass variable, m_{eff}, defined as the scalar sum of the p_{T} of the two leading large-R jets and $E_{\mathrm{T}}^{\mathrm{miss}}$, is used to select events with hard kinematics together with $E_{\mathrm{T}}^{\mathrm{miss}}$. Selections of $E_{\mathrm{T}}^{\mathrm{miss}}>300(200)$ GeV and $m_{\mathrm{eff}}>1300(1000)$ GeV are applied in the 4Q (2B2Q) regions. Event shape information is also useful in distinguishing the signals from the backgrounds. Signal events have a relatively spherical shape, where the jets tend to be isolated from $E_{\mathrm{T}}^{\mathrm{miss}}$, indicating that the heavy electroweakinos are produced nearly at rest. Background events, meanwhile, have a higher chance of containing a jet aligned with a W/Z boson, due to boosted top decays in $t\bar{t}$ events or the emission of collinear radiation in $Z+\mathrm{jets}$ and $W+\mathrm{jets}$ events. The minimum azimuthal angle separation between $E_{\mathrm{T}}^{\mathrm{miss}}$ and any signal small-R jets must satisfy $\min\Delta\phi(E_{\mathrm{T}}^{\mathrm{miss}},j)>1.0$ for both SR categories. The use of small-R jets is motivated by the need to effectively identify low-p_{T} jets and it also provides better resolution in terms of jet alignment with $E_{\mathrm{T}}^{\mathrm{miss}}$. In 2B2Q, the stransverse mass variable m_{T2} [151,152] is also used, constructed by assigning each of the two leading large-R jets to the visible particle legs. A selection of $m_{\mathrm{T2}}>250$ GeV is found to effectively suppress the SM backgrounds, particularly $t\bar{t}$ which exhibits a kinematic cutoff at $m_{\mathrm{T2}}\sim200$ GeV, driven by the top-quark mass constraint.[11]

The cut values of the kinematic selection are equivalent within the SR-4Q and SR-2B2Q categories. The selection criteria that define the SR-4Q, SR-2B2Q-Wh, and SR-2B2Q-Vh regions are obtained by optimizing the sensitivity to the $(\tilde{W},\tilde{B})$ model with $(m(\tilde{\chi}_1^{\pm}),m(\tilde{\chi}_1^0))\approx(800,100)$ GeV, while those for SR-2B2Q-WZ, SR-2B2Q-ZZ, and SR-2B2Q-VZ are determined by optimizing the sensitivity to the $(\tilde{H},\tilde{G})$ model with $m_{\tilde{\chi}_1^0}\approx800$ GeV. The discovery significance is used as the metric of sensitivity. The obtained cuts are also found to be nearly optimal for the other signal models.

The acceptance times efficiency for signal events ranges from 1 to 4% depending on $\Delta m(\tilde{\chi}_{\mathrm{heavy}},\tilde{\chi}_{\mathrm{light}})$ and the SR. For example, it is about 1–2% (1.5%) in SR-4Q-VV (SR-2B2Q-Vh) for the C1N2-WZ (C1N2-Wh) signals with $\Delta m(\tilde{\chi}_{\mathrm{heavy}},\tilde{\chi}_{\mathrm{light}})=600$ GeV, and 3–4% (2–3%) with $\Delta m(\tilde{\chi}_{\mathrm{heavy}},\tilde{\chi}_{\mathrm{light}})=1$ TeV.

[11]The hypothetical missing-particle mass is set to 100 GeV and this offset is subtracted from the calculated m_{T2}, although the dependency on the choice of missing-particle mass is very small.

TABLE III. Summary of selections for the SRs, CRs, and VRs. $n(V_{qq})$ ($n(!V_{qq})$) represents the number of large-R jets passing (failing) the V_{qq} tagging of the two highest-p_{T} large-R jets. The same selection is applied to the SR (VR) and CR in the same category except for the V_{qq} tagging and some kinematic selections that are explicitly indicated in parentheses. The trigger selection and event cleaning described in Sec. V are also applied. VRTTX is a validation region used to validate the $t\bar{t}+X$ modeling as described in Sec. VII A. $p_{\mathrm{T}}(W)$ is the vector sum of the p_{T} of the lepton and $E_{\mathrm{T}}^{\mathrm{miss}}$ in the 1L regions. In the 1L (1Y) regions, $E_{\mathrm{T}}^{\mathrm{miss}}$ is replaced by $p_{\mathrm{T}}(W)$ ($p_{\mathrm{T}}(\gamma)$) when calculating the kinematic variables m_{eff}, $\min\Delta\phi(E_{\mathrm{T}}^{\mathrm{miss}}, j)$ and m_{T2}. Details are given in Sec. VII B.

	SR(CR0L)		VR(CR)1L		VR(CR)1Y		
	4Q	2B2Q	4Q	2B2Q	4Q	2B2Q	VRTTX
$n_{\text{Large-}R\text{ jets}}$	≥ 2		≥ 2		≥ 2		$=1$
n_{lepton}	$=0$		$=1$		$=0$		$=3$
$p_{\mathrm{T}}(\ell_1)$ [GeV]	⋯		>30		⋯		>30
n_{photon}	⋯		⋯		$=1$		⋯
$n(V_{qq})$	$=2(=1)$	$=1(=0)$	$=2(=1)$	$=1(=0)$	$=2(=1)$	$=1(=0)$	⋯
$n(!V_{qq})$	$=0(=1)$	$=0(=1)$	$=0(=1)$	$=0(=1)$	$=0(=1)$	$=0(=1)$	⋯
$n(J_{bb})$	$=0$	$=1$	$=0$	$=1$	$=0$	$=1$	$=1$
$m(J_{bb})$ [GeV]	⋯	$\in[70, 135(150)]$	⋯	$\in[70, 150]$	⋯	$\in[70, 150]$	⋯
$n_{b\text{-jet}}^{\text{unmatched}}$	$=0$		$=0$		$=0$		⋯
$n_{b\text{-jet}}$	≤ 1	⋯	$=0$	⋯	≤ 1	⋯	⋯
$E_{\mathrm{T}}^{\mathrm{miss}}$	>300	>200	>50		<200		⋯
$p_{\mathrm{T}}(W)$	⋯		>200		⋯		⋯
$p_{\mathrm{T}}(\gamma)$	⋯		⋯		>200		⋯
m_{eff}	>1300	$>1000(>900)$	>1000	>900	>1000	>900	⋯
$\min\Delta\phi(E_{\mathrm{T}}^{\mathrm{miss}}, j)$	>1.0		>1.0		>1.0		⋯
m_{T2}	⋯	>250	⋯	>250	⋯	>250	⋯

VII. BACKGROUND ESTIMATION

The main SM background process in the SRs is $Z(\to\nu\nu)+\text{jets}$ (∼50%), followed by $W(\to\ell\nu)+\text{jets}$ (15–20%), and VV (10–20%). The rest consists of VVV events in SR-4Q (5–10%), or $t\bar{t}$, single-top and $t\bar{t}+X$ events in SR-2B2Q (10–20%).

The estimation strategy varies between the "reducible" and "irreducible" backgrounds. The irreducible backgrounds in this search are due to SM events including at least two hadronic $W/Z/h$ decays and large $E_{\mathrm{T}}^{\mathrm{miss}}$ from high-p_{T} neutrinos. These consist of VVV and $t\bar{t}+X$, and are estimated using MC simulation. The contributions from fully hadronic VV and $t\bar{t}$ are negligible due to the stringent $E_{\mathrm{T}}^{\mathrm{miss}}$ requirement.

The reducible backgrounds are all that remain, including the dominant $Z(\to\nu\nu)+\text{jets}$ production. These backgrounds are characterized by the presence of at least one large-R jet that originates from a process other than a $W/Z\to qq$ decay and is referred to as a "fake boson jet." The fake boson jets are typically caused by two collimated high-p_{T} initial-state radiation (ISR) jets that are clustered together as a single large-R jet. A partly data-driven method is used to estimate the reducible backgrounds; a control region (CR0L)[12] is defined in the phase space adjacent to a SR, where the MC sample is normalized to the CR data. The SR expectation is obtained using the normalized MC sample, assuming the modeling of the SR/CR0L yield ratio ("0L transfer factor") is reliable. This assumption is tested in a number of VRs in data. A CR0L is defined for each 4Q and 2B2Q category by reversing the V_{qq}-tagging requirement on one of the two leading large-R jets in the SR, and is denoted by CR0L-4Q and CR0L-2B2Q, respectively. The multijet and noncollision background contributions are found to be negligible using the data-driven methods or from the estimation in a similar phase space carried out in Ref. [153].

The following subsections discuss the methodology and results of the irreducible and reducible background estimations.

A. Irreducible background estimation

The VVV ($t\bar{t}+X$) events account for at most 10% of the total background in SR-4Q (SR-2B2Q), and are negligible in SR-2B2Q (SR-4Q). Given their minor contribution, these backgrounds are estimated directly from the MC predictions and assigned conservative uncertainties.

The dominant $t\bar{t}+X$ component in SR-2B2Q is $t\bar{t}(\to bqqbqq)+Z(\to\nu\nu)$. To validate the MC modeling, a dedicated validation region VRTTX is defined in a three-lepton region populated by $t\bar{t}(\to b\ell\nu bqq)+Z(\to\ell\ell)$. The selections are summarized in Table III. Exactly three baseline and signal leptons are required, with the leading

[12]"0L" stands for regions with no baseline leptons.

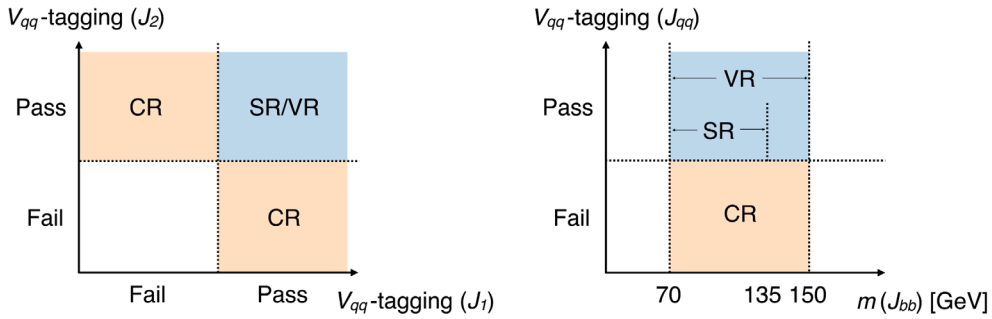

(a) 4Q (b) 2B2Q

FIG. 6. Schematics illustrating the relation between the SRs, VRs, and CRs in the (a) 4Q and (b) 2B2Q categories. A CR is constructed by inverting the V_{qq}-tagging requirement for one of the two leading large-R jets in the corresponding SR (VR). In 2B2Q, the J_{bb} mass window cut in the CRs and VRs is loosened. See Table III for details.

lepton of $p_{\mathrm{T}} > 30$ GeV firing the single-lepton trigger. At least one large-R jet is required in the event, and it must contain exactly two b-tagged track jets. No further kinematic cuts are applied, in order to maintain a sufficient data sample size in the region. The $t\bar{t} + X$ purity in this region is about 70%. Sixty-eight data events are observed in VRTTX, while 46.5 events are predicted by MC simulation (31.5 from $t\bar{t} + X$, 12.1 from VV, and 2.9 from the others). A 70% uncertainty is therefore assigned to the $t\bar{t} + X$ normalization to fully cover the observed discrepancy; this has only a small impact on the total background estimation, given the minor contribution in the SRs.

The VVV contribution to SR-4Q is mainly from $VV(\to qqqq) + Z(\to \nu\nu)$ processes. The VVV process has only recently been observed at the LHC [154,155]. As the data sample size in that phase-space region is insufficient and loosening the selection leads to poor VVV purity, no control or validation regions were designed and this background is estimated directly from the MC prediction. A 50% uncertainty is assigned for the normalization based on the precision of the WWZ production cross-section measurement performed by the CMS experiment [155].

B. Reducible background estimation

The CR0L-4Q is defined by the same selection as SR-4Q-VV except that one of the two leading large-R jets must fail the V_{qq}-tagging, and the CR0L-2B2Q is constructed as the logical union of SR-2B2Q-VZ and SR-2B2Q-Vh with the J_{qq} failing the V_{qq} tagging. For the reducible backgrounds, the extrapolation from a CR0L to the SR is mainly characterized by the V_{qq}-tagging response for a fake boson jet. In order to maintain a sufficient data sample size and to suppress signal contamination, the m_{eff} selection and the J_{bb} mass window cut for CR0L-2B2Q are loosened relative to the SR, from $m_{\mathrm{eff}} > 1000$ GeV to $m_{\mathrm{eff}} > 900$ GeV and from $70 < m(J_{bb}) < 135$ GeV to $70 < m(J_{bb}) < 150$ GeV. The signal contamination in CR0L-4Q and CR0L-2B2Q is evaluated using the $(\tilde{W}, \tilde{B})$-SIM and $(\tilde{H}, \tilde{G})$ samples. While a contribution of up to 15% (24%) of the expected backgrounds in CR0L-4Q (CR0L-2B2Q) can be caused by the nonexcluded signals, the introduced bias in the estimate is still smaller than the total uncertainty in the SRs and VRs, and therefore has only a small impact on the final sensitivity. The selections are summarized in Table III, and the relation with the SR is illustrated in Fig. 6.

One advantage of this CR0L definition is that all physics processes contributing to the background ($Z +$ jets, $W +$ jets, $t\bar{t}$, etc.) have comparable 0L transfer factors. This is because the fake boson jets have similar origins and kinematics, and therefore the same boson tagging efficiency, confirmed by the simulation. Consequently, they can be treated as a single combined component with a common normalization factor assigned to correct their normalizations at once. The normalization is performed in 4Q and 2B2Q separately with an independent normalization factor, based on the "background-only fits" described in Sec. IX A.

Good MC modeling of the 0L transfer factor is essential for the estimation. Data events with exactly one lepton or one photon are utilized for the validation. This is motivated by the fact that in these regions the main backgrounds, $Z(\to \nu\nu) +$ jets in SR/CR0L, $W(\to \ell\nu) +$ jets in the one-lepton region and $\gamma +$ jets in the one-photon region, have similar ISR jet kinematics and, relative to the minor backgrounds, contribute similarly to the respective regions when a compatible kinematic phase space is chosen. The one-lepton (one-photon) regions corresponding to CR0L and the SR are constructed, denoted by CR1L(1Y) and VR1L(1Y), respectively. The level of data-vs-MC agreement in the ratio VR1L(1Y)/CR1L(1Y) ["1L(1Y) transfer factor"] is validated as a proxy for the MC modeling of the 0L transfer factor.

The selections applied for VR(CR)1L and VR(CR)1Y are listed in Table III. The VR(CR)1L is defined by requiring exactly one baseline lepton and a signal lepton with $p_{\mathrm{T}} > 30$ GeV that fires the single-lepton trigger. In addition, $E_{\mathrm{T}}^{\mathrm{miss}} > 50$ GeV is required to suppress contributions from

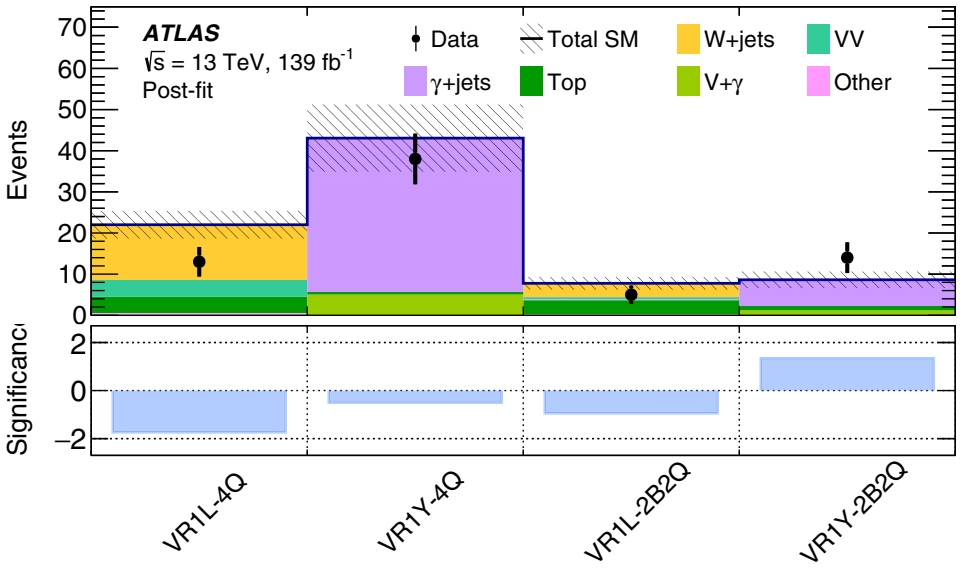

FIG. 7. Comparison between the observed data and the postfit SM background prediction in VR1L and VR1Y. The background predictions are obtained using the background-only fit described in Sec. IX A. "Top" includes $t\bar{t}$, $t + X$, and $t\bar{t} + X$ production. The total systematic uncertainty of the background prediction is shown by the hatched band. The bottom panel shows the statistical significance of the discrepancy between the observed number of events and the SM expectation, following the prescription described in Ref. [158].

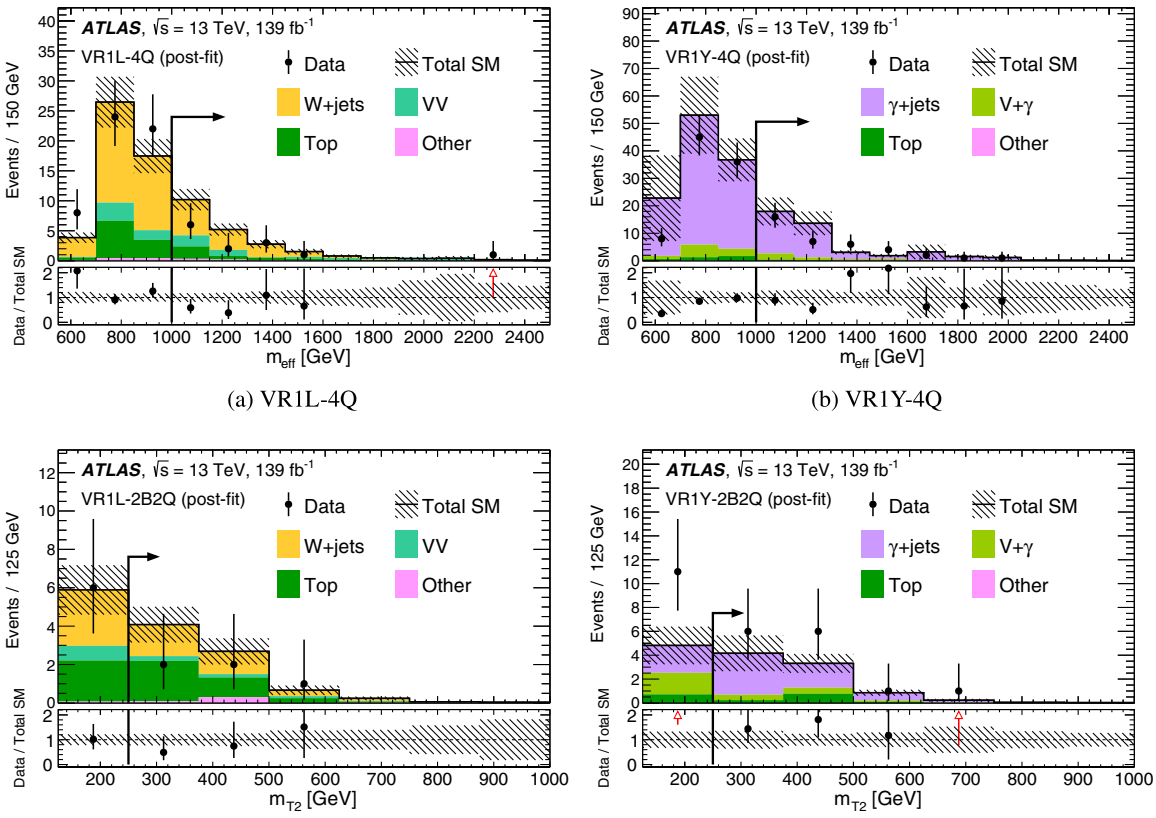

(a) VR1L-4Q (b) VR1Y-4Q

(c) VR1L-2B2Q (d) VR1Y-2B2Q

FIG. 8. m_{eff} distributions in VR1L-4Q/VR1Y-4Q and m_{T2} distributions in VR1L-2B2Q/VR1Y-2B2Q. The postfit SM background expectation using the background-only fit is shown in a histogram stack. "Top" includes $t\bar{t}$, $t + X$, and $t\bar{t} + X$ production. The hatched bands indicate the combined statistical and systematic uncertainty of the background. The bottom panels show the ratio of the observed data to the background expectation. The selection criterion for the variable shown by each plot is removed, while the arrow indicates the cut value used to define the region.

QCD multijet events with poorly measured $E_{\mathrm{T}}^{\mathrm{miss}}$. The VR (CR)1Y requires exactly one baseline and signal photon to fire the single-photon trigger, and vetoes events with at least one baseline lepton. For both VR(CR)1L and VR(CR)1Y, at least two large-R jets are required, and the events are separated into the 4Q and 2B2Q categories, based on the absence or presence of J_{bb}, respectively A b-jet veto strategy similar to that for the SRs and the CR0L bins is applied: $n_{b\text{-jet}}^{\mathrm{unmatched}} = 0$ in all the regions, $n_{b\text{-jet}} \leq 1$ in the 4Q regions. A stricter veto of $n_{b\text{-jet}} = 0$ is applied in CR(VR)1L-4Q to suppress the large single-top contribution relative to the other 4Q regions.

The kinematic selection in the 1L (1Y) regions is applied with $E_{\mathrm{T}}^{\mathrm{miss}}$ replaced by $p_{\mathrm{T}}(W)$ ($p_{\mathrm{T}}(\gamma)$) in the variables. This is to ensure that compatible phase spaces are probed for $Z(\to \nu\nu) + \mathrm{jets}$ in SR/CR0L, $W(\to \ell\nu) + \mathrm{jets}$ in VR1L/CR1L, and $\gamma + \mathrm{jets}$ in VR1Y/CR1Y, since $E_{\mathrm{T}}^{\mathrm{miss}}$ in $Z(\to \nu\nu) + \mathrm{jets}$ events typically represents the p_{T} of the Z boson. The $p_{\mathrm{T}}(W)$ variable is defined as the vector sum of the p_{T} of the lepton and $E_{\mathrm{T}}^{\mathrm{miss}}$ in the 1L regions. The $E_{\mathrm{T}}^{\mathrm{miss}}$, $p_{\mathrm{T}}(W)$, and $p_{\mathrm{T}}(\gamma)$ are collectively denoted by $p_{\mathrm{T}}(V)$.

TABLE IV. Number of observed data events and the postfit SM background prediction in the VR1L (1Y) bins and the corresponding CR1L (1Y) bins. Negligibly small contributions are indicated by "dots." Within each CR the reducible backgrounds have the same relative uncertainty in their expected yield because a common normalization factor is assigned to all of them in the fit.

Region	CR1L-4Q	VR1L-4Q	CR1L-2B2Q	VR1L-2B2Q
Observed	439	13	96	5
Post-fit	439 ± 21	22.0 ± 3.4	96 ± 10	7.8 ± 1.5
$W + \mathrm{jets}$	325 ± 16	13.4 ± 2.2	48 ± 5	3.4 ± 0.7
$Z + \mathrm{jets}$	4.45 ± 0.21	0.198 ± 0.035	0.58 ± 0.06	0.044 ± 0.012
$\gamma + \mathrm{jets}$	<1	…	0.57 ± 0.06	0.22 ± 0.10
VV	65.4 ± 3.1	4.1 ± 0.8	6.9 ± 0.7	0.55 ± 0.15
$V\gamma$	<1	…	< 0.1	…
VVV	1.3 ± 0.6	0.52 ± 0.28	0.14 ± 0.08	0.09 ± 0.05
$t\bar{t}$	30.4 ± 1.5	2.7 ± 0.4	24.0 ± 2.5	1.8 ± 0.4
$t + X$	11.0 ± 0.5	0.91 ± 0.21	13.2 ± 1.4	1.27 ± 0.34
$t\bar{t} + X$	1.5 ± 1.2	0.16 ± 0.12	1.5 ± 1.1	0.4 ± 0.4
Vh	< 0.1	< 0.001	0.69 ± 0.07	0.046 ± 0.009

Region	CR1Y-4Q	VR1Y-4Q	CR1Y-2B2Q	VR1Y-2B2Q
Observed	1001	38	127	14
Postfit	1001 ± 32	43 ± 8	127 ± 11	8.6 ± 2.0
$W + \mathrm{jets}$	2.59 ± 0.08	< 0.1	< 0.1	…
$Z + \mathrm{jets}$	<1	…	< 0.01	…
$\gamma + \mathrm{jets}$	856 ± 28	37 ± 7	107 ± 11	6.4 ± 1.6
VV	<1	…	…	…
$V\gamma$	131 ± 4	5.0 ± 0.9	12.6 ± 1.3	1.13 ± 0.27
VVV	< 0.1	< 0.01	…	…
$t\bar{t}$	1.28 ± 0.04	…	0.57 ± 0.06	0.28 ± 0.18
$t + X$	<1	…	< 0.1	…
$t\bar{t} + X$	9 ± 6	0.6 ± 0.5	7 ± 5	0.8 ± 0.6
Vh	< 0.001	…	< 0.01	…

The $\min \Delta\phi(E_{\mathrm{T}}^{\mathrm{miss}}, j)$ variable, as well as those analogously derived from $p_{\mathrm{T}}(W)$ and $p_{\mathrm{T}}(\gamma)$, are collectively denoted by $\min \Delta\phi(V, j)$. The cuts in $p_{\mathrm{T}}(V)$ and m_{eff} are moderately loosened relative to the SRs to ensure a data sample size sufficient for the validation. For 2B2Q regions, the J_{bb} mass window cut for the Z_{bb}/h_{bb} tagging is loosened to $70 < m_J < 150$ GeV to match CR0L-2B2Q, further increasing the data sample size. The contributions from events containing fake leptons and fake photons are estimated by data-driven methods [156,157] and are found to be negligible.

The same estimation procedure used to estimate the backgrounds in the SRs is employed to predict the backgrounds in the VRs. A background-only fit, described in Sec. IX A, is performed, where the sum of the reducible backgrounds in MC samples is normalized to the data in each CR1L (CR1Y). The modeling of the transfer factor is examined using the level of agreement between the data and the postfit background expectation in the corresponding VR1L (VR1Y). Four sets of fits are performed in the 1L-4Q, 1L-2B2Q, 1Y-4Q, and 1Y-2B2Q categories separately. Including all the systematic uncertainties discussed in Sec. VIII, the observed data event yields and the postfit background expectations in the VRs are summarized in Table IV, and compared graphically in Fig. 7. The distributions of m_{eff} in VR1L(1Y)-4Q and m_{T2} in VR1L(1Y)-2B2Q are shown in Fig. 8. The data agree reasonably well with the estimated backgrounds across the VRs. The largest disagreement is found in VR1L-4Q, corresponding to a statistical significance of 1.8σ.

VIII. SYSTEMATIC UNCERTAINTIES

Uncertainties in the expected signal and background yields account for the statistical uncertainties of the MC samples, the experimental systematic uncertainties associated with the detector measurements and reconstruction, and the theoretical systematic uncertainties in the MC simulation modeling. For the signals and irreducible backgrounds, the uncertainties are assigned directly to the event yields. For the reducible backgrounds, however, they are assigned to the SR(VR)/CR ratio ("transfer factor," TF) as a consequence of the normalization performed in the CRs. The reducible backgrounds are also subject to uncertainties due to the limited data sample size in the CRs. Each systematic uncertainty is treated as fully correlated across the analysis regions but not across physics processes, unless explicitly stated otherwise. A summary of the background prediction uncertainties is shown in Fig. 9. The postfit values are quoted after a background-only fit described in Sec. IX. The MC statistical uncertainties give the largest contribution to the systematic uncertainty, mainly from the limited size of the $Z(\to \nu\nu) + \mathrm{jets}$ background sample used for the extrapolation. However, this is not a limiting factor for the analysis sensitivity since the total uncertainty in the SRs is dominated by the statistical uncertainty due to the low number of data events in the SRs.

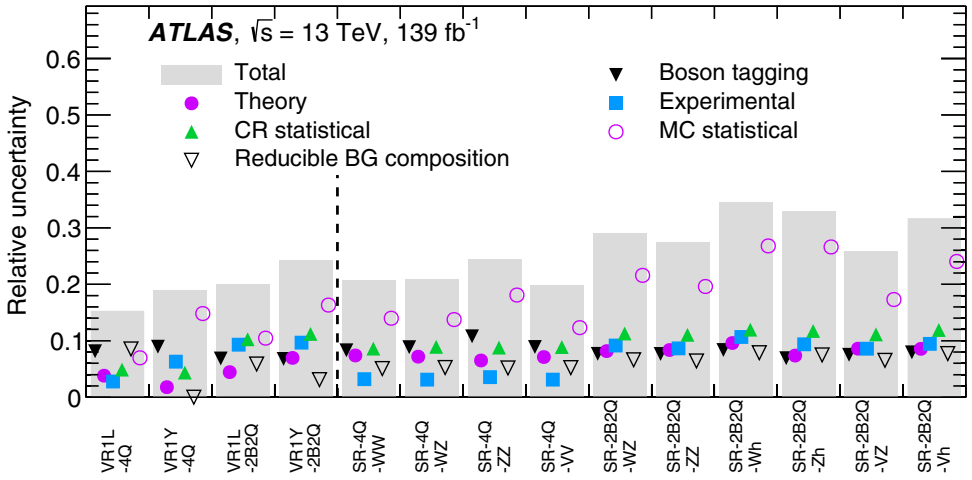

FIG. 9. The total postfit uncertainty and the breakdown in each of the SRs and VRs. "MC statistical" and "CR statistical" present the statistical uncertainty due to the limited sample size either in MC simulation [mainly due to the $Z(\to \nu\nu)$ + jets sample size] or in the CR data, respectively. "Boson tagging" indicates the uncertainty in the $W_{qq}(Z_{qq})$-tagging efficiency, while "experimental" shows the contribution from the rest of the experimental uncertainties. "Reducible BG composition" refers to the uncertainty in the reducible background estimation due to the relative composition uncertainty. "Theory" represents the total uncertainty from all the theoretical uncertainties.

Details of the experimental and theoretical systematic uncertainties are described in the following subsections.

A. Experimental uncertainties

The first class of experimental uncertainties is related to the reconstruction and identification efficiencies for large-R jets, small-R jets, leptons and photons considered in the analysis. These are assigned as uncertainties in the efficiency correction factors applied to the MC samples, which correct for discrepancies between the efficiency predicted by MC simulation and the efficiency in data, as measured using dedicated control samples.

TABLE V. Number of observed data events and the SM backgrounds in the SRs and the CR0L bins. The SM backgrounds are predicted by the background-only fits. Negligible contributions are indicated by "dots." Within each CR the reducible backgrounds have the same relative uncertainty in their expected yield because a common normalization factor is assigned to all of them in the fit.

Region	CR0L-4Q	CR0L-2B2Q	SR-4Q-WW	SR-4Q-WZ	SR-4Q-ZZ	SR-4Q-VV
Observed	129	83	2	3	1	3
Postfit	129 ± 11	83 ± 9	1.9 ± 0.4	3.4 ± 0.7	1.9 ± 0.5	3.9 ± 0.8
W + jets	24.2 ± 2.2	16.6 ± 2.0	0.37 ± 0.08	0.60 ± 0.13	0.26 ± 0.07	0.69 ± 0.15
Z + jets	78 ± 7	44 ± 5	1.0 ± 0.21	1.8 ± 0.4	1.26 ± 0.32	2.1 ± 0.4
VV	21.5 ± 1.9	7.1 ± 0.9	0.35 ± 0.11	0.73 ± 0.24	0.26 ± 0.09	0.79 ± 0.25
VVV	0.9 ± 0.4	0.10 ± 0.05	0.17 ± 0.09	0.19 ± 0.10	0.11 ± 0.07	0.23 ± 0.12
$t\bar{t}$	1.38 ± 0.12	7.8 ± 0.9	0.039 ± 0.009	0.060 ± 0.018	0.025 ± 0.010	0.063 ± 0.018
$t + X$	1.32 ± 0.12	2.87 ± 0.34	0.015 ± 0.006	0.039 ± 0.016	0.012 ± 0.005	0.039 ± 0.016
$t\bar{t} + X$	1.3 ± 0.9	3.7 ± 2.6	…	…	…	…
Other	< 0.1	0.95 ± 0.11	< 0.001	< 0.001	< 0.001	< 0.001

Region	SR-2B2Q-WZ	SR-2B2Q-Wh	SR-2B2Q-ZZ	SR-2B2Q-Zh	SR-2B2Q-VZ	SR-2B2Q-Vh
Observed	2	0	2	1	2	1
Postfit	1.6 ± 0.4	1.9 ± 0.7	1.7 ± 0.5	1.6 ± 0.5	2.2 ± 0.6	2.5 ± 0.8
W + jets	0.11 ± 0.06	0.24 ± 0.09	0.23 ± 0.08	0.26 ± 0.10	0.26 ± 0.09	0.26 ± 0.09
Z + jets	0.84 ± 0.27	1.3 ± 0.5	0.78 ± 0.23	0.66 ± 0.24	1.15 ± 0.33	1.4 ± 0.5
VV	0.33 ± 0.11	0.09 ± 0.03	0.32 ± 0.10	0.085 ± 0.032	0.37 ± 0.11	0.085 ± 0.030
VVV	0.047 ± 0.027	< 0.01	0.051 ± 0.032	0.011 ± 0.007	0.06 ± 0.04	0.011 ± 0.007
$t\bar{t}$	0.016 ± 0.006	0.13 ± 0.04	0.064 ± 0.019	0.40 ± 0.16	0.072 ± 0.021	0.46 ± 0.18
$t + X$	0.11 ± 0.05	0.07 ± 0.04	0.11 ± 0.05	0.041 ± 0.022	0.11 ± 0.05	0.10 ± 0.05
$t\bar{t} + X$	0.10 ± 0.08	$0.07^{+0.10}_{-0.07}$	0.14 ± 0.12	$0.08^{+0.09}_{-0.08}$	0.18 ± 0.14	$0.10^{+0.11}_{-0.10}$
Other	< 0.01	0.03 ± 0.01	< 0.01	0.024 ± 0.008	< 0.01	0.037 ± 0.011

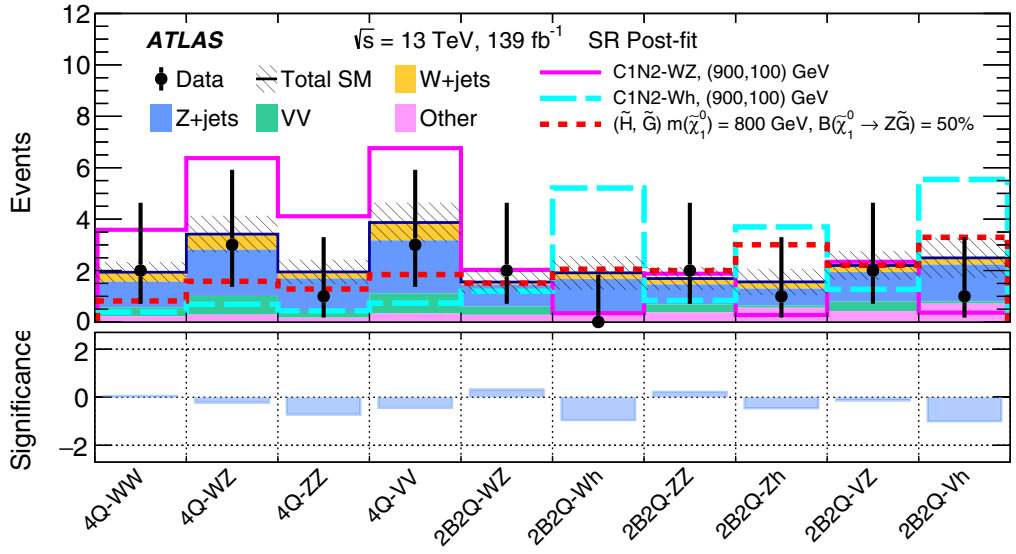

FIG. 10. Summary of the observed data and predicted SM background in all SRs. The background prediction in SR-4Q (SR-2B2Q) is obtained by a background-only fit to CR0L-4Q (CR0L-2B2Q). The total systematic uncertainty in the background prediction is shown by the hatched area. Distributions of a few representative signals are overlaid. For the $(\tilde{W},\tilde{B})$-SIM models, the label (900, 100) GeV indicates $(m(\tilde{\chi}_1^{\pm}), m(\tilde{\chi}_1^0))$. The bottom panel shows the statistical significance of the discrepancy between the observed number of events and the SM expectation, following the prescription described in Ref. [158].

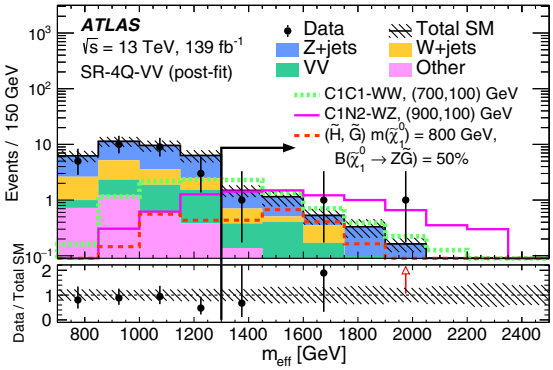

(a) SR-4Q-VV

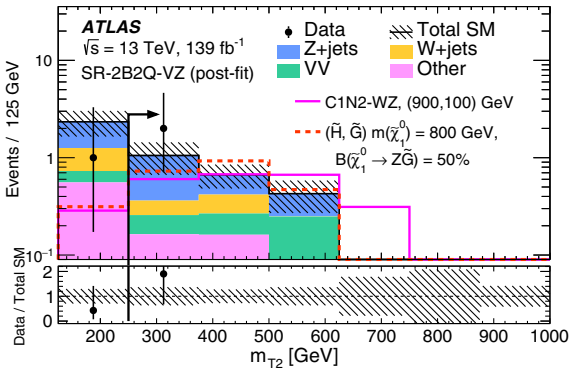

(b) SR-2B2Q-VZ

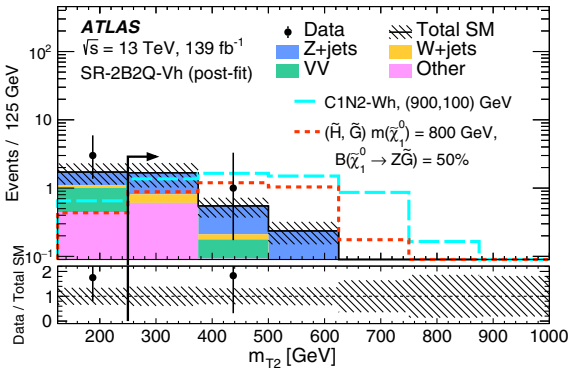

(c) SR-2B2Q-Vh

FIG. 11. (a) m_{eff} distribution in SR-4Q-VV. (b), (c) m_{T2} distributions in SR-2B2Q-VZ and SR-2B2Q-Vh. The postfit SM background expectation using the background-only fit is shown in a histogram stack. Distributions of a few representative signals are overlaid. The bottom panels show the ratio of the observed data to the background prediction. The selection criterion for the variable shown by each plot is removed, while the arrow indicates the cut value used to define the region. For the $(\tilde{W},\tilde{B})$-SIM models, the labels (700, 100) GeV and (900, 100) GeV indicate $(m(\tilde{\chi}_1^{\pm}), m(\tilde{\chi}_1^0))$.

The uncertainty in $W_{qq}(Z_{qq})$ tagging contributes the most to this class of efficiency uncertainties. It originates from the MC modeling uncertainty in the jet substructure variable distributions (m_J, D_2, and n_{track}), as well as the precision of the efficiency determination in data. The MC modeling uncertainty is evaluated by comparing samples from different MC generator configurations [137]. The W_{qq}-tagging efficiency in data is measured using $t\bar{t}$ for signal jets (large-R jets that contain the $W \to qq$ decays) and QCD multijet/γ + jets for background jets, following the prescription described in Ref. [137]. The total uncertainty of the W_{qq}-tagging efficiency correction factor ranges from 12 to 23% for signal jets, and from 7 to 15% for background jets, depending on the p_{T}. The same efficiency correction factors are applied to the Z_{qq}-tagging selection, with a simulation-based additional uncertainty of 4–5% to account for differences between W and Z bosons.

The uncertainty in the $Z_{bb}(h_{bb})$ tagging is obtained from the b-tagging efficiency uncertainty and the J_{bb} mass distribution's shape uncertainty. For the b-tagging uncertainty, 1–10%, 15–50%, and 50–100% uncertainties are assigned to the MC correction factor for b jets, c-jet mistagging, and light-flavor jet mistagging, respectively, driven by theoretical uncertainties in the MC-simulated efficiency and the precision of the efficiency measurement in data. The J_{bb} mass scale uncertainty is estimated using the R_{trk} method [132], and a relative scale uncertainty of 2–8% is assigned depending on $p_{\text{T},J}$ and m_J. A 20% relative uncertainty is assigned for the J_{bb} mass resolution based on the variation in the simulation [159].

Other efficiency uncertainties related to triggering, identification, reconstruction, and isolation requirements of electrons [75,141], muons [142] and photons [75], and the jet vertex tagger selection for small-R jets, are found to be negligible.

The second class of experimental uncertainties is related to the energy (or momentum) determination for the reconstructed objects, namely large-R jets [132], small-R jets [145], electrons [141], muons [160] and photons [141]. These typically come from the precision of simulation-based and *in situ* calibrations of the energy (or momentum) scale and resolution. These per-object uncertainties are propagated through the $E_{\text{T}}^{\text{miss}}$ calculation, with additional uncertainties accounting for the scale and resolution of the soft term [146].

Additionally, an uncertainty in the integrated luminosity used to normalize the MC samples is considered. A 1.7% uncertainty is quoted for the combined 2015–2018 integrated luminosity obtained primarily using the LUCID-2 detector [161]. Finally, a pileup modeling uncertainty is assigned to account for the discrepancy between the predicted and measured inelastic cross sections [162].

B. Theoretical uncertainties

Theoretical uncertainties in the main reducible backgrounds (W/Z + jets, γ + jets, and VV production) are estimated with varied generator parameters. Uncertainties due to the choice of QCD renormalization and factorization scales are evaluated by varying them up and down by a factor of 2 relative to their nominal values [163]. For W/Z + jets, the uncertainties related to the choice of CKKW merging scale are also considered. These are assessed by shifting the merging scale to 15 or 30 GeV from the default scale of 20 GeV. For the $t\bar{t}$ background, the nominal POWHEG+PYTHIA 8 sample is compared with two alternative samples: one from MADGRAPH5_AMC@NLO to estimate the hard-scatter modeling uncertainty, and the other from POWHEGBOX interfaced to HERWIG 7.0.4 [164] and H7UE set of tuned parameters [164] to assess the uncertainty due to the choice of parton shower scheme and hadronization model. Variations in the $t\bar{t}$ initial- and final-state radiation modeling, and renormalization and factorization scales, are also considered following the prescription described in Ref. [165]. Uncertainties related to the choice of NNPDF3.0NNLO PDF sets are assigned to the W/Z + jets, γ + jets, VV, $t\bar{t}$ and single-top backgrounds. These are derived by taking the envelope of the eigenvector variations from 100 propagated uncertainties.

For the reducible background estimation, an additional uncertainty is assigned for the modeling of the relative background composition. This is because different physics processes (Z + jets, W + jets, $t\bar{t}$, etc.) are considered as a

TABLE VI. Left to right: 95% C.L. upper limits on the visible cross section ($\langle\epsilon\sigma\rangle_{\text{obs}}^{95}$). S_{obs}^{95} (S_{exp}^{95}) shows the 95% C.L. upper limit on the number of signal events, given the observed number (expected number and $\pm1\sigma$ excursions) of background events. The last two columns indicate the CL_b value and the discovery p value [$p(s=0)$] with the corresponding Gaussian significance (Z). CL_b provides a measure of compatibility of the observed data with the 95% C.L. signal strength hypothesis relative to fluctuations of the background, and $p(s=0)$ measures compatibility of the observed data with the background-only (zero signal strength) hypothesis relative to fluctuations of the background. Larger values indicate greater relative compatibility. $p(s=0)$ is not calculated in signal regions with a deficit with respect to the nominal background prediction.

Signal region	$\langle\epsilon\sigma\rangle_{\text{obs}}^{95}$ [fb]	S_{obs}^{95}	$S_{\text{exp}}^{95}(\pm1\sigma)$	CL_b	$p(s=0)$ (Z)
SR-4Q-WW	0.032	4.5	$4.2^{+1.8}_{-1.0}$	0.55	0.44 (0.15)
SR-4Q-WZ	0.036	5.0	$5.1^{+2.1}_{-1.3}$	0.46	…
SR-4Q-ZZ	0.025	3.6	$4.1^{+1.8}_{-1.0}$	0.30	…
SR-4Q-VV	0.034	4.7	$5.3^{+2.3}_{-1.5}$	0.38	…
SR-2B2Q-WZ	0.033	4.7	$4.0^{+1.7}_{-0.7}$	0.66	0.33 (0.44)
SR-2B2Q-Wh	0.022	3.1	$3.9^{+1.3}_{-0.7}$	0.28	…
SR-2B2Q-ZZ	0.033	4.5	$4.1^{+1.7}_{-0.9}$	0.63	0.37 (0.32)
SR-2B2Q-Zh	0.026	3.6	$3.9^{+1.4}_{-0.7}$	0.38	…
SR-2B2Q-VZ	0.032	4.4	$4.4^{+1.8}_{-1.0}$	0.50	…
SR-2B2Q-Vh	0.026	3.6	$4.4^{+1.7}_{-1.0}$	0.24	…
Disc-SR-2B2Q	0.034	4.8	$5.6^{+2.4}_{-1.6}$	0.30	…
Disc-SR-Incl	0.042	5.9	$7.2^{+2.2}_{-2.0}$	0.27	…

single component in the fits, and therefore its composition is predicted solely by the simulation. While the estimation is insensitive to the composition at first order since the TFs of those physics processes are similar, the residual TF difference can cause a bias in the estimation when the composition is significantly mismodeled by the simulation. The impact of the potential composition mismodeling is evaluated by the variation in the combined TF when shifting the normalization of each physics process up and down by a factor of 2. An uncertainty of about 2–8% is assigned in the 4Q category, while 7–10% is assigned for those in the 2B2Q category.

For the irreducible backgrounds, cross-section uncertainties are assigned to account for their normalization. A 50% uncertainty is quoted for VVV production based on the cross-section measurement by the CMS experiment [155], while a 70% normalization uncertainty is assigned to $t\bar{t}+X$ based on the data/MC discrepancy observed in VRTTX, as discussed in Sec. VII A.

The uncertainty in the signal yields consists of the cross-section uncertainty and the shape uncertainties. The cross-section uncertainty ranges from 6 to 20% for the production of electroweakinos with masses between 400 GeV and 1 TeV, driven mainly by the PDF uncertainty [125]. The shape uncertainties comprise uncertainties in the choice of renormalization/factorization scales and parton shower modeling, affecting the signal acceptance by 5–10%.

IX. RESULTS

A. Statistical analysis

Final background estimates are obtained by performing a profile log-likelihood fit [166] simultaneously in all CRs and

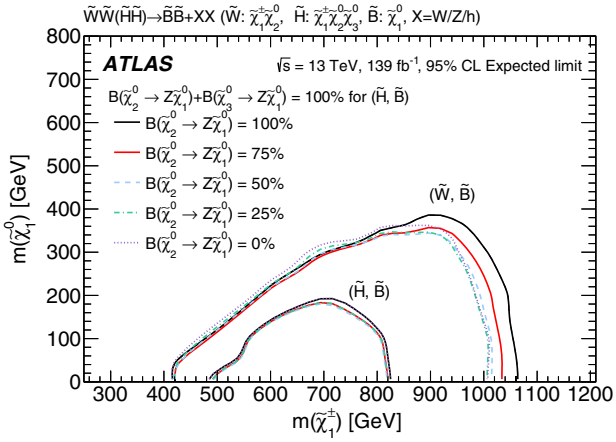

(a) Expected limits with various $\mathcal{B}(\tilde{\chi}_2^0 \to Z\tilde{\chi}_1^0)$

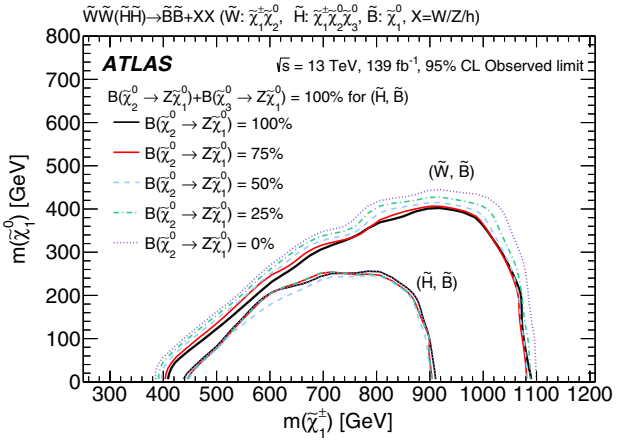

(b) Observed limits with various $\mathcal{B}(\tilde{\chi}_2^0 \to Z\tilde{\chi}_1^0)$

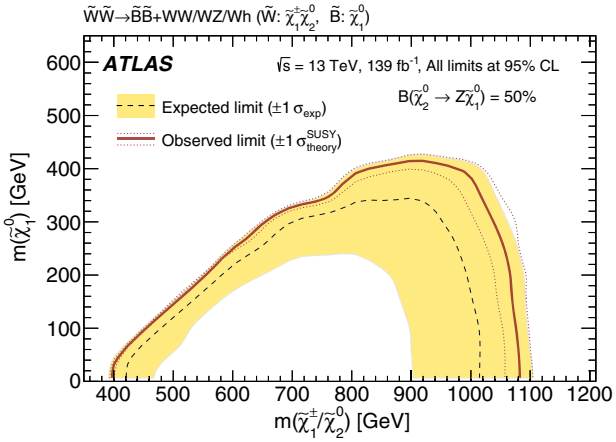

(c) $(\widetilde{W},\widetilde{B})$ with $\mathcal{B}(\tilde{\chi}_2^0 \to Z\tilde{\chi}_1^0) = 50\%$

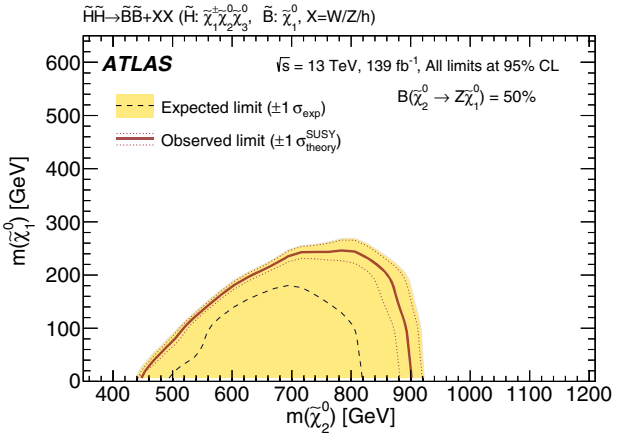

(d) $(\widetilde{H},\widetilde{B})$ with $\mathcal{B}(\tilde{\chi}_2^0 \to Z\tilde{\chi}_1^0) = 50\%$

FIG. 12. Exclusion limits for the $(\tilde{W},\tilde{B})$ and $(\tilde{H},\tilde{B})$ models shown as a function of the wino/higgsino chargino mass $m(\tilde{\chi}_1^{\pm})$ and the bino LSP mass $m(\tilde{\chi}_1^0)$. The (a) expected and (b) observed limits for various $\mathcal{B}(\tilde{\chi}_2^0 \to Z\tilde{\chi}_1^0)$ hypotheses are overlaid. The outer and inner bundles correspond to the limits for the $(\tilde{W},\tilde{B})$ and $(\tilde{H},\tilde{B})$ models, respectively. The limits set on the $(\tilde{H},\tilde{B})$ models are highly consistent and thus the contour lines are highly overlapped. Expected (dashed) and observed (solid red) 95% C.L. exclusion limits are shown for the (c) $(\tilde{W},\tilde{B})$ and (d) $(\tilde{H},\tilde{B})$ models with a representative branching ratio $\mathcal{B}(\tilde{\chi}_2^0 \to Z\tilde{\chi}_1^0) = 50\%$.

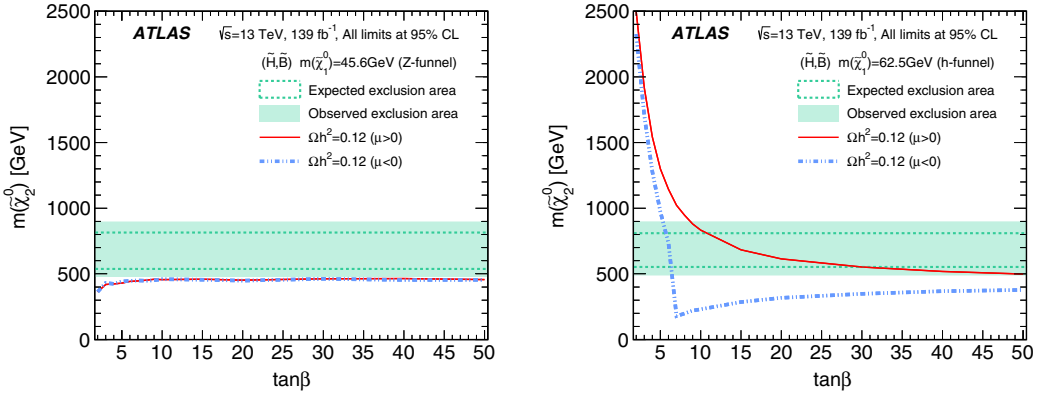

(a) $m(\tilde{\chi}_1^0) = m_Z/2$ (Z-funnel) (b) $m(\tilde{\chi}_1^0) = m_h/2$ (h-funnel)

FIG. 13. Expected (dashed green lines) and observed (green band) 95% C.L. exclusion limits on the Z/h-funnel dark matter model described in Sec. II A, where the mass of binolike LSP ($\tilde{\chi}_1^0$) is (a) half of the Z boson mass (42.6 GeV) or (b) half of the h boson mass (62.5 GeV). The areas surrounded by the green bands or dashed lines represent the excluded range of $\tilde{\chi}_2^0$. The overlaid red solid (blue dashed) line indicates for $\mu > 0$ ($\mu < 0$) the $\tilde{\chi}_2^0$ mass that reproduces the observed dark matter relic density ($\Omega h^2 = 0.12$) as function of $\tan\beta$ [55]; below (above) these lines the predicted dark matter relic density is too small (too large).

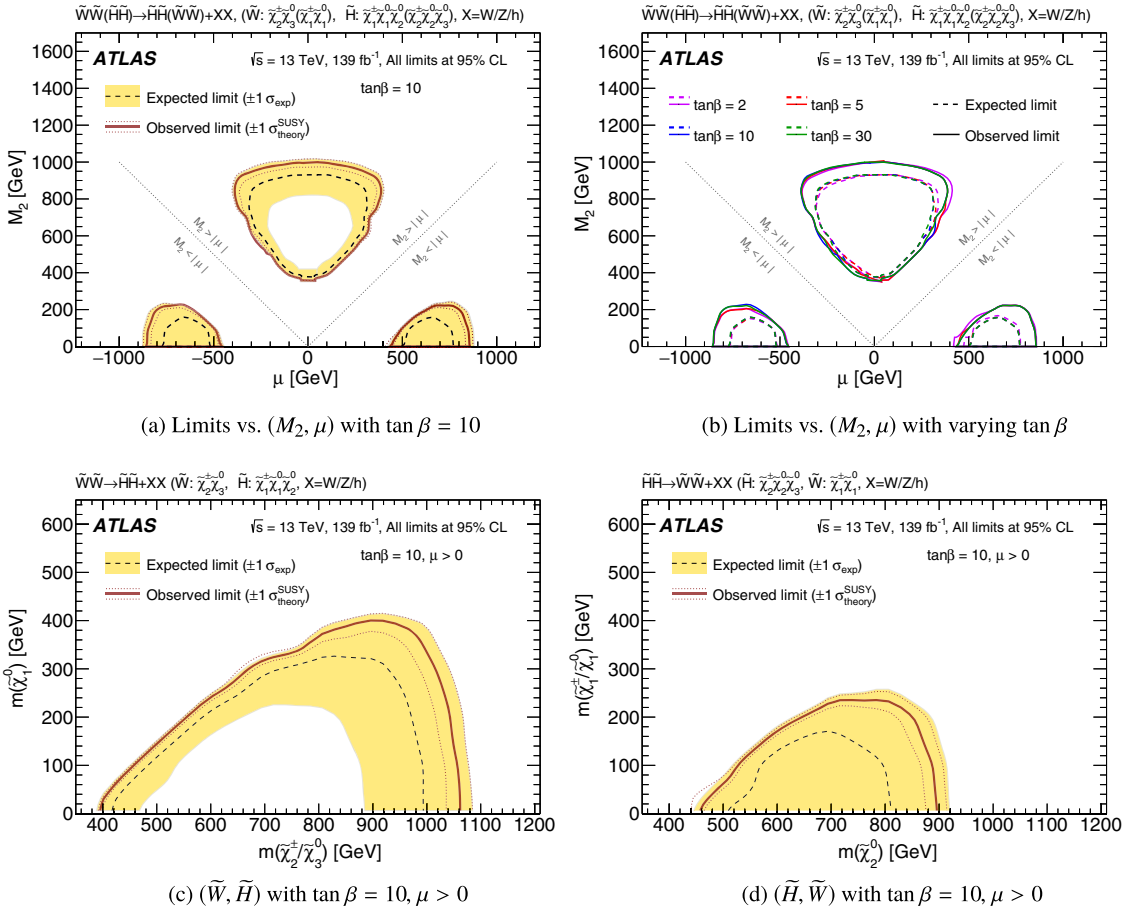

(a) Limits vs. (M_2, μ) with $\tan\beta = 10$ (b) Limits vs. (M_2, μ) with varying $\tan\beta$

(c) $(\tilde{W}, \tilde{H})$ with $\tan\beta = 10, \mu > 0$ (d) $(\tilde{H}, \tilde{W})$ with $\tan\beta = 10, \mu > 0$

FIG. 14. 95% C.L. exclusion limits for the $(\tilde{W}, \tilde{H})$ and $(\tilde{H}, \tilde{W})$ models. The limits are projected onto a two-dimensional plane either as a function of the wino/higgsino mass parameters (M_2, μ) (top figures), or of the physical electroweakino masses $(m(\tilde{\chi}_2^{\pm}), m(\tilde{\chi}_1^0))$ representing $(m(\tilde{\chi}_{\text{heavy}}), m(\tilde{\chi}_{\text{light}}))$ (bottom figures). For the limits shown on the (M_2, μ) plane, the excluded regions are indicated by the area inside the contours. The round excluded area in the top part corresponds to the excluded parameter space in the $(\tilde{W}, \tilde{H})$ model ($M_2 > |\mu|$), while the two small areas at the bottom are that in the $(\tilde{H}, \tilde{W})$ model ($M_2 < |\mu|$).

SRs relevant to a given interpretation. The HistFitter [167] framework is employed. Systematic uncertainties are treated as Gaussian-distributed nuisance parameters in the likelihood, while the statistical uncertainties of the MC samples are treated as Poisson-distributed nuisance parameters.

Three types of fit configurations are used to derive the results.

(i) A "*background-only fit*" is performed considering only the CRs and assuming no contribution from signals. The normalization of the total reducible background is allowed to float and is constrained by the fit using the data in the CRs. The normalization factors and nuisance parameters are adjusted by maximizing the likelihood. Three independent sets of fits are performed in the 0L, 1L, and 1Y categories, respectively. The 4Q and 2B2Q regions in each category are fitted simultaneously, but with independent normalization factors assigned in 4Q and 2B2Q. The normalization factors obtained from the fits range from 0.7 to 1.3.

(ii) A "*discovery fit*" performs the hypothesis test for a generic beyond-the-SM (BSM) signal, setting upper limits on the number of events and visible cross section for the signal. The fit uses only a single SR and the associated CR0L bin(s), constraining the backgrounds following the same method as in the background-only fit. Any contribution from signals is allowed only in the SR, and the signal-strength parameter is defined to be strictly positive.

(iii) An "*exclusion fit*" is performed to set the exclusion limit for a given signal model. The SRs and the corresponding CR0L bins are fit simultaneously to determine the reducible background normalization factors and constrain the systematic uncertainties. The signal contamination in CR0L is also taken into account according to the model predictions.

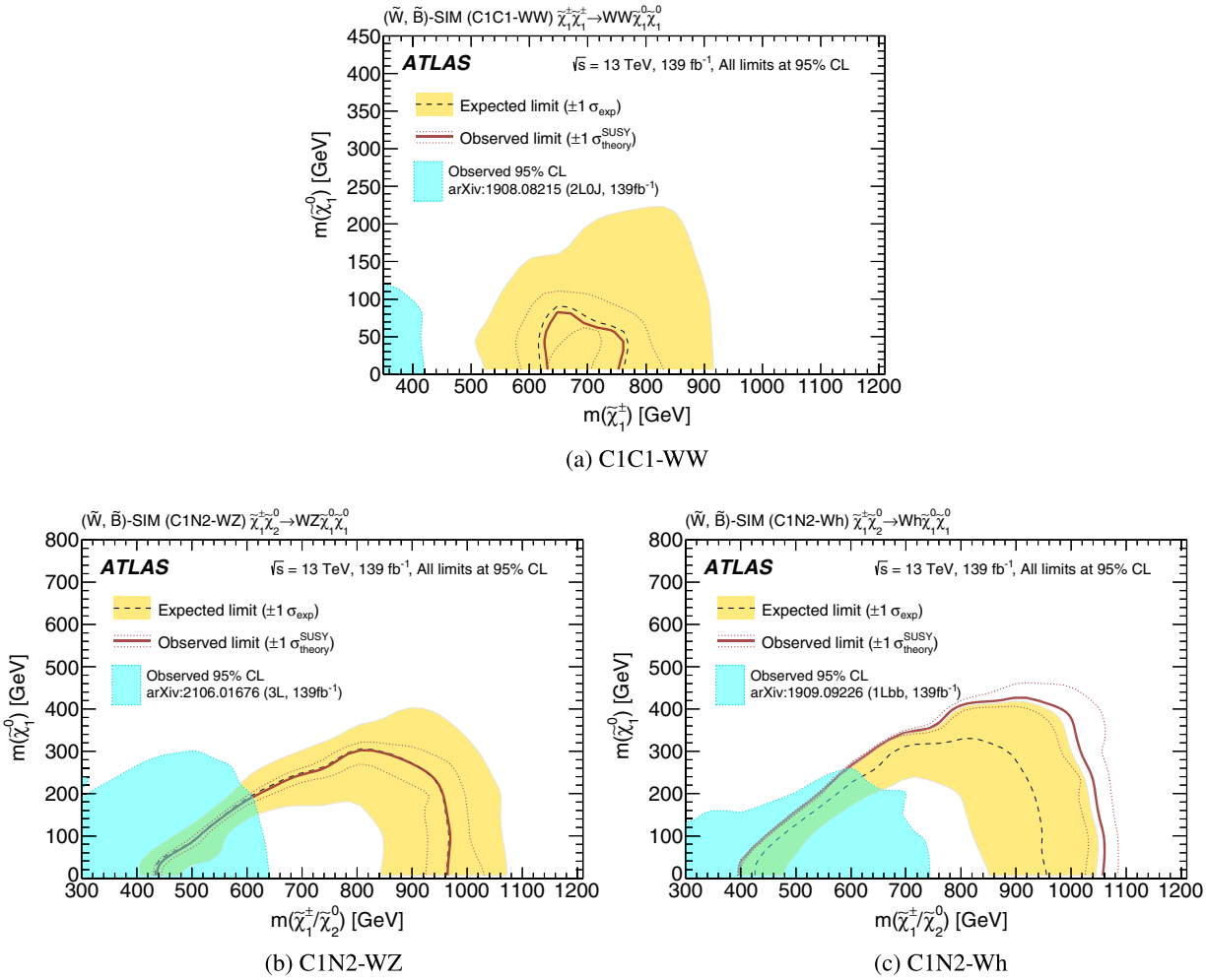

(a) C1C1-WW

(b) C1N2-WZ

(c) C1N2-Wh

FIG. 15. Exclusion limits for $(\tilde{W},\tilde{B})$-SIM as a function of the produced wino mass $m(\tilde{\chi}_1^{\pm}/\tilde{\chi}_2^0)$ and the bino LSP mass $m(\tilde{\chi}_1^0)$. Expected (dashed) and observed (solid) 95% C.L. exclusion limits on $(\tilde{W},\tilde{B})$ simplified models are shown for (a) C1C1-WW, (b) C1N2-WZ, and (c) C1N2-Wh. The limits from the previous ATLAS searches on C1C1-WW [23], C1N2-WZ [24], and C1N2-Wh [29] are shown by the shaded areas.

For each discovery or exclusion fit, the compatibility of the observed data with the background-only or signal-plus-background hypotheses is quantified by calculating a one-sided p_0 value with the profile likelihood ratio used as a test statistic [166]. The upper limits and exclusion are derived using the CL_s prescription [168] where the 95% confidence level (C.L.) exclusion is defined by $CL_s < 0.05$.

B. Signal region yields

The observed data yields in each SR and CR0L together with their SM background expectations are summarized in Table V and shown in Fig. 10. No significant excess is found in any of the SRs. The distributions of m_{eff} in SR-4Q-VV and m_{T2} in SR-2B2Q-VZ and SR-2B2Q-Vh are shown in Fig. 11 with some representative signal samples overlaid to illustrate the sensitivity.

C. Model-independent upper limits

A discovery fit is performed for each SR to derive the expected and observed 95% C.L. upper limits on the number of BSM signal events (S^{95}_{exp} and S^{95}_{obs}) as well as the one-sided p value (p_0) of the background-only hypothesis. Pseudoexperiments with toy MC are used for the calculation. An upper limit on the cross section, $\langle \epsilon\sigma \rangle^{95}_{\text{obs}}$ where ϵ represents the efficiency times acceptance of the SR for the given signal, is obtained by dividing S^{95}_{obs} by the integrated luminosity. The upper limits and the p_0 value associated with each SR are summarized in Table VI. Two additional "discovery SRs" are defined in order to set model-independent upper limits in the inclusive phase space. First, Disc-SR-2B2Q is defined as the logical union of SR-2B2Q-VZ and SR-2B2Q-Vh, and then the inclusive discovery signal region Disc-SR-Incl is defined as the logical union of SR-4Q-VV and Disc-SR-2B2Q. When evaluating Disc-SR-Incl, both CR0L-4Q and CR0L-2B2Q are included in the simultaneous fit and each has its own floating normalization factor for the reducible backgrounds.

D. Model-dependent exclusion limits

The results are also interpreted in the context of the specific signal models discussed in Sec. II. An exclusion fit is performed for each point in the model space, and a CL_s value is assigned based on the hypothesis test. The expected and observed 95% C.L. exclusion regions correspond to values of $CL_s < 0.05$. Given the large number of models tested, an asymptotic approximation [166] is employed in the CL_s calculation instead of the full calculation using pseudoexperiments. The validity is checked and the CL_s values of the two methods typically agree within 5%, and maximally within 10%.

The SRs participating in the simultaneous fit vary with the signal model being tested, as summarized in Table I. CR0L-4Q (CR0L-2B2Q) is included in the fit when at least one SR-4Q (SR-2B2Q) bin is used in deriving the limit, while both of the CR0L bins are included when the SR bins from both SR-4Q and SR-2B2Q participate in the fit.

1. Exclusion limits on $(\tilde{W},\tilde{B})$, $(\tilde{H},\tilde{B})$, $(\tilde{W},\tilde{H})$, and $(\tilde{H},\tilde{W})$ models

The exclusion limits on the $(\tilde{W},\tilde{B})$ and $(\tilde{H},\tilde{B})$ models are summarized in Fig. 12. As discussed in Sec. II A, different $\mathcal{B}(\tilde{\chi}^0_2 \to Z\tilde{\chi}^0_1)$ hypotheses are examined, and these are shown to result in very similar limits in Figs. 12(a) and 12(b).

The expected and observed limits for a representative slice $\mathcal{B}(\tilde{\chi}^0_2 \to Z\tilde{\chi}^0_1) = 50\%$ are shown in Figs. 12(c) and 12(d), for $(\tilde{W},\tilde{B})$ and $(\tilde{H},\tilde{B})$ models respectively.

The $(\tilde{H},\tilde{B})$ limits are also interpreted for the Z/h-funnel dark matter model described in Sec. II A. The exclusion limits are shown in Fig. 13, overlaid with theoretical predictions of higgsino masses ($\tilde{\chi}^0_2$) reproducing the observed dark matter relic density ($\Omega h^2 = 0.12$) [55]. While the relic density depends drastically on $\tan\beta$, the exclusion limits obtained by the search are assumed to be constant along $\tan\beta$ since they do not change when varying $\mathcal{B}(\tilde{\chi}^0_2 \to Z\tilde{\chi}^0_1)$, and are interpreted from the exclusion limits for the $\mathcal{B}(\tilde{\chi}^0_2 \to Z\tilde{\chi}^0_1) = 50\%$ hypothesis in Fig. 12(d). For the h-funnel case, where $m(\tilde{\chi}^0_1) = m_h/2$, the excluded regions are $\tan\beta > 8.5$ for $\mu > 0$ and $5.5 < \tan\beta < 7$ for $\mu < 0$.

The exclusion limits set on the $(\tilde{W},\tilde{H})$ and $(\tilde{H},\tilde{W})$ models are evaluated in a three-dimensional model space defined by $(M_2,\mu,\tan\beta)$. For each model point, the mass spectra and the branching ratios are determined using the

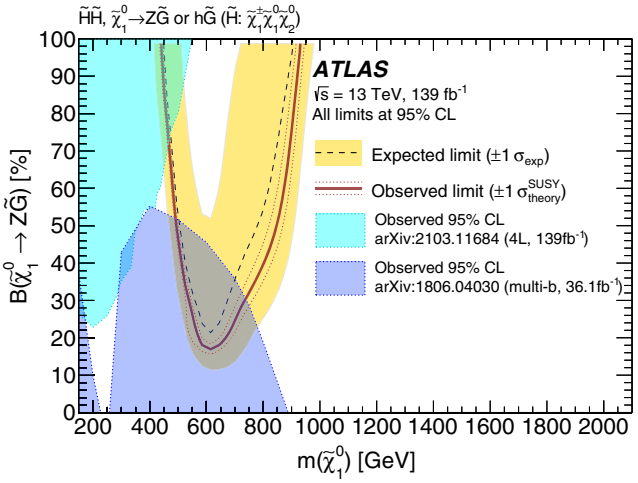

FIG. 16. Expected (dashed) and observed (solid red) 95% C.L. exclusion limits derived for the $(\tilde{H},\tilde{G})$ model, as a function of the lightest higgsino mass $m(\tilde{\chi}^0_1)$ and the branching ratio $\mathcal{B}(\tilde{\chi}^0_1 \to Z\tilde{G})$ $(= 1 - \mathcal{B}(\tilde{\chi}^0_1 \to h\tilde{G}))$. The excluded region is indicated by the area inside the contour. The exclusion limits from the previous ATLAS search using four-lepton final states [30] (cyan, denoted by "4L"), or final states with three or more b jets [37] (violet, denoted by "multi-b") are shown by the shaded areas.

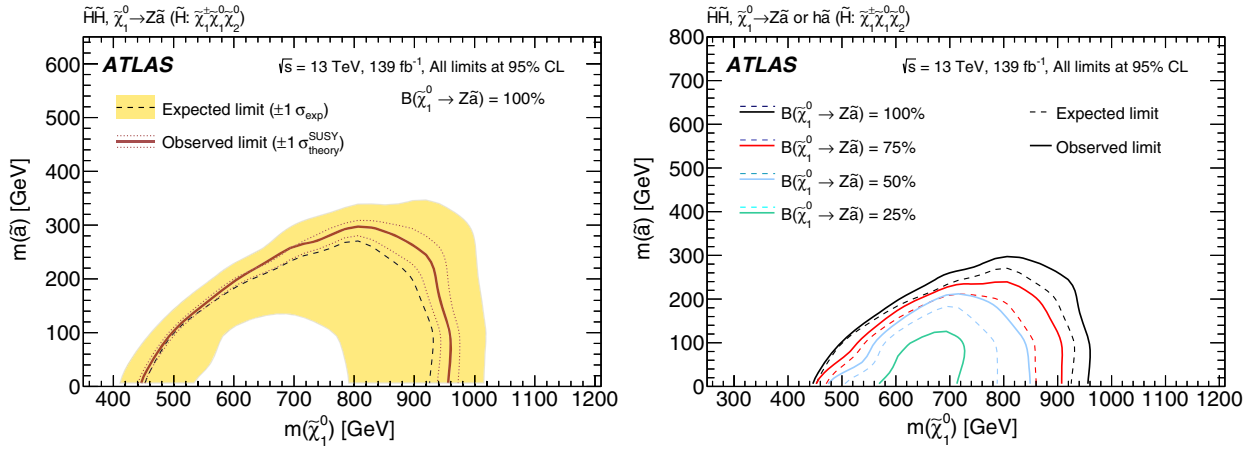

(a) $\mathcal{B}(\tilde{\chi}_1^0 \to Z\tilde{a}) = 100\%$ (b) Variable $\mathcal{B}(\tilde{\chi}_1^0 \to Z\tilde{a})$

FIG. 17. 95% C.L. exclusion limits for the $(\tilde{H}, \tilde{a})$ model as a function of axino mass $m(\tilde{a})$ and lightest higgsino mass $m(\tilde{\chi}_1^0)$. (a) Expected (dashed line) and observed (solid red line) limits calculated for $\mathcal{B}(\tilde{\chi}_1^0 \to Z\tilde{a}) = 100\%$. (b) Expected (dashed lines) and observed (solid lines) limits with various $\mathcal{B}(\tilde{\chi}_1^0 \to Z\tilde{a})$ $(= 1 - \mathcal{B}(\tilde{\chi}_1^0 \to h\tilde{a}))$ hypotheses. No expected limit is derived for the case with $\mathcal{B}(\tilde{\chi}_1^0 \to Z\tilde{a}) = 25\%$ as no mass point on the plane can be excluded.

prescription described in Sec. II A. Figure 14(a) shows the expected limit and observed limit as a function of (M_2, μ) with a fixed $\tan\beta = 10$. Figure 14(b) shows that varying $\tan\beta$ or the sign of μ (sign(μ)) has very little effect on the sensitivity. The limits are also interpreted as a function of the physical electroweakino masses so that they can be directly compared with the other models. For a given set of $(\tan\beta, \text{sign}(\mu))$, a pair of $(M_2, |\mu|)$ can be projected one to one to $(m(\tilde{\chi}_2^{\pm}), m(\tilde{\chi}_1^0))$ when all the other MSSM parameters are fixed. Figure 14(c) and Figure 14(d) show the limits for the $(\tilde{W}, \tilde{H})$ model $(M_2 > |\mu|)$ and $(\tilde{H}, \tilde{W})$ model $(M_2 < |\mu|)$, respectively, assuming $\tan\beta = 10$ and $\mu > 0$.

The mass exclusion limits are shown to be highly stable with respect to the internal variations within each model. The limits for $(\tilde{W}, \tilde{B})$ and $(\tilde{W}, \tilde{H})$ (or for $(\tilde{H}, \tilde{B})$ and $(\tilde{H}, \tilde{W})$) are also very similar, despite the branching ratios of $\tilde{\chi}_{\text{heavy}}$ being substantially different between the models. This model dependency is small mostly due to the statistical combination of SR-4Q and SR-2B2Q, and the inclusive SR bins (SR-4Q-VV, SR-2B2Q-VZ, and SR-2B2Q-Vh), which are designed to be agnostic with regard to the difference between W and Z bosons.

To summarize, a wino mass between 400 and 1060 GeV is excluded for the wino production models for $m(\tilde{\chi}_1^0) < 400$ GeV; and a higgsino mass between 450 and 900 GeV is excluded for the higgsino production models for $m(\tilde{\chi}_1^0) < 240$ GeV.

2. Exclusion limits on $(\tilde{W}, \tilde{B})$ simplified model: $(\tilde{W}, \tilde{B})$-SIM

The exclusion limits for the $(\tilde{W}, \tilde{B})$ simplified models (C1C1-WW, C1N2-WZ, and C1N2-Wh) are also derived, in order to directly compare the search sensitivity with the previous ATLAS analyses. Figure 15 shows the obtained exclusion as a function of the produced wino mass $m(\tilde{\chi}_1^{\pm}/\tilde{\chi}_2^0)$ and the bino LSP mass $m(\tilde{\chi}_1^0)$. For C1C1-WW, $m(\tilde{\chi}_1^{\pm})$ between 630 and 760 GeV is excluded for $m(\tilde{\chi}_1^0) < 80$ GeV. For C1N2-WZ (C1N2-Wh), $m(\tilde{\chi}_1^{\pm}/\tilde{\chi}_2^0)$ between 440 and 960 GeV (400 and 1060 GeV) is excluded for $m(\tilde{\chi}_1^0) < 300$ GeV(420 GeV).[13]

The sensitivity to high-mass winos is significantly improved relative to ATLAS searches using the other final states and the same dataset. For example, the expected limits on C1N2-WZ (C1N2-Wh) are typically extended by about 300 (140) GeV in $m(\tilde{\chi}_1^{\pm}/\tilde{\chi}_2^0)$, corresponding to exclusion of signals with a 7.5 (2.4) times smaller production cross section than in the search using final states with three leptons [24] (one lepton and two b jets [29]). This result also sets the most stringent limit on the model to date from the LHC experiments.

3. Exclusion limits on $(\tilde{H}, \tilde{G})$ model

The exclusion for the $(\tilde{H}, \tilde{G})$ model is presented in Fig. 16, as the function of the mass of the lightest higgsino, $m(\tilde{\chi}_1^0)$, and the branching ratio $\mathcal{B}(\tilde{\chi}_1^0 \to Z\tilde{G})$. For $\mathcal{B}(\tilde{\chi}_1^0 \to Z\tilde{G}) = 100\%(50\%)$, $m(\tilde{\chi}_1^0)$ between 450 (500) and 940 (850) GeV is excluded, while the exclusion reaches $\mathcal{B}(\tilde{\chi}_1^0 \to Z\tilde{G}) \sim 20\%$ for $m(\tilde{\chi}_1^0) \sim 600$ GeV. This complements the sensitivity achieved by previous ATLAS searches using four-lepton final states to target signals with decays

[13]The obtained limits are generally weaker than those set on the $(\tilde{W}, \tilde{B})$ model shown in Sec. IX D 1. This is because only one production mode is considered in these simplified models, while multiple production modes are included in the signals in the $(\tilde{W}, \tilde{B})$ model.

into ZZ [30] and final states with three or more b jets to target signals with decays into hh [37].

4. Exclusion limits on $(\tilde{H},\tilde{a})$ model

Lastly, Fig. 17 shows the exclusion limits on the $(\tilde{H},\tilde{a})$ model as the function of the mass of the axino, $m(\tilde{a})$, and the lightest higgsino, $m(\tilde{\chi}_1^0)$. Similarly to the $(\tilde{H},\tilde{G})$ model, different branching ratio hypotheses of $\mathcal{B}(\tilde{\chi}_1^0 \to Z\tilde{a})(=1-\mathcal{B}(\tilde{\chi}_1^0 \to h\tilde{a}))$ are tested. For $\mathcal{B}(\tilde{\chi}_1^0 \to Z\tilde{a}) = 100\%$, a higgsino mass between 450 and 940 GeV is excluded when the axino mass is less than 300 GeV. The sensitivity decreases with decreasing $\mathcal{B}(\tilde{\chi}_1^0 \to Z\tilde{a})$. For $\mathcal{B}(\tilde{\chi}_1^0 \to Z\tilde{a}) = 50\%$, the observed limit excludes higgsino masses of 500–850 GeV when the axino mass is less than 210 GeV.

X. CONCLUSION

A search for electroweakino pair production using final states consisting of $E_{\mathrm{T}}^{\mathrm{miss}}$ and two boosted hadronically decaying heavy SM bosons (W, Z, or h) is reported. Signatures with large mass splitting between the produced electroweakino and the lightest SUSY particle are targeted.

The use of fully hadronic final states takes advantage of the large SM boson branching ratios, while the backgrounds are efficiently suppressed by reconstructing the W, Z, and h bosons using boosted boson-tagging techniques. Using 139 fb^{-1} of proton-proton collision data at $\sqrt{s} =$ 13 TeV recorded by the ATLAS detector at the LHC, this strategy provides unprecedented sensitivity to the production of heavy electroweakinos.

No excess over the SM background prediction is observed, and 95% C.L. exclusion limits are set for signal models in various R-parity conserving scenarios. For wino pair production with direct decays into a bino or higgsino LSP, wino masses between 400 and 1060 GeV are excluded when the LSP mass is below 400 GeV and the mass splitting is larger than 400 GeV. For higgsino pair production with direct decays into a bino or wino LSP, higgsino masses between 450 and 900 GeV are excluded when the LSP mass is below 240 GeV and the mass splitting is larger than 450 GeV. The limits are also examined for various wino (higgsino) branching ratio assumptions, by directly scanning over relevant branching ratios (for the bino LSP models) or over the MSSM parameters that dictate them (M_2, μ, and $\tan\beta$ for the wino/higgsino LSP models). The results are shown to be highly consistent for the variations.

The results are also interpreted in the context of simplified models of wino production with decays into a bino LSP, which are more conventionally explored in electroweakino searches at the LHC. For chargino pair production, with each decaying into a W boson and an LSP, a chargino mass between 630 and 760 GeV is excluded for a LSP mass below 80 GeV. For chargino-neutralino pair production involving decays into WZ (Wh) and two LSPs, a wino mass between 440 (400) and 960 (1060) GeV is excluded for a LSP mass below 300 (420) GeV. These extend significantly beyond the exclusion limits set by the previous searches at the LHC using different final states.

Finally, exclusion limits are set on higgsino production with decays into a massless gravitino LSP or a massless/massive axino LSP, motivated by the GGM or new physics models involving the axion, respectively. A higgsino mass between 450 (500) and 940 (850) GeV is excluded for the gravitino LSP model with $\mathcal{B}(\tilde{\chi}_1^0 \to Z\tilde{G}) = 100\%(50\%)$, and a mass between 450 (500) and 940 (850) GeV is excluded for the axino LSP model with $\mathcal{B}(\tilde{\chi}_1^0 \to Z\tilde{G}) = 100\%(50\%)$ when the axino LSP mass is below 300 (210) GeV.

ACKNOWLEDGMENTS

We thank CERN for the very successful operation of the LHC, as well as the support staff from our institutions without whom ATLAS could not be operated efficiently. We acknowledge the support of ANPCyT, Argentina; YerPhI, Armenia; ARC, Australia; BMWFW and FWF, Austria; ANAS, Azerbaijan; SSTC, Belarus; CNPq and FAPESP, Brazil; NSERC, NRC and CFI, Canada; CERN; ANID, Chile; CAS, MOST and NSFC, China; Minciencias, Colombia; MSMT CR, MPO CR and VSC CR, Czech Republic; DNRF and DNSRC, Denmark; IN2P3-CNRS and CEA-DRF/IRFU, France; SRNSFG, Georgia; BMBF, HGF and MPG, Germany; GSRI, Greece; RGC and Hong Kong SAR, China; ISF and Benoziyo Center, Israel; INFN, Italy; MEXT and JSPS, Japan; CNRST, Morocco; NWO, Netherlands; RCN, Norway; MNiSW and NCN, Poland; FCT, Portugal; MNE/IFA, Romania; JINR; MES of Russia and NRC KI, Russian Federation; MESTD, Serbia; MSSR, Slovakia; ARRS and MIZŠ, Slovenia; DSI/NRF, South Africa; MICINN, Spain; SRC and Wallenberg Foundation, Sweden; SERI, SNSF and Cantons of Bern and Geneva, Switzerland; MOST, Taiwan; TAEK, Turkey; STFC, United Kingdom; DOE and NSF, United States of America. In addition, individual groups and members have received support from BCKDF, CANARIE, Compute Canada and CRC, Canada; COST, ERC, ERDF, Horizon 2020 and Marie Skłodowska-Curie Actions, European Union; Investissements d'Avenir Labex, Investissements d'Avenir Idex and ANR, France; DFG and AvH Foundation, Germany; Herakleitos, Thales and Aristeia programmes co-financed by EU-ESF and the Greek NSRF, Greece; BSF-NSF and GIF, Israel; Norwegian Financial Mechanism 2014–2021, Norway; La Caixa Banking Foundation, CERCA Programme Generalitat de Catalunya and PROMETEO and GenT Programmes Generalitat Valenciana, Spain; Göran Gustafssons Stiftelse, Sweden; The Royal Society and Leverhulme Trust, United Kingdom. The crucial computing support from all WLCG partners is acknowledged gratefully, in

particular from CERN, the ATLAS Tier-1 facilities at TRIUMF (Canada), NDGF (Denmark, Norway, Sweden), CC-IN2P3 (France), KIT/GridKA (Germany), INFN-CNAF (Italy), NL-T1 (Netherlands), PIC (Spain), ASGC (Taiwan), RAL (UK) and BNL (USA), the Tier-2 facilities worldwide and large non-WLCG resource providers. Major contributors of computing resources are listed in Ref. [169].

[1] Y. Golfand and E. Likhtman, Extension of the Algebra of Poincare Group Generators and Violation of P Invariance, Pis'ma Zh. Eksp. Teor. Fiz. **13**, 452 (1971), http://jetpletters.ru/ps/1584/article_24309.shtml [JETP Lett. **13**, 323 (1971)].
[2] D. Volkov and V. Akulov, Is the neutrino a goldstone particle?, Phys. Lett. **46B**, 109 (1973).
[3] J. Wess and B. Zumino, Supergauge transformations in four dimensions, Nucl. Phys. **B70**, 39 (1974).
[4] J. Wess and B. Zumino, Supergauge invariant extension of quantum electrodynamics, Nucl. Phys. **B78**, 1 (1974).
[5] S. Ferrara and B. Zumino, Supergauge invariant Yang-Mills theories, Nucl. Phys. **B79**, 413 (1974).
[6] A. Salam and J. Strathdee, Super-symmetry and non-Abelian gauges, Phys. Lett. **51B**, 353 (1974).
[7] P. Fayet, Supersymmetry and weak, electromagnetic and strong interactions, Phys. Lett. **64B**, 159 (1976).
[8] P. Fayet, Spontaneously broken supersymmetric theories of weak, electromagnetic and strong interactions, Phys. Lett. **69B**, 489 (1977).
[9] H. Goldberg, Constraint on the Photino Mass from Cosmology, Phys. Rev. Lett. **50**, 1419 (1983); **103**, 099905(E) (2009).
[10] J. Ellis, J. Hagelin, D. V. Nanopoulos, K. A. Olive, and M. Srednicki, Supersymmetric relics from the big bang, Nucl. Phys. **B238**, 453 (1984).
[11] G. R. Farrar and P. Fayet, Phenomenology of the production, decay, and detection of new hadronic states associated with supersymmetry, Phys. Lett. **76B**, 575 (1978).
[12] J. Hisano, S. Matsumot, M. Nagai, O. Saito, and M. Senami, Non-perturbative effect on thermal relic abundance of dark matter, Phys. Lett. B **646**, 34 (2007).
[13] T. Han, S. Mukhopadhyay, and X. Wang, Electroweak dark matter at future hadron colliders, Phys. Rev. D **98**, 035026 (2018).
[14] R. Barbieri and D. Pappadopulo, S-particles at their naturalness limits, J. High Energy Phys. 10 (2009) 061.
[15] H. Baer, V. Barger, and P. Huang, Hidden SUSY at the LHC: The light higgsino-world scenario and the role of a lepton collider, J. High Energy Phys. 11 (2011) 031.
[16] M. Papucci, J. T. Ruderman, and A. Weiler, Natural SUSY endures, J. High Energy Phys. 09 (2012) 035.
[17] H. Baer, V. Barger, P. Huang, A. Mustafayev, and X. Tata, Radiative Natural Supersymmetry with a 125 GeV Higgs Boson, Phys. Rev. Lett. **109**, 161802 (2012).
[18] T. Albahri *et al.*, Measurement of the anomalous precession frequency of the muon in the Fermilab muon $g-2$ experiment, Phys. Rev. D **103**, 072002 (2021).
[19] T. Aoyama *et al.*, The anomalous magnetic moment of the muon in the Standard Model, Phys. Rep. **887**, 1 (2020).
[20] T. Moroi, Muon anomalous magnetic dipole moment in the minimal supersymmetric standard model, Phys. Rev. D **53**, 6565 (1996); **56**, 4424(E) (1997).
[21] L. L. Everett, G. L. Kane, S. Rigolin, and L.-T.Wang, Implications of Muon $g-2$ for Supersymmetry and for Discovering Superpartners Directly, Phys. Rev. Lett. **86**, 3484 (2001).
[22] M. Endo, K. Hamaguchi, S. Iwamoto, and T. Kitahara, Muon $g-2$ vs LHC Run 2 in supersymmetric models, J. High Energy Phys. 4 (2020) 165.
[23] ATLAS Collaboration, Search for electroweak production of charginos and sleptons decaying into final states with two leptons and missing transverse momentum in $\sqrt{s}=$ 13 TeV pp collisions using the ATLAS detector, Eur. Phys. J. C **80**, 123 (2020).
[24] ATLAS Collaboration, Search for chargino–neutralino pair production in final states with three leptons and missing transverse momentum in $\sqrt{s}=13$ TeV pp collisions with the ATLAS detector, arXiv:2106.01676.
[25] ATLAS Collaboration, Search for chargino–neutralino production using recursive jigsaw reconstruction in final states with two or three charged leptons in proton–proton collisions at $\sqrt{s}=13$ TeV with the ATLAS detector, Phys. Rev. D **98**, 092012 (2018).
[26] ATLAS Collaboration, Search for chargino–neutralino production with mass splittings near the electroweak scale in three-lepton final states in $\sqrt{s}=13$ TeV pp collisions with the ATLAS detector, Phys. Rev. D **101**, 072001 (2020).
[27] ATLAS Collaboration, Search for chargino and neutralino production in final states with a Higgs boson and missing transverse momentum at $\sqrt{s}=13$ TeV with the ATLAS detector, Phys. Rev. D **100**, 012006 (2019).
[28] ATLAS Collaboration, Search for direct production of electroweakinos in final states with missing transverse momentum and a Higgs boson decaying into photons in pp collisions at $\sqrt{s}=13$ TeV with the ATLAS detector, J. High Energy Phys. 10 (2020) 005.
[29] ATLAS Collaboration, Search for direct production of electroweakinos in final states with one lepton, missing transverse momentum and a Higgs boson decaying into two b-jets in pp collisions at $\sqrt{s}=13$ TeV with the ATLAS detector, Eur. Phys. J. C **80**, 691 (2020).
[30] ATLAS Collaboration, Search for supersymmetry in events with four or more charged leptons in 139 fb^{-1} of $\sqrt{s}=13$ TeV pp collisions with the ATLAS detector, arXiv:2103.11684.

[31] CMS Collaboration, Searches for pair production of charginos and top squarks in final states with two oppositely charged leptons in proton–proton collisions at $\sqrt{s} =$ 13 TeV, J. High Energy Phys. 11 (2018) 079.

[32] CMS Collaboration, Search for supersymmetry in final states with two oppositely charged same-flavor leptons and missing transverse momentum in proton–proton collisions at $\sqrt{s} = 13$ TeV, J. High Energy Phys. 04 (2021) 123.

[33] CMS Collaboration, Search for electroweak production of charginos and neutralinos in proton-proton collisions at $\sqrt{s} = 13$ TeV, arXiv:2106.14246.

[34] CMS Collaboration, Search for electroweak production of charginos and neutralinos in multilepton final states in proton–proton collisions at $\sqrt{s} = 13$ TeV, J. High Energy Phys. 03 (2018) 166.

[35] CMS Collaboration, Search for chargino-neutralino production in events with Higgs and W bosons using 137 fb^{-1} of proton-proton collisions at $\sqrt{s} = 13$ TeV, arXiv:2107.12553.

[36] CMS Collaboration, Search for supersymmetry with Higgs boson to diphoton decays using the razor variables at $\sqrt{s} = 13$ TeV, Phys. Lett. B **779**, 166 (2018).

[37] ATLAS Collaboration, Search for pair production of higgsinos in final states with at least three b-tagged jets in $\sqrt{s} = 13$ TeV pp collisions using the ATLAS detector, Phys. Rev. D **98**, 092002 (2018).

[38] CMS Collaboration, Search for Higgsino pair production in pp collisions at $\sqrt{s} = 13$ TeV in final states with large missing transverse momentum and two Higgs bosons decaying via $H \to b\bar{b}$, Phys. Rev. D **97**, 032007 (2018).

[39] ATLAS Collaboration, Performance of top-quark and W-boson tagging with ATLAS in Run 2 of the LHC, Eur. Phys. J. C **79**, 375 (2019).

[40] ATLAS Collaboration, Identification of boosted Higgs bosons decaying into b-quark pairs with the ATLAS detector at 13 TeV, Eur. Phys. J. C **79**, 836 (2019).

[41] CMS Collaboration, Identification techniques for highly boosted W bosons that decay into hadrons, J. High Energy Phys. 12 (2014) 017.

[42] CMS Collaboration, Identification of heavy-flavour jets with the CMS detector in pp collisions at 13 TeV, J. Instrum. **13**, P05011 (2018).

[43] P. Meade, N. Seiberg, and D. Shih, General gauge mediation, Prog. Theor. Phys. Suppl. **177**, 143 (2009).

[44] C. Cheung, A. L. Fitzpatrick, and D. Shih, (Extra)ordinary gauge mediation, J. High Energy Phys. 07 (2008) 054.

[45] M. Dine and W. Fischler, A phenomenological model of particle physics based on supersymmetry, Phys. Lett. **110B**, 227 (1982).

[46] L. Alvarez-Gaumé, M. Claudson, and M. B. Wise, Low-energy supersymmetry, Nucl. Phys. **B207**, 96 (1982).

[47] C. R. Nappi and B. A. Ovrut, Supersymmetric extension of the $\text{SU}(3) \times \text{SU}(2) \times \text{U}(1)$ model, Phys. Lett. B **113B**, 175 (1982).

[48] G. Giudice and A. Romanino, Split supersymmetry, Nucl. Phys. **B699**, 65 (2004); **B706**, 65(E) (2005).

[49] N. Arkani-Hamed and S. Dimopoulos, Supersymmetric unification without low energy supersymmetry and signatures for fine-tuning at the LHC, J. High Energy Phys. 06 (2005) 073.

[50] M. Drees and M. M. Nojiri, Neutralino relic density in minimal $N = 1$ supergravity, Phys. Rev. D **47**, 376 (1993).

[51] A. Pierce, Dark matter in the finely tuned minimal supersymmetric standard model, Phys. Rev. D **70**, 075006 (2004).

[52] T. Han, Z. Liu, and A. Natarajan, Dark matter and Higgs bosons in the MSSM, J. High Energy Phys. 11 (2013) 008.

[53] L. Calibbi, J. M. Lindert, T. Ota, and Y. Takanishi, LHC tests of light neutralino dark matter without light sfermions, J. High Energy Phys. 11 (2014) 106.

[54] M. Chakraborti, U. Chattopadhyay, A. Choudhury, A. Datta, and S. Poddar, Reduced LHC constraints for higgsino-like heavier electroweakinos, J. High Energy Phys. 11 (2015) 050.

[55] K. Hamaguchi and K. Ishikawa, Prospects for Higgs- and Z-resonant neutralino dark matter, Phys. Rev. D **93**, 055009 (2016).

[56] J. Bramante, Nishita Desai, Patrick Fox, Adam Martin, Bryan Ostdiek, and Tilman Plehn, Towards the final word on neutralino dark matter, Phys. Rev. D **93**, 063525 (2016).

[57] T. Han, F. Kling, S. Su, and Y. Wu, Unblinding the dark matter blind spots, J. High Energy Phys. 02 (2017) 057.

[58] G. Pozzo and Y. Zhang, Constraining resonant dark matter with combined LHC electroweakino searches, Phys. Lett. B **789**, 582 (2019).

[59] T. Han, S. Padhi, and S. Su, Electroweakinos in the light of the Higgs boson, Phys. Rev. D **88**, 115010 (2013).

[60] B. C. Allanach, SOFTSUSY: A program for calculating supersymmetric spectra, Comput. Phys. Commun. **143**, 305 (2002).

[61] B. C. Allanach and T. Cridge, The calculation of sparticle and Higgs decays in the minimal and next-to-minimal supersymmetric standard models: SOFTSUSY4.0, Comput. Phys. Commun. **220**, 417 (2017).

[62] R. D. Peccei and H. R. Quinn, CP Conservation in the Presence of Pseudoparticles, Phys. Rev. Lett. **38**, 1440 (1977).

[63] S. Weinberg, A New Light Boson?, Phys. Rev. Lett. **40**, 223 (1978).

[64] F. Wilczek, Problem of Strong P and T Invariance in the Presence of Instantons, Phys. Rev. Lett. **40**, 279 (1978).

[65] G. Barenboim, E. J. Chun, S. Jung, and W. I. Park, Implications of an axino LSP for naturalness, Phys. Rev. D **90**, 035020 (2014).

[66] L. Covi, H. B. Kim, J. E. Kim, and L. Roszkowski, Axinos as dark matter, J. High Energy Phys. 05 (2001) 033.

[67] K. J. Bae, E. J. Chun, and S. H. Im, Cosmology of the DFSZ axino, J. Cosmol. Astropart. Phys. 03 (2012) 013.

[68] ATLAS Collaboration, Search for electroweak production of supersymmetric particles in final states with two or three leptons at $\sqrt{s} = 13$ TeV with the ATLAS detector, Eur. Phys. J. C **78**, 995 (2018).

[69] ATLAS Collaboration, The ATLAS experiment at the CERN large hadron collider, J. Instrum. **3**, S08003 (2008).

[70] B. Abbott *et al.*, Production and integration of the ATLAS Insertable B-Layer, J. Instrum. **13**, T05008 (2018).

[71] ATLAS Collaboration, Performance of the ATLAS trigger system in 2015, Eur. Phys. J. C **77**, 317 (2017).

[72] ATLAS Collaboration, The ATLAS Collaboration software and firmware, Report No. ATL-SOFT-PUB-2021-001, 2021, https://cds.cern.ch/record/2767187.
[73] ATLAS Collaboration, ATLAS data quality operations and performance for 2015–2018 data-taking, J. Instrum. **15**, P04003 (2020).
[74] ATLAS Collaboration, Performance of the missing transverse momentum triggers for the ATLAS detector during Run-2 data taking, J. High Energy Phys. 08 (2020) 080.
[75] ATLAS Collaboration, Performance of electron and photon triggers in ATLAS during LHC Run 2, Eur. Phys. J. C **80**, 47 (2020).
[76] ATLAS Collaboration, Performance of the ATLAS muon triggers in Run 2, J. Instrum. **15**, P09015 (2020).
[77] ATLAS Collaboration, The ATLAS simulation infrastructure, Eur. Phys. J. C **70**, 823 (2010).
[78] S. Agostinelli *et al.* (GEANT4 Collaboration), Geant4—a simulation toolkit, Nucl. Instrum. Methods Phys. Res., Sect. A **506**, 250 (2003).
[79] T. Sjöstrand, S. Mrenna, and P. Skands, A brief introduction to PYTHIA 8.1, Comput. Phys. Commun. **178**, 852 (2008).
[80] ATLAS Collaboration, The Pythia 8 A3 tune description of ATLAS minimum bias and inelastic measurements incorporating the Donnachie–Landshoff diffractive model, Report No. ATL-PHYS-PUB-2016-017, 2016, https://cds.cern.ch/record/2206965.
[81] R. D. Ball *et al.*, Parton distributions with LHC data, Nucl. Phys. **B867**, 244 (2013).
[82] E. Bothmann *et al.*, Event generation with Sherpa 2.2, SciPost Phys. **7**, 034 (2019).
[83] T. Gleisberg and S. Höche, Comix, a new matrix element generator, J. High Energy Phys. 12 (2008) 039.
[84] F. Cascioli, P. Maierhöfer, and S. Pozzorini, Scattering Amplitudes with Open Loops, Phys. Rev. Lett. **108**, 111601 (2012).
[85] A. Denner, S. Dittmaier, and L. Hofer, Collier: A fortran-based complex one-loop library in extended regularizations, Comput. Phys. Commun. **212**, 220 (2017).
[86] S. Höche, F. Krauss, M. Schönherr, and F. Siegert, A critical appraisal of NLO + PS matching methods, J. High Energy Phys. 09 (2012) 049.
[87] S. Catani, F. Krauss, R. Kuhn, and B. R. Webber, QCD matrix elements + parton showers, J. High Energy Phys. 11 (2001) 063.
[88] S. Höche, F. Krauss, S. Schumann, and F. Siegert, QCD matrix elements and truncated showers, J. High Energy Phys. 05 (2009) 053.
[89] S. Höche, F. Krauss, M. Schönherr, and F. Siegert, QCD matrix elements + parton showers. The NLO case, J. High Energy Phys. 04 (2013) 027.
[90] R. D. Ball *et al.*, Parton distributions for the LHC run II, J. High Energy Phys. 04 (2015) 040.
[91] S. Frixione, Isolated photons in perturbative QCD, Phys. Lett. B **429**, 369 (1998).
[92] S. Frixione, P. Nason, and G. Ridolfi, A positive-weight next-to-leading-order Monte Carlo for heavy flavour hadroproduction, J. High Energy Phys. 09 (2007) 126.
[93] P. Nason, A new method for combining NLO QCD with shower Monte Carlo algorithms, J. High Energy Phys. 11 (2004) 040.
[94] S. Frixione, P. Nason, and C. Oleari, Matching NLO QCD computations with parton shower simulations: The POWHEG method, J. High Energy Phys. 11 (2007) 070.
[95] S. Alioli, P. Nason, C. Oleari, and E. Re, A general framework for implementing NLO calculations in shower Monte Carlo programs: The POWHEG BOX, J. High Energy Phys. 06 (2010) 043.
[96] ATLAS Collaboration, Studies on top-quark Monte Carlo modelling for Top2016, Report No. ATL-PHYSPUB-2016-020, 2016, https://cds.cern.ch/record/2216168.
[97] ATLAS Collaboration, ATLAS Pythia 8 tunes to 7 TeV data, Report No. ATL-PHYS-PUB-2014-021, 2014, https://cds.cern.ch/record/1966419.
[98] D. J. Lange, The EvtGen particle decay simulation package, Nucl. Instrum. Methods Phys. Res., Sect. A **462**, 152 (2001).
[99] S. Frixione, E. Laenen, P. Motylinski, C. White, and B. R. Webber, Single-top hadroproduction in association with a W boson, J. High Energy Phys. 07 (2008) 029.
[100] J. Alwall, R. Frederix, S. Frixione, V. Hirschi, F. Maltoni, O. Mattelaer, H.-S. Shao, T. Stelzer, P. Torrielli, and M. Zaro, The automated computation of tree-level and next-to-leading order differential cross sections, and their matching to parton shower simulations, J. High Energy Phys. 07 (2014) 079.
[101] M. Beneke, P. Falgari, S. Klein, and C. Schwinn, Hadronic top-quark pair production with NNLL threshold resummation, Nucl. Phys. **B855**, 695 (2012).
[102] M. Cacciari, M. Czakon, M. Mangano, A. Mitov, and P. Nason, Top-pair production at hadron colliders with next-to-next-to-leading logarithmic soft-gluon resummation, Phys. Lett. B **710**, 612 (2012).
[103] P. Bärnreuther, M. Czakon, and A. Mitov, Percent-Level-Precision Physics at the Tevatron: Next-to-Next-to-Leading Order QCD Corrections to $q\bar{q} \to t\bar{t} + X$, Phys. Rev. Lett. **109**, 132001 (2012).
[104] M. Czakon and A. Mitov, NNLO corrections to top-pair production at hadron colliders: The all-fermionic scattering channels, J. High Energy Phys. 12 (2012) 054.
[105] M. Czakon and A. Mitov, NNLO corrections to top pair production at hadron colliders: The quark-gluon reaction, J. High Energy Phys. 01 (2013) 080.
[106] M. Czakon, P. Fiedler, and A. Mitov, Total Top-Quark Pair-Production Cross Section at Hadron Colliders Through $O(\alpha_S^4)$, Phys. Rev. Lett. **110**, 252004 (2013).
[107] M. Czakon and A. Mitov, Top++: A program for the calculation of the top-pair cross-section at hadron colliders, Comput. Phys. Commun. **185**, 2930 (2014).
[108] P. Kant, O. M. Kind, T. Kintscher, T. Lohse, T. Martini, S. Mölbitz, P. Rieck, and P. Uwer, HatHor for single top-quark production: Updated predictions and uncertainty estimates for single top-quark production in hadronic collisions, Comput. Phys. Commun. **191**, 74 (2015).
[109] M. Aliev, H. Lacker, U. Langenfeld, S. Moch, P. Uwer, and M. Wiedermann, HATHOR—Hadronic Top and Heavy quarks cross section calculator, Comput. Phys. Commun. **182**, 1034 (2011).
[110] N. Kidonakis, Next-to-next-to-leading-order collinear and soft gluon corrections for t-channel single top quark production, Phys. Rev. D **83**, 091503 (2011).

[111] N. Kidonakis, Two-loop soft anomalous dimensions for single top quark associated production with a W^- or H^-, Phys. Rev. D **82**, 054018 (2010).

[112] A. Lazopoulos, T. McElmurry, K. Melnikov, and F. Petriello, Next-to-leading order QCD corrections to $t\bar{t}Z$ production at the LHC, Phys. Lett. B **666**, 62 (2008).

[113] J. M. Campbell and R. K. Ellis, $t\bar{t}W^{\pm}$ production and decay at NLO, J. High Energy Phys. 07 (2012) 052.

[114] J. M. Campbell, R. K. Ellis, and C. Williams, Vector boson pair production at the LHC, J. High Energy Phys. 07 (2011) 018.

[115] C. Anastasiou, L. J. Dixon, K. Melnikov, and F. Petriello, High precision QCD at hadron colliders: Electroweak gauge boson rapidity distributions at next-to-next-to leading order, Phys. Rev. D **69**, 094008 (2004).

[116] T. Sjöstrand, Stefan Ask, Jesper R. Christiansen, Richard Corke, Nishita Desai, Philip Ilten, Stephen Mrenna, Stefan Prestel, Christine O. Rasmussen, and Peter Z. Skands, An introduction to PYTHIA 8.2, Comput. Phys. Commun. **191**, 159 (2015).

[117] P. Artoisenet, R. Frederix, O. Mattelaer, and R. Rietkerk, Automatic spin-entangled decays of heavy resonances in Monte Carlo simulations, J. High Energy Phys. 03 (2013) 015.

[118] S. Frixione, E. Laenen, P. Motylinski, and B. R. Webber, Angular correlations of lepton pairs from vector boson and top quark decays in Monte Carlo simulations, J. High Energy Phys. 04 (2007) 081.

[119] W. Beenakker, M. Klasen, M. Krämer, T. Plehn, M. Spira, and P. M. Zerwas, Production of Charginos, Neutralinos, and Sleptons at Hadron Colliders, Phys. Rev. Lett. **83**, 3780 (1999); **100**, 029901(E) (2008).

[120] J. Debove, B. Fuks, and M. Klasen, Threshold resummation for gaugino pair production at hadron colliders, Nucl. Phys. **B842**, 51 (2011).

[121] B. Fuks, M. Klasen, D. R. Lamprea, and M. Rothering, Gaugino production in proton-proton collisions at a center-of-mass energy of 8 TeV, J. High Energy Phys. 10 (2012) 081.

[122] B. Fuks, M. Klasen, D. R. Lamprea, and M. Rothering, Precision predictions for electroweak superpartner production at hadron colliders with resummino, Eur. Phys. J. C **73**, 2480 (2013).

[123] J. Fiaschi and M. Klasen, Neutralino-chargino pair production at NLO + NLL with resummationimproved parton density functions for LHC Run II, Phys. Rev. D **98**, 055014 (2018).

[124] C. Borschensky, Michael Krämer, Anna Kulesza, Michelangelo Mangano, Sanjay Padhi, Tilman Plehn, and Xavier Portell, Squark and gluino production cross sections in pp collisions at $\sqrt{s} = 13$, 14, 33 and 100 TeV, Eur. Phys. J. C **74**, 3174 (2014).

[125] J. Butterworth *et al.*, PDF4LHC recommendations for LHC Run II, J. Phys. G **43**, 023001 (2016).

[126] ATLAS Collaboration, Topological cell clustering in the ATLAS calorimeters and its performance in LHC run 1, Eur. Phys. J. C **77**, 490 (2017).

[127] M. Cacciari, G. P. Salam, and G. Soyez, The anti-k_t jet clustering algorithm, J. High Energy Phys. 04 (2008) 063.

[128] M. Cacciari, G. P. Salam, and G. Soyez, FastJet user manual, Eur. Phys. J. C **72**, 1896 (2012).

[129] D. Krohn, J. Thaler, and L.-T. Wang, Jet trimming, J. High Energy Phys. 02 (2010) 084.

[130] S. D. Ellis and D. E. Soper, Successive combination jet algorithm for hadron collisions, Phys. Rev. D **48**, 3160 (1993).

[131] ATLAS Collaboration, Jet mass reconstruction with the ATLAS Detector in early Run 2 data, Report No. ATLAS-CONF-2016-035, 2016, https://cds.cern.ch/record/2200211.

[132] ATLAS Collaboration, In situ calibration of large-radius jet energy and mass in 13 TeV proton–proton collisions with the ATLAS detector, Eur. Phys. J. C **79**, 135 (2019).

[133] ATLAS Collaboration, Variable radius, exclusive-k_T, and center-of-mass subjet reconstruction for Higgs($\to b\bar{b}$) tagging in ATLAS, Report No. ATL-PHYS-PUB-2017-010, 2017, https://cds.cern.ch/record/2268678.

[134] ATLAS Collaboration, ATLAS b-jet identification performance and efficiency measurement with $t\bar{t}$ events in pp collisions at $\sqrt{s} = 13$ TeV, Eur. Phys. J. C **79**, 970 (2019).

[135] ATLAS Collaboration, Calibration of the ATLAS b-tagging algorithm in $t\bar{t}$ semileptonic events, Report No. ATLAS-CONF-2018-045, 2018, https://cds.cern.ch/record/2638455.

[136] ATLAS Collaboration, Calibration of light-flavour b-jet mistagging rates using ATLAS proton–proton collision data at $\sqrt{s} = 13$ TeV, Report No. ATLAS-CONF-2018-006, 2018 https://cds.cern.ch/record/2314418.

[137] ATLAS Collaboration, Boosted hadronic vector boson and top quark tagging with ATLAS using Run 2 data, Report No. ATL-PHYS-PUB-2020-017, 2020 https://cds.cern.ch/record/2724149.

[138] A. J. Larkoski, G. P. Salam, and J. Thaler, Energy correlation functions for jet substructure, J. High Energy Phys. 06 (2013) 108.

[139] A. J. Larkoski, I. Moult, and D. Neill, Power counting to better jet observables, J. High Energy Phys. 12 (2014) 009.

[140] M. Cacciari, G. P. Salam, and G. Soyez, The catchment area of jets, J. High Energy Phys. 04 (2008) 005.

[141] ATLAS Collaboration, Electron and photon performance measurements with the ATLAS detector using the 2015–2017 LHC proton–proton collision data, J. Instrum. **14**, P12006 (2019).

[142] ATLAS Collaboration, Muon reconstruction and identification efficiency in ATLAS using the full Run 2pp collision data set at $\sqrt{s} = 13$ TeV, Eur. Phys. J. C **81**, 578 (2020).

[143] ATLAS Collaboration, Jet reconstruction and performance using particle flow with the ATLAS Detector, Eur. Phys. J. C **77**, 466 (2017).

[144] ATLAS Collaboration, Performance of pile-up mitigation techniques for jets in pp collisions at $\sqrt{s} = 8$ TeV using the ATLAS detector, Eur. Phys. J. C **76**, 581 (2016).

[145] ATLAS Collaboration, Jet energy scale measurements and their systematic uncertainties in proton–proton collisions at $\sqrt{s} = 13$ TeV with the ATLAS detector, Phys. Rev. D **96**, 072002 (2017).

[146] ATLAS Collaboration, Performance of missing transverse momentum reconstruction with the ATLAS detector using

proton–proton collisions at $\sqrt{s} = 13$ TeV, Eur. Phys. J. C **78**, 903 (2018).
[147] ATLAS Collaboration, Tagging and suppression of pileup jets with the ATLAS detector, Report No. ATLASCONF-2014-018, 2014, https://cds.cern.ch/record/1700870.
[148] ATLAS Collaboration, Vertex Reconstruction Performance of the ATLAS Detector at $\sqrt{s} = 13$ TeV, Report No. ATL-PHYS-PUB-2015-026, 2015, https://cds.cern.ch/record/2037717.
[149] ATLAS Collaboration, Non-collision backgrounds as measured by the ATLAS detector during the 2010 proton–proton run, Report No. ATLAS-CONF-2011-137, 2011, https://cds.cern.ch/record/1383840.
[150] ATLAS Collaboration, Selection of jets produced in 13 TeV proton–proton collisions with the ATLAS detector, Report No. ATLAS-CONF-2015-029, 2015, https://cds.cern.ch/record/2037702.
[151] C. G. Lester and D. J. Summers, Measuring masses of semi-invisibly decaying particles pair produced at hadron colliders, Phys. Lett. B **463**, 99 (1999).
[152] A. Barr, C. Lester, and P. Stephens, A variable for measuring masses at hadron colliders when missing energy is expected; m_{T2}: The truth behind the glamour, J. Phys. G **29**, 2343 (2003).
[153] ATLAS Collaboration, Search for squarks and gluinos in final states with jets and missing transverse momentum using 139 fb^{-1} of $\sqrt{s} = 13$ TeV pp collision data with the ATLAS detector, J. High Energy Phys. 02 (2021) 143.
[154] ATLAS Collaboration, Evidence for the production of three massive vector bosons with the ATLAS detector, Phys. Lett. B **798**, 134913 (2019).
[155] CMS Collaboration, Observation of the Production of Three Massive Gauge Bosons at $\sqrt{s} = 13$ TeV, Phys. Rev. Lett. **125**, 151802 (2020).
[156] ATLAS Collaboration, Measurement of the WW cross section in $\sqrt{s} = 7$ TeV pp collisions with the ATLAS detector and limits on anomalous gauge couplings, Phys. Lett. B **712**, 289 (2012).
[157] ATLAS Collaboration, Measurement of the inclusive isolated prompt photon cross section in pp collisions at $\sqrt{s} = 7$ TeV with the ATLAS detector, Phys. Rev. D **83**, 052005 (2011).
[158] R. D. Cousins, J. T. Linnemann, and J. Tucker, Evaluation of three methods for calculating statistical significance when incorporating a systematic uncertainty into a test of the background-only hypothesis for a Poisson process, Nucl. Instrum. Methods Phys. Res., Sect. A **595**, 480 (2008).
[159] ATLAS Collaboration, Jet mass and substructure of inclusive jets in $\sqrt{s} = 7$ TeV pp collisions with the ATLAS experiment, J. High Energy Phys. 05 (2012) 128.
[160] ATLAS Collaboration, Muon reconstruction performance of the ATLAS detector in proton–proton collision data at $\sqrt{s} = 13$ TeV, Eur. Phys. J. C **76**, 292 (2016).
[161] G. Avoni *et al.*, The new LUCID-2 detector for luminosity measurement and monitoring in ATLAS, J. Instrum. **13**, P07017 (2018).
[162] ATLAS Collaboration, Measurement of the Inelastic Proton–Proton Cross Section at $\sqrt{s} = 13$ TeV with the ATLAS Detector at the LHC, Phys. Rev. Lett. **117**, 182002 (2016).
[163] ATLAS Collaboration, Monte Carlo generators for the production of a W or Z/γ^* boson in association with jets at ATLAS in run 2, Report No. ATL-PHYS-PUB-2016-003, 2016, https://cds.cern.ch/record/2120133.
[164] J. Bellm *et al.*, Herwig 7.0/Herwig++ 3.0 release note, Eur. Phys. J. C **76**, 196 (2016).
[165] ATLAS Collaboration, Improvements in $t\bar{t}$ modelling using NLO + PS Monte Carlo generators for Run 2, Report No. ATL-PHYS-PUB-2018-009, 2018, https://cds.cern.ch/record/2630327.
[166] G. Cowan, K. Cranmer, E. Gross, and O. Vitells, Asymptotic formulae for likelihood-based tests of new physics, Eur. Phys. J. C **71**, 1554 (2011); **73**, 2501(E) (2013).
[167] M. Baak, G. J. Besjes, D. Côté, A. Koutsman, J. Lorenz, and D. Short, HistFitter software framework for statistical data analysis, Eur. Phys. J. C **75**, 153 (2015).
[168] A. L. Read, Presentation of search results: The CL_S technique, J. Phys. G **28**, 2693 (2002).
[169] ATLAS Collaboration, ATLAS Computing Acknowledgements, Report No. ATL-SOFT-PUB-2021-003, https://cds.cern.ch/record/2776662.

G. Aad,[99] B. Abbott,[124] D. C. Abbott,[100] A. Abed Abud,[34] K. Abeling,[51] D. K. Abhayasinghe,[91] S. H. Abidi,[27] H. Abramowicz,[157] H. Abreu,[156] Y. Abulaiti,[5] A. C. Abusleme Hoffman,[142a] B. S. Acharya,[64a,64b,b] B. Achkar,[51] L. Adam,[97] C. Adam Bourdarios,[4] L. Adamczyk,[81a] L. Adamek,[162] S. V. Addepalli,[24] J. Adelman,[117] A. Adiguzel,[11c,c] S. Adorni,[52] T. Adye,[139] A. A. Affolder,[141] Y. Afik,[156] C. Agapopoulou,[62] M. N. Agaras,[12] J. Agarwala,[68a,68b] A. Aggarwal,[115] C. Agheorghiesei,[25c] J. A. Aguilar-Saavedra,[135f,135a,d] A. Ahmad,[34] F. Ahmadov,[77] W. S. Ahmed,[101] X. Ai,[44] G. Aielli,[71a,71b] I. Aizenberg,[175] S. Akatsuka,[83] M. Akbiyik,[97] T. P. A. Åkesson,[94] A. V. Akimov,[108] K. Al Khoury,[37] G. L. Alberghi,[21b] J. Albert,[171] P. Albicocco,[49] M. J. Alconada Verzini,[86] S. Alderweireldt,[48] M. Aleksa,[34] I. N. Aleksandrov,[77] C. Alexa,[25b] T. Alexopoulos,[9] A. Alfonsi,[116] F. Alfonsi,[21b] M. Alhroob,[124] B. Ali,[137] S. Ali,[154] M. Aliev,[161] G. Alimonti,[66a] C. Allaire,[34] B. M. M. Allbrooke,[152] P. P. Allport,[19] A. Aloisio,[67a,67b] F. Alonso,[86] C. Alpigiani,[144] E. Alunno Camelia,[71a,71b] M. Alvarez Estevez,[96] M. G. Alviggi,[67a,67b] Y. Amaral Coutinho,[78b] A. Ambler,[101] L. Ambroz,[130] C. Amelung,[34] D. Amidei,[103] S. P. Amor Dos Santos,[135a] S. Amoroso,[44] C. S. Amrouche,[52] C. Anastopoulos,[145] N. Andari,[140] T. Andeen,[10]

J. K. Anders,[18] S. Y. Andrean,[43a,43b] A. Andreazza,[66a,66b] S. Angelidakis,[8] A. Angerami,[37] A. V. Anisenkov,[118b,118a] A. Annovi,[69a] C. Antel,[52] M. T. Anthony,[145] E. Antipov,[125] M. Antonelli,[49] D. J. A. Antrim,[16] F. Anulli,[70a] M. Aoki,[79] J. A. Aparisi Pozo,[169] M. A. Aparo,[152] L. Aperio Bella,[44] N. Aranzabal,[34] V. Araujo Ferraz,[78a] C. Arcangeletti,[49] A. T. H. Arce,[47] E. Arena,[88] J-F. Arguin,[107] S. Argyropoulos,[50] J.-H. Arling,[44] A. J. Armbruster,[34] A. Armstrong,[166] O. Arnaez,[162] H. Arnold,[34] Z. P. Arrubarrena Tame,[111] G. Artoni,[130] H. Asada,[113] K. Asai,[122] S. Asai,[159] N. A. Asbah,[57] E. M. Asimakopoulou,[167] L. Asquith,[152] J. Assahsah,[33d] K. Assamagan,[27] R. Astalos,[26a] R. J. Atkin,[31a] M. Atkinson,[168] N. B. Atlay,[17] H. Atmani,[58b] P. A. Atmasiddha,[103] K. Augsten,[137] S. Auricchio,[67a,67b] V. A. Austrup,[177] G. Avner,[156] G. Avolio,[34] M. K. Ayoub,[13c] G. Azuelos,[107,e] D. Babal,[26a] H. Bachacou,[140] K. Bachas,[158] A. Bachiu,[32] F. Backman,[43a,43b] A. Badea,[57] P. Bagnaia,[70a,70b] H. Bahrasemani,[148] A. J. Bailey,[169] V. R. Bailey,[168] J. T. Baines,[139] C. Bakalis,[9] O. K. Baker,[178] P. J. Bakker,[116] E. Bakos,[14] D. Bakshi Gupta,[7] S. Balaji,[153] R. Balasubramanian,[116] E. M. Baldin,[118b,118a] P. Balek,[138] E. Ballabene,[66a,66b] F. Balli,[140] W. K. Balunas,[130] J. Balz,[97] E. Banas,[82] M. Bandieramonte,[134] A. Bandyopadhyay,[17] S. Bansal,[22] L. Barak,[157] E. L. Barberio,[102] D. Barberis,[53b,53a] M. Barbero,[99] G. Barbour,[92] K. N. Barends,[31a] T. Barillari,[112] M-S. Barisits,[34] J. Barkeloo,[127] T. Barklow,[149] B. M. Barnett,[139] R. M. Barnett,[16] A. Baroncelli,[58a] G. Barone,[27] A. J. Barr,[130] L. Barranco Navarro,[43a,43b] F. Barreiro,[96] J. Barreiro Guimarães da Costa,[13a] U. Barron,[157] S. Barsov,[133] F. Bartels,[59a] R. Bartoldus,[149] G. Bartolini,[99] A. E. Barton,[87] P. Bartos,[26a] A. Basalaev,[44] A. Basan,[97] I. Bashta,[72a,72b] A. Bassalat,[62] M. J. Basso,[162] C. R. Basson,[98] R. L. Bates,[55] S. Batlamous,[33e] J. R. Batley,[30] B. Batool,[147] M. Battaglia,[141] M. Bauce,[70a,70b] F. Bauer,[140,a] P. Bauer,[22] H. S. Bawa,[29] A. Bayirli,[11c] J. B. Beacham,[47] T. Beau,[131] P. H. Beauchemin,[165] F. Becherer,[50] P. Bechtle,[22] H. P. Beck,[18,f] K. Becker,[173] C. Becot,[44] A. J. Beddall,[11a] V. A. Bednyakov,[77] C. P. Bee,[151] T. A. Beermann,[177] M. Begalli,[78b] M. Begel,[27] A. Behera,[151] J. K. Behr,[44] C. Beirao Da Cruz E Silva,[34] J. F. Beirer,[51,34] F. Beisiegel,[22] M. Belfkir,[4] G. Bella,[157] L. Bellagamba,[21b] A. Bellerive,[32] P. Bellos,[19] K. Beloborodov,[118b,118a] K. Belotskiy,[109] N. L. Belyaev,[109] D. Benchekroun,[33a] Y. Benhammou,[157] D. P. Benjamin,[27] M. Benoit,[27] J. R. Bensinger,[24] S. Bentvelsen,[116] L. Beresford,[34] M. Beretta,[49] D. Berge,[17] E. Bergeaas Kuutmann,[167] N. Berger,[4] B. Bergmann,[137] L. J. Bergsten,[24] J. Beringer,[16] S. Berlendis,[6] G. Bernardi,[131] C. Bernius,[149] F. U. Bernlochner,[22] T. Berry,[91] P. Berta,[138] A. Berthold,[46] I. A. Bertram,[87] O. Bessidskaia Bylund,[177] S. Bethke,[112] A. Betti,[40] A. J. Bevan,[90] S. Bhatta,[151] D. S. Bhattacharya,[172] P. Bhattarai,[24] V. S. Bhopatkar,[5] R. Bi,[134] R. M. Bianchi,[134] O. Biebel,[111] R. Bielski,[127] N. V. Biesuz,[69a,69b] M. Biglietti,[72a] T. R. V. Billoud,[137] M. Bindi,[51] A. Bingul,[11d] C. Bini,[70a,70b] S. Biondi,[21b,21a] A. Biondini,[88] C. J. Birch-sykes,[98] G. A. Bird,[19,139] M. Birman,[175] T. Bisanz,[34] J. P. Biswal,[2] D. Biswas,[176,g] A. Bitadze,[98] C. Bittrich,[46] K. Bjørke,[129] I. Bloch,[44] C. Blocker,[24] A. Blue,[55] U. Blumenschein,[90] J. Blumenthal,[97] G. J. Bobbink,[116] V. S. Bobrovnikov,[118b,118a] M. Boehler,[50] D. Bogavac,[12] A. G. Bogdanchikov,[118b,118a] C. Bohm,[43a] V. Boisvert,[91] P. Bokan,[44] T. Bold,[81a] M. Bomben,[131] M. Bona,[90] M. Boonekamp,[140] C. D. Booth,[91] A. G. Borbély,[55] H. M. Borecka-Bielska,[107] L. S. Borgna,[92] G. Borissov,[87] D. Bortoletto,[130] D. Boscherini,[21b] M. Bosman,[12] J. D. Bossio Sola,[34] K. Bouaouda,[33a] J. Boudreau,[134] E. V. Bouhova-Thacker,[87] D. Boumediene,[36] R. Bouquet,[131] A. Boveia,[123] J. Boyd,[34] D. Boye,[27] I. R. Boyko,[77] A. J. Bozson,[91] J. Bracinik,[19] N. Brahimi,[58d,58c] G. Brandt,[177] O. Brandt,[30] F. Braren,[44] B. Brau,[100] J. E. Brau,[127] W. D. Breaden Madden,[55] K. Brendlinger,[44] R. Brener,[175] L. Brenner,[34] R. Brenner,[167] S. Bressler,[175] B. Brickwedde,[97] D. L. Briglin,[19] D. Britton,[55] D. Britzger,[112] I. Brock,[22] R. Brock,[104] G. Brooijmans,[37] W. K. Brooks,[142d] E. Brost,[27] P. A. Bruckman de Renstrom,[82] B. Brüers,[44] D. Bruncko,[26b] A. Bruni,[21b] G. Bruni,[21b] M. Bruschi,[21b] N. Bruscino,[70a,70b] L. Bryngemark,[149] T. Buanes,[15] Q. Buat,[151] P. Buchholz,[147] A. G. Buckley,[55] I. A. Budagov,[77] M. K. Bugge,[129] O. Bulekov,[109] B. A. Bullard,[57] T. J. Burch,[117] S. Burdin,[88] C. D. Burgard,[44] A. M. Burger,[125] B. Burghgrave,[7] J. T. P. Burr,[44] C. D. Burton,[10] J. C. Burzynski,[100] V. Büscher,[97] P. J. Bussey,[55] J. M. Butler,[23] C. M. Buttar,[55] J. M. Butterworth,[92] W. Buttinger,[139] C. J. Buxo Vazquez,[104] A. R. Buzykaev,[118b,118a] G. Cabras,[21b] S. Cabrera Urbán,[169] D. Caforio,[54] H. Cai,[134] V. M. M. Cairo,[149] O. Cakir,[3a] N. Calace,[34] P. Calafiura,[16] G. Calderini,[131] P. Calfayan,[63] G. Callea,[55] L. P. Caloba,[78b] S. Calvente Lopez,[96] D. Calvet,[36] S. Calvet,[36] T. P. Calvet,[99] M. Calvetti,[69a,69b] R. Camacho Toro,[131] S. Camarda,[34] D. Camarero Munoz,[96] P. Camarri,[71a,71b] M. T. Camerlingo,[72a,72b] D. Cameron,[129] C. Camincher,[171] M. Campanelli,[92] A. Camplani,[38] V. Canale,[67a,67b] A. Canesse,[101] M. Cano Bret,[75] J. Cantero,[125] Y. Cao,[168] F. Capocasa,[24] M. Capua,[39b,39a] A. Carbone,[66a,66b] R. Cardarelli,[71a] J. C. J. Cardenas,[7] F. Cardillo,[169] G. Carducci,[39b,39a] T. Carli,[34] G. Carlino,[67a] B. T. Carlson,[134] E. M. Carlson,[171,163a] L. Carminati,[66a,66b] M. Carnesale,[70a,70b] R. M. D. Carney,[149] S. Caron,[115] E. Carquin,[142d] S. Carrá,[44] G. Carratta,[21b,21a] J. W. S. Carter,[162] T. M. Carter,[48] D. Casadei,[31c] M. P. Casado,[12,h] A. F. Casha,[162] E. G. Castiglia,[178] F. L. Castillo,[59a] L. Castillo Garcia,[12] V. Castillo Gimenez,[169] N. F. Castro,[135a,135e] A. Catinaccio,[34] J. R. Catmore,[129] A. Cattai,[34] V. Cavaliere,[27] N. Cavalli,[21b,21a] V. Cavasinni,[69a,69b] E. Celebi,[11b] F. Celli,[130]

M. S. Centonze,[65a,65b] K. Cerny,[126] A. S. Cerqueira,[78a] A. Cerri,[152] L. Cerrito,[71a,71b] F. Cerutti,[16] A. Cervelli,[21b] S. A. Cetin,[11b] Z. Chadi,[33a] D. Chakraborty,[117] M. Chala,[135f] J. Chan,[176] W. S. Chan,[116] W. Y. Chan,[88] J. D. Chapman,[30] B. Chargeishvili,[155b] D. G. Charlton,[19] T. P. Charman,[90] M. Chatterjee,[18] S. Chekanov,[5] S. V. Chekulaev,[163a] G. A. Chelkov,[77,i] A. Chen,[103] B. Chen,[157] C. Chen,[58a] C. H. Chen,[76] H. Chen,[13c] H. Chen,[27] J. Chen,[58c] J. Chen,[24] S. Chen,[132] S. J. Chen,[13c] X. Chen,[58c] X. Chen,[13b] Y. Chen,[58a] Y-H. Chen,[44] C. L. Cheng,[176] H. C. Cheng,[60a] A. Cheplakov,[77] E. Cheremushkina,[44] E. Cherepanova,[77] R. Cherkaoui El Moursli,[33e] E. Cheu,[6] K. Cheung,[61] L. Chevalier,[140] V. Chiarella,[49] G. Chiarelli,[69a] G. Chiodini,[65a] A. S. Chisholm,[19] A. Chitan,[25b] Y. H. Chiu,[171] M. V. Chizhov,[77,j] K. Choi,[10] A. R. Chomont,[70a,70b] Y. Chou,[100] Y. S. Chow,[116] L. D. Christopher,[31f] M. C. Chu,[60a] X. Chu,[13a,13d] J. Chudoba,[136] J. J. Chwastowski,[82] D. Cieri,[112] K. M. Ciesla,[82] V. Cindro,[89] I. A. Cioară,[25b] A. Ciocio,[16] F. Cirotto,[67a,67b] Z. H. Citron,[175,k] M. Citterio,[66a] D. A. Ciubotaru,[25b] B. M. Ciungu,[162] A. Clark,[52] P. J. Clark,[48] J. M. Clavijo Columbie,[44] S. E. Clawson,[98] C. Clement,[43a,43b] L. Clissa,[21b,21a] Y. Coadou,[99] M. Cobal,[64a,64c] A. Coccaro,[53b] J. Cochran,[76] R. F. Coelho Barrue,[135a] R. Coelho Lopes De Sa,[100] S. Coelli,[66a] H. Cohen,[157] A. E. C. Coimbra,[34] B. Cole,[37] J. Collot,[56] P. Conde Muiño,[135a,135h] S. H. Connell,[31c] I. A. Connelly,[55] E. I. Conroy,[130] F. Conventi,[67a,l] H. G. Cooke,[19] A. M. Cooper-Sarkar,[130] F. Cormier,[170] L. D. Corpe,[34] M. Corradi,[70a,70b] E. E. Corrigan,[94] F. Corriveau,[101,m] M. J. Costa,[169] F. Costanza,[4] D. Costanzo,[145] B. M. Cote,[123] G. Cowan,[91] J. W. Cowley,[30] K. Cranmer,[121] S. Crépé-Renaudin,[56] F. Crescioli,[131] M. Cristinziani,[147] M. Cristoforetti,[73a,73b,n] V. Croft,[165] G. Crosetti,[39b,39a] A. Cueto,[34] T. Cuhadar Donszelmann,[166] H. Cui,[13a,13d] A. R. Cukierman,[149] W. R. Cunningham,[55] P. Czodrowski,[34] M. M. Czurylo,[59b] M. J. Da Cunha Sargedas De Sousa,[58a] J. V. Da Fonseca Pinto,[78b] C. Da Via,[98] W. Dabrowski,[81a] T. Dado,[45] S. Dahbi,[31f] T. Dai,[103] C. Dallapiccola,[100] M. Dam,[38] G. D'amen,[27] V. D'Amico,[72a,72b] J. Damp,[97] J. R. Dandoy,[132] M. F. Daneri,[28] M. Danninger,[148] V. Dao,[34] G. Darbo,[53b] S. Darmora,[5] A. Dattagupta,[127] S. D'Auria,[66a,66b] C. David,[163b] T. Davidek,[138] D. R. Davis,[47] B. Davis-Purcell,[32] I. Dawson,[90] K. De,[7] R. De Asmundis,[67a] M. De Beurs,[116] S. De Castro,[21b,21a] N. De Groot,[115] P. de Jong,[116] H. De la Torre,[104] A. De Maria,[13c] D. De Pedis,[70a] A. De Salvo,[70a] U. De Sanctis,[71a,71b] M. De Santis,[71a,71b] A. De Santo,[152] J. B. De Vivie De Regie,[56] D. V. Dedovich,[77] J. Degens,[116] A. M. Deiana,[40] J. Del Peso,[96] Y. Delabat Diaz,[44] F. Deliot,[140] C. M. Delitzsch,[6] M. Della Pietra,[67a,67b] D. Della Volpe,[52] A. Dell'Acqua,[34] L. Dell'Asta,[66a,66b] M. Delmastro,[4] P. A. Delsart,[56] S. Demers,[178] M. Demichev,[77] S. P. Denisov,[119] L. D'Eramo,[117] D. Derendarz,[82] J. E. Derkaoui,[33d] F. Derue,[131] P. Dervan,[88] K. Desch,[22] K. Dette,[162] C. Deutsch,[22] P. O. Deviveiros,[34] F. A. Di Bello,[70a,70b] A. Di Ciaccio,[71a,71b] L. Di Ciaccio,[4] C. Di Donato,[67a,67b] A. Di Girolamo,[34] G. Di Gregorio,[69a,69b] A. Di Luca,[73a,73b] B. Di Micco,[72a,72b] R. Di Nardo,[72a,72b] C. Diaconu,[99] F. A. Dias,[116] T. Dias Do Vale,[135a] M. A. Diaz,[142a] F. G. Diaz Capriles,[22] J. Dickinson,[16] M. Didenko,[169] E. B. Diehl,[103] J. Dietrich,[17] S. Díez Cornell,[44] C. Diez Pardos,[147] A. Dimitrievska,[16] W. Ding,[13b] J. Dingfelder,[22] I-M. Dinu,[25b] S. J. Dittmeier,[59b] F. Dittus,[34] F. Djama,[99] T. Djobava,[155b] J. I. Djuvsland,[15] M. A. B. Do Vale,[143] D. Dodsworth,[24] C. Doglioni,[94] J. Dolejsi,[138] Z. Dolezal,[138] M. Donadelli,[78c] B. Dong,[58c] J. Donini,[36] A. D'onofrio,[13c] M. D'Onofrio,[88] J. Dopke,[139] A. Doria,[67a] M. T. Dova,[86] A. T. Doyle,[55] E. Drechsler,[148] E. Dreyer,[148] T. Dreyer,[51] A. S. Drobac,[165] D. Du,[58b] T. A. du Pree,[116] F. Dubinin,[108] M. Dubovsky,[26a] A. Dubreuil,[52] E. Duchovni,[175] G. Duckeck,[111] O. A. Ducu,[34,25b] D. Duda,[112] A. Dudarev,[34] M. D'uffizi,[98] L. Duflot,[62] M. Dührssen,[34] C. Dülsen,[177] A. E. Dumitriu,[25b] M. Dunford,[59a] S. Dungs,[45] K. Dunne,[43a,43b] A. Duperrin,[99] H. Duran Yildiz,[3a] M. Düren,[54] A. Durglishvili,[155b] B. Dutta,[44] G. I. Dyckes,[132] M. Dyndal,[81a] S. Dysch,[98] B. S. Dziedzic,[82] B. Eckerova,[26a] M. G. Eggleston,[47] E. Egidio Purcino De Souza,[78b] L. F. Ehrke,[52] T. Eifert,[7] G. Eigen,[15] K. Einsweiler,[16] T. Ekelof,[167] Y. El Ghazali,[33b] H. El Jarrari,[33e] A. El Moussaouy,[33a] V. Ellajosyula,[167] M. Ellert,[167] F. Ellinghaus,[177] A. A. Elliot,[90] N. Ellis,[34] J. Elmsheuser,[27] M. Elsing,[34] D. Emeliyanov,[139] A. Emerman,[37] Y. Enari,[159] J. Erdmann,[45] A. Ereditato,[18] P. A. Erland,[82] M. Errenst,[177] M. Escalier,[62] C. Escobar,[169] O. Estrada Pastor,[169] E. Etzion,[157] G. Evans,[135a] H. Evans,[63] M. O. Evans,[152] A. Ezhilov,[133] F. Fabbri,[55] L. Fabbri,[21b,21a] V. Fabiani,[115] G. Facini,[173] V. Fadeyev,[141] R. M. Fakhrutdinov,[119] S. Falciano,[70a] P. J. Falke,[22] S. Falke,[34] J. Faltova,[138] Y. Fan,[13a] Y. Fang,[13a] Y. Fang,[13a] G. Fanourakis,[42] M. Fanti,[66a,66b] M. Faraj,[58c] A. Farbin,[7] A. Farilla,[72a] E. M. Farina,[68a,68b] T. Farooque,[104] S. M. Farrington,[48] P. Farthouat,[34] F. Fassi,[33e] D. Fassouliotis,[8] M. Faucci Giannelli,[71a,71b] W. J. Fawcett,[30] L. Fayard,[62] O. L. Fedin,[133,o] M. Feickert,[168] L. Feligioni,[99] A. Fell,[145] C. Feng,[58b] M. Feng,[13b] M. J. Fenton,[166] A. B. Fenyuk,[119] S. W. Ferguson,[41] J. Ferrando,[44] A. Ferrari,[167] P. Ferrari,[116] R. Ferrari,[68a] D. Ferrere,[52] C. Ferretti,[103] F. Fiedler,[97] A. Filipčič,[89] F. Filthaut,[115] M. C. N. Fiolhais,[135a,135c,p] L. Fiorini,[169] F. Fischer,[147] W. C. Fisher,[104] T. Fitschen,[19] I. Fleck,[147] P. Fleischmann,[103] T. Flick,[177] B. M. Flierl,[111] L. Flores,[132] L. R. Flores Castillo,[60a] F. M. Follega,[73a,73b] N. Fomin,[15] J. H. Foo,[162] B. C. Forland,[63] A. Formica,[140] F. A. Förster,[12] A. C. Forti,[98] E. Fortin,[99] M. G. Foti,[130] D. Fournier,[62] H. Fox,[87] P. Francavilla,[69a,69b] S. Francescato,[57]

M. Franchini,[21b,21a] S. Franchino,[59a] D. Francis,[34] L. Franco,[4] L. Franconi,[18] M. Franklin,[57] G. Frattari,[70a,70b] A. C. Freegard,[90] P. M. Freeman,[19] W. S. Freund,[78b] E. M. Freundlich,[45] D. Froidevaux,[34] J. A. Frost,[130] Y. Fu,[58a] M. Fujimoto,[122] E. Fullana Torregrosa,[169] J. Fuster,[169] A. Gabrielli,[21b,21a] A. Gabrielli,[34] P. Gadow,[44] G. Gagliardi,[53b,53a] L. G. Gagnon,[16] G. E. Gallardo,[130] E. J. Gallas,[130] B. J. Gallop,[139] R. Gamboa Goni,[90] K. K. Gan,[123] S. Ganguly,[175] J. Gao,[58a] Y. Gao,[48] Y. S. Gao,[29,q] F. M. Garay Walls,[142a] C. García,[169] J. E. García Navarro,[169] J. A. García Pascual,[13a] M. Garcia-Sciveres,[16] R. W. Gardner,[35] D. Garg,[75] S. Gargiulo,[50] C. A. Garner,[162] V. Garonne,[129] S. J. Gasiorowski,[144] P. Gaspar,[78b] G. Gaudio,[68a] P. Gauzzi,[70a,70b] I. L. Gavrilenko,[108] A. Gavrilyuk,[120] C. Gay,[170] G. Gaycken,[44] E. N. Gazis,[9] A. A. Geanta,[25b] C. M. Gee,[141] C. N. P. Gee,[139] J. Geisen,[94] M. Geisen,[97] C. Gemme,[53b] M. H. Genest,[56] S. Gentile,[70a,70b] S. George,[91] W. F. George,[19] T. Geralis,[42] L. O. Gerlach,[51] P. Gessinger-Befurt,[34] M. Ghasemi Bostanabad,[171] M. Ghneimat,[147] A. Ghosh,[166] A. Ghosh,[75] B. Giacobbe,[21b] S. Giagu,[70a,70b] N. Giangiacomi,[162] P. Giannetti,[69a] A. Giannini,[67a,67b] S. M. Gibson,[91] M. Gignac,[141] D. T. Gil,[81b] B. J. Gilbert,[37] D. Gillberg,[32] G. Gilles,[116] N. E. K. Gillwald,[44] D. M. Gingrich,[2,e] M. P. Giordani,[64a,64c] P. F. Giraud,[140] G. Giugliarelli,[64a,64c] D. Giugni,[66a] F. Giuli,[71a,71b] I. Gkialas,[8,r] P. Gkountoumis,[9] L. K. Gladilin,[110] C. Glasman,[96] G. R. Gledhill,[127] M. Glisic,[127] I. Gnesi,[39b,s] M. Goblirsch-Kolb,[24] D. Godin,[107] S. Goldfarb,[102] T. Golling,[52] D. Golubkov,[119] J. P. Gombas,[104] A. Gomes,[135a,135b] R. Goncalves Gama,[51] R. Gonçalo,[135a,135c] G. Gonella,[127] L. Gonella,[19] A. Gongadze,[77] F. Gonnella,[19] J. L. Gonski,[37] S. González de la Hoz,[169] S. Gonzalez Fernandez,[12] R. Gonzalez Lopez,[88] C. Gonzalez Renteria,[16] R. Gonzalez Suarez,[167] S. Gonzalez-Sevilla,[52] G. R. Gonzalvo Rodriguez,[169] R. Y. González Andana,[142a] L. Goossens,[34] N. A. Gorasia,[19] P. A. Gorbounov,[120] H. A. Gordon,[27] B. Gorini,[34] E. Gorini,[65a,65b] A. Gorišek,[89] A. T. Goshaw,[47] M. I. Gostkin,[77] C. A. Gottardo,[115] M. Gouighri,[33b] V. Goumarre,[44] A. G. Goussiou,[144] N. Govender,[31c] C. Goy,[4] I. Grabowska-Bold,[81a] K. Graham,[32] E. Gramstad,[129] S. Grancagnolo,[17] M. Grandi,[152] V. Gratchev,[133] P. M. Gravila,[25f] F. G. Gravili,[65a,65b] H. M. Gray,[16] C. Grefe,[22] I. M. Gregor,[44] P. Grenier,[149] K. Grevtsov,[44] C. Grieco,[12] N. A. Grieser,[124] A. A. Grillo,[141] K. Grimm,[29,t] S. Grinstein,[12,u] J.-F. Grivaz,[62] S. Groh,[97] E. Gross,[175] J. Grosse-Knetter,[51] C. Grud,[103] A. Grummer,[114] J. C. Grundy,[130] L. Guan,[103] W. Guan,[176] C. Gubbels,[170] J. Guenther,[34] J. G. R. Guerrero Rojas,[169] F. Guescini,[112] D. Guest,[17] R. Gugel,[97] A. Guida,[44] T. Guillemin,[4] S. Guindon,[34] J. Guo,[58c] L. Guo,[62] Y. Guo,[103] R. Gupta,[44] S. Gurbuz,[22] G. Gustavino,[124] M. Guth,[52] P. Gutierrez,[124] L. F. Gutierrez Zagazeta,[132] C. Gutschow,[92] C. Guyot,[140] C. Gwenlan,[130] C. B. Gwilliam,[88] E. S. Haaland,[129] A. Haas,[121] M. Habedank,[17] C. Haber,[16] H. K. Hadavand,[7] A. Hadef,[97] S. Hadzic,[112] M. Haleem,[172] J. Haley,[125] J. J. Hall,[145] G. Halladjian,[104] G. D. Hallewell,[99] L. Halser,[18] K. Hamano,[171] H. Hamdaoui,[33e] M. Hamer,[22] G. N. Hamity,[48] K. Han,[58a] L. Han,[13c] L. Han,[58a] S. Han,[16] Y. F. Han,[162] K. Hanagaki,[79,v] M. Hance,[141] M. D. Hank,[35] R. Hankache,[98] E. Hansen,[94] J. B. Hansen,[38] J. D. Hansen,[38] M. C. Hansen,[22] P. H. Hansen,[38] K. Hara,[164] T. Harenberg,[177] S. Harkusha,[105] Y. T. Harris,[130] P. F. Harrison,[173] N. M. Hartman,[149] N. M. Hartmann,[111] Y. Hasegawa,[146] A. Hasib,[48] S. Hassani,[140] S. Haug,[18] R. Hauser,[104] M. Havranek,[137] C. M. Hawkes,[19] R. J. Hawkings,[34] S. Hayashida,[113] D. Hayden,[104] C. Hayes,[103] R. L. Hayes,[170] C. P. Hays,[130] J. M. Hays,[90] H. S. Hayward,[88] S. J. Haywood,[139] F. He,[58a] Y. He,[160] Y. He,[131] M. P. Heath,[48] V. Hedberg,[94] A. L. Heggelund,[129] N. D. Hehir,[90] C. Heidegger,[50] K. K. Heidegger,[50] W. D. Heidorn,[76] J. Heilman,[32] S. Heim,[44] T. Heim,[16] B. Heinemann,[44,w] J. G. Heinlein,[132] J. J. Heinrich,[127] L. Heinrich,[34] J. Hejbal,[136] L. Helary,[44] A. Held,[121] S. Hellesund,[129] C. M. Helling,[141] S. Hellman,[43a,43b] C. Helsens,[34] R. C. W. Henderson,[87] L. Henkelmann,[30] A. M. Henriques Correia,[34] H. Herde,[149] Y. Hernández Jiménez,[151] H. Herr,[97] M. G. Herrmann,[111] T. Herrmann,[46] G. Herten,[50] R. Hertenberger,[111] L. Hervas,[34] N. P. Hessey,[163a] H. Hibi,[80] S. Higashino,[79] E. Higón-Rodriguez,[169] K. K. Hill,[27] K. H. Hiller,[44] S. J. Hillier,[19] M. Hils,[46] I. Hinchliffe,[16] F. Hinterkeuser,[22] M. Hirose,[128] S. Hirose,[164] D. Hirschbuehl,[177] B. Hiti,[89] O. Hladik,[136] J. Hobbs,[151] R. Hobincu,[25e] N. Hod,[175] M. C. Hodgkinson,[145] B. H. Hodkinson,[30] A. Hoecker,[34] J. Hofer,[44] D. Hohn,[50] T. Holm,[22] T. R. Holmes,[35] M. Holzbock,[112] L. B. A. H. Hommels,[30] B. P. Honan,[98] J. Hong,[58c] T. M. Hong,[134] J. C. Honig,[50] A. Hönle,[112] B. H. Hooberman,[168] W. H. Hopkins,[5] Y. Horii,[113] L. A. Horyn,[35] S. Hou,[154] J. Howarth,[55] J. Hoya,[86] M. Hrabovsky,[126] A. Hrynevich,[106] T. Hryn'ova,[4] P. J. Hsu,[61] S.-C. Hsu,[144] Q. Hu,[37] S. Hu,[58c] Y. F. Hu,[13a,13d,x] D. P. Huang,[92] X. Huang,[13c] Y. Huang,[58a] Y. Huang,[13a] Z. Hubacek,[137] F. Hubaut,[99] M. Huebner,[22] F. Huegging,[22] T. B. Huffman,[130] M. Huhtinen,[34] R. Hulsken,[56] N. Huseynov,[77,y] J. Huston,[104] J. Huth,[57] R. Hyneman,[149] S. Hyrych,[26a] G. Iacobucci,[52] G. Iakovidis,[27] I. Ibragimov,[147] L. Iconomidou-Fayard,[62] P. Iengo,[34] R. Iguchi,[159] T. Iizawa,[52] Y. Ikegami,[79] A. Ilg,[18] N. Ilic,[162] H. Imam,[33a] T. Ingebretsen Carlson,[43a,43b] G. Introzzi,[68a,68b] M. Iodice,[72a] V. Ippolito,[70a,70b] M. Ishino,[159] W. Islam,[125] C. Issever,[17,44] S. Istin,[11c,z] J. M. Iturbe Ponce,[60a] R. Iuppa,[73a,73b] A. Ivina,[175] J. M. Izen,[41] V. Izzo,[67a] P. Jacka,[136] P. Jackson,[1] R. M. Jacobs,[44] B. P. Jaeger,[148] C. S. Jagfeld,[111] G. Jäkel,[177] K. Jakobs,[50] T. Jakoubek,[175] J. Jamieson,[55] K. W. Janas,[81a]

G. Jarlskog,[94] A. E. Jaspan,[88] N. Javadov,[77,y] T. Javůrek,[34] M. Javurkova,[100] F. Jeanneau,[140] L. Jeanty,[127] J. Jejelava,[155a,aa] P. Jenni,[50,bb] S. Jézéquel,[4] J. Jia,[151] Z. Jia,[13c] Y. Jiang,[58a] S. Jiggins,[50] J. Jimenez Pena,[112] S. Jin,[13c] A. Jinaru,[25b] O. Jinnouchi,[160] H. Jivan,[31f] P. Johansson,[145] K. A. Johns,[6] C. A. Johnson,[63] D. M. Jones,[30] E. Jones,[173] R. W. L. Jones,[87] T. J. Jones,[88] J. Jovicevic,[51] X. Ju,[16] J. J. Junggeburth,[34] A. Juste Rozas,[12,u] S. Kabana,[142c] A. Kaczmarska,[82] M. Kado,[70a,70b] H. Kagan,[123] M. Kagan,[149] A. Kahn,[37] C. Kahra,[97] T. Kaji,[174] E. Kajomovitz,[156] C. W. Kalderon,[27] A. Kamenshchikov,[119] M. Kaneda,[159] N. J. Kang,[141] S. Kang,[76] Y. Kano,[113] J. Kanzaki,[79] D. Kar,[31f] K. Karava,[130] M. J. Kareem,[163b] I. Karkanias,[158] S. N. Karpov,[77] Z. M. Karpova,[77] V. Kartvelishvili,[87] A. N. Karyukhin,[119] E. Kasimi,[158] C. Kato,[58d] J. Katzy,[44] K. Kawade,[146] K. Kawagoe,[85] T. Kawaguchi,[113] T. Kawamoto,[140] G. Kawamura,[51] E. F. Kay,[171] F. I. Kaya,[165] S. Kazakos,[12] V. F. Kazanin,[118b,118a] Y. Ke,[151] J. M. Keaveney,[31a] R. Keeler,[171] J. S. Keller,[32] D. Kelsey,[152] J. J. Kempster,[19] J. Kendrick,[19] K. E. Kennedy,[37] O. Kepka,[136] S. Kersten,[177] B. P. Kerševan,[89] S. Ketabchi Haghighat,[162] M. Khandoga,[131] A. Khanov,[125] A. G. Kharlamov,[118b,118a] T. Kharlamova,[118b,118a] E. E. Khoda,[144] T. J. Khoo,[17] G. Khoriauli,[172] E. Khramov,[77] J. Khubua,[155b] S. Kido,[80] M. Kiehn,[34] A. Kilgallon,[127] E. Kim,[160] Y. K. Kim,[35] N. Kimura,[92] A. Kirchhoff,[51] D. Kirchmeier,[46] C. Kirfel,[22] J. Kirk,[139] A. E. Kiryunin,[112] T. Kishimoto,[159] D. P. Kisliuk,[162] V. Kitali,[44] C. Kitsaki,[9] O. Kivernyk,[22] T. Klapdor-Kleingrothaus,[50] M. Klassen,[59a] C. Klein,[32] L. Klein,[172] M. H. Klein,[103] M. Klein,[88] U. Klein,[88] P. Klimek,[34] A. Klimentov,[27] F. Klimpel,[34] T. Klingl,[22] T. Klioutchnikova,[34] F. F. Klitzner,[111] P. Kluit,[116] S. Kluth,[112] E. Kneringer,[74] T. M. Knight,[162] A. Knue,[50] D. Kobayashi,[85] M. Kobel,[46] M. Kocian,[149] T. Kodama,[159] P. Kodys,[138] D. M. Koeck,[152] P. T. Koenig,[22] T. Koffas,[32] N. M. Köhler,[34] M. Kolb,[140] I. Koletsou,[4] T. Komarek,[126] K. Köneke,[50] A. X. Y. Kong,[1] T. Kono,[122] V. Konstantinides,[92] N. Konstantinidis,[92] B. Konya,[94] R. Kopeliansky,[63] S. Koperny,[81a] K. Korcyl,[82] K. Kordas,[158] G. Koren,[157] A. Korn,[92] S. Korn,[51] I. Korolkov,[12] E. V. Korolkova,[145] N. Korotkova,[110] B. Kortman,[116] O. Kortner,[112] S. Kortner,[112] W. H. Kostecka,[117] V. V. Kostyukhin,[145,161] A. Kotsokechagia,[62] A. Kotwal,[47] A. Koulouris,[34] A. Kourkoumeli-Charalampidi,[68a,68b] C. Kourkoumelis,[8] E. Kourlitis,[5] O. Kovanda,[152] R. Kowalewski,[171] W. Kozanecki,[140] A. S. Kozhin,[119] V. A. Kramarenko,[110] G. Kramberger,[89] D. Krasnopevtsev,[58a] M. W. Krasny,[131] A. Krasznahorkay,[34] J. A. Kremer,[97] J. Kretzschmar,[88] K. Kreul,[17] P. Krieger,[162] F. Krieter,[111] S. Krishnamurthy,[100] A. Krishnan,[59b] M. Krivos,[138] K. Krizka,[16] K. Kroeninger,[45] H. Kroha,[112] J. Kroll,[136] J. Kroll,[132] K. S. Krowpman,[104] U. Kruchonak,[77] H. Krüger,[22] N. Krumnack,[76] M. C. Kruse,[47] J. A. Krzysiak,[82] A. Kubota,[160] O. Kuchinskaia,[161] S. Kuday,[3b] D. Kuechler,[44] J. T. Kuechler,[44] S. Kuehn,[34] T. Kuhl,[44] V. Kukhtin,[77] Y. Kulchitsky,[105,cc] S. Kuleshov,[142b] M. Kumar,[31f] N. Kumari,[99] M. Kuna,[56] A. Kupco,[136] T. Kupfer,[45] O. Kuprash,[50] H. Kurashige,[80] L. L. Kurchaninov,[163a] Y. A. Kurochkin,[105] A. Kurova,[109] M. G. Kurth,[13a,13d] E. S. Kuwertz,[34] M. Kuze,[160] A. K. Kvam,[144] J. Kvita,[126] T. Kwan,[101] K. W. Kwok,[60a] C. Lacasta,[169] F. Lacava,[70a,70b] H. Lacker,[17] D. Lacour,[131] N. N. Lad,[92] E. Ladygin,[77] R. Lafaye,[4] B. Laforge,[131] T. Lagouri,[142c] S. Lai,[51] I. K. Lakomiec,[81a] N. Lalloue,[56] J. E. Lambert,[124] S. Lammers,[63] W. Lampl,[6] C. Lampoudis,[158] E. Lançon,[27] U. Landgraf,[50] M. P. J. Landon,[90] V. S. Lang,[50] J. C. Lange,[51] R. J. Langenberg,[100] A. J. Lankford,[166] F. Lanni,[27] K. Lantzsch,[22] A. Lanza,[68a] A. Lapertosa,[53b,53a] J. F. Laporte,[140] T. Lari,[66a] F. Lasagni Manghi,[21b] M. Lassnig,[34] V. Latonova,[136] T. S. Lau,[60a] A. Laudrain,[97] A. Laurier,[32] M. Lavorgna,[67a,67b] S. D. Lawlor,[91] Z. Lawrence,[98] M. Lazzaroni,[66a,66b] B. Le,[98] B. Leban,[89] A. Lebedev,[76] M. LeBlanc,[34] T. LeCompte,[5] F. Ledroit-Guillon,[56] A. C. A. Lee,[92] G. R. Lee,[15] L. Lee,[57] S. C. Lee,[154] S. Lee,[76] L. L. Leeuw,[31c] B. Lefebvre,[163a] H. P. Lefebvre,[91] M. Lefebvre,[171] C. Leggett,[16] K. Lehmann,[148] N. Lehmann,[18] G. Lehmann Miotto,[34] W. A. Leight,[44] A. Leisos,[158,dd] M. A. L. Leite,[78c] C. E. Leitgeb,[44] R. Leitner,[138] K. J. C. Leney,[40] T. Lenz,[22] S. Leone,[69a] C. Leonidopoulos,[48] A. Leopold,[131] C. Leroy,[107] R. Les,[104] C. G. Lester,[30] M. Levchenko,[133] J. Levêque,[4] D. Levin,[103] L. J. Levinson,[175] D. J. Lewis,[19] B. Li,[13b] B. Li,[58b] C. Li,[58a] C-Q. Li,[58c,58d] H. Li,[58a] H. Li,[58b] H. Li,[58b] J. Li,[58c] K. Li,[144] L. Li,[58c] M. Li,[13a,13d] Q. Y. Li,[58a] S. Li,[58d,58c,ee] T. Li,[58b] X. Li,[44] Y. Li,[44] Z. Li,[58b] Z. Li,[130] Z. Li,[101] Z. Li,[88] Z. Liang,[13a] M. Liberatore,[44] B. Liberti,[71a] K. Lie,[60c] K. Lin,[104] R. A. Linck,[63] R. E. Lindley,[6] J. H. Lindon,[2] A. Linss,[44] E. Lipeles,[132] A. Lipniacka,[15] T. M. Liss,[168,ff] A. Lister,[170] J. D. Little,[7] B. Liu,[13a] B. X. Liu,[148] J. B. Liu,[58a] J. K. K. Liu,[35] K. Liu,[58d,58c] M. Liu,[58a] M. Y. Liu,[58a] P. Liu,[13a] X. Liu,[58a] Y. Liu,[44] Y. Liu,[13c,13d] Y. L. Liu,[103] Y. W. Liu,[58a] M. Livan,[68a,68b] A. Lleres,[56] J. Llorente Merino,[148] S. L. Lloyd,[90] E. M. Lobodzinska,[44] P. Loch,[6] S. Loffredo,[71a,71b] T. Lohse,[17] K. Lohwasser,[145] M. Lokajicek,[136] J. D. Long,[168] I. Longarini,[70a,70b] L. Longo,[34] R. Longo,[168] I. Lopez Paz,[12] A. Lopez Solis,[44] J. Lorenz,[111] N. Lorenzo Martinez,[4] A. M. Lory,[111] A. Lösle,[50] X. Lou,[43a,43b] X. Lou,[13a] A. Lounis,[62] J. Love,[5] P. A. Love,[87] J. J. Lozano Bahilo,[169] G. Lu,[13a] M. Lu,[58a] S. Lu,[132] Y. J. Lu,[61] H. J. Lubatti,[144] C. Luci,[70a,70b] F. L. Lucio Alves,[13c] A. Lucotte,[56] F. Luehring,[63] I. Luise,[151] L. Luminari,[70a] O. Lundberg,[150] B. Lund-Jensen,[150] N. A. Luongo,[127] M. S. Lutz,[157] D. Lynn,[27] H. Lyons,[88] R. Lysak,[136] E. Lytken,[94] F. Lyu,[13a] V. Lyubushkin,[77] T. Lyubushkina,[77] H. Ma,[27] L. L. Ma,[58b] Y. Ma,[92] D. M. Mac Donell,[171] G. Maccarrone,[49]

C. M. Macdonald,[145] J. C. MacDonald,[145] R. Madar,[36] W. F. Mader,[46] M. Madugoda Ralalage Don,[125] N. Madysa,[46] J. Maeda,[80] T. Maeno,[27] M. Maerker,[46] V. Magerl,[50] J. Magro,[64a,64c] D. J. Mahon,[37] C. Maidantchik,[78b] A. Maio,[135a,135b,135d] K. Maj,[81a] O. Majersky,[26a] S. Majewski,[127] N. Makovec,[62] B. Malaescu,[131] Pa. Malecki,[82] V. P. Maleev,[133] F. Malek,[56] D. Malito,[39b,39a] U. Mallik,[75] C. Malone,[30] S. Maltezos,[9] S. Malyukov,[77] J. Mamuzic,[169] G. Mancini,[49] J. P. Mandalia,[90] I. Mandić,[89] L. Manhaes de Andrade Filho,[78a] I. M. Maniatis,[158] M. Manisha,[140] J. Manjarres Ramos,[46] K. H. Mankinen,[94] A. Mann,[111] A. Manousos,[74] B. Mansoulie,[140] I. Manthos,[158] S. Manzoni,[116] A. Marantis,[158,dd] G. Marchiori,[131] M. Marcisovsky,[136] L. Marcoccia,[71a,71b] C. Marcon,[94] M. Marjanovic,[124] Z. Marshall,[16] S. Marti-Garcia,[169] T. A. Martin,[173] V. J. Martin,[48] B. Martin dit Latour,[15] L. Martinelli,[70a,70b] M. Martinez,[12,u] P. Martinez Agullo,[169] V. I. Martinez Outschoorn,[100] S. Martin-Haugh,[139] V. S. Martoiu,[25b] A. C. Martyniuk,[92] A. Marzin,[34] S. R. Maschek,[112] L. Masetti,[97] T. Mashimo,[159] J. Masik,[98] A. L. Maslennikov,[118b,118a] L. Massa,[21b] P. Massarotti,[67a,67b] P. Mastrandrea,[69a,69b] A. Mastroberardino,[39b,39a] T. Masubuchi,[159] D. Matakias,[27] T. Mathisen,[167] A. Matic,[111] N. Matsuzawa,[159] J. Maurer,[25b] B. Maček,[89] D. A. Maximov,[118b,118a] R. Mazini,[154] I. Maznas,[158] S. M. Mazza,[141] C. Mc Ginn,[27] J. P. Mc Gowan,[101] S. P. Mc Kee,[103] T. G. McCarthy,[112] W. P. McCormack,[16] E. F. McDonald,[102] A. E. McDougall,[116] J. A. Mcfayden,[152] G. Mchedlidze,[155b] M. A. McKay,[40] K. D. McLean,[171] S. J. McMahon,[139] P. C. McNamara,[102] R. A. McPherson,[171,m] J. E. Mdhluli,[31f] Z. A. Meadows,[100] S. Meehan,[34] T. Megy,[36] S. Mehlhase,[111] A. Mehta,[88] B. Meirose,[41] D. Melini,[156] B. R. Mellado Garcia,[31f] A. H. Melo,[51] F. Meloni,[44] A. Melzer,[22] E. D. Mendes Gouveia,[135a] A. M. Mendes Jacques Da Costa,[19] H. Y. Meng,[162] L. Meng,[34] S. Menke,[112] M. Mentink,[34] E. Meoni,[39b,39a] C. Merlassino,[130] P. Mermod,[52,a] L. Merola,[67a,67b] C. Meroni,[66a] G. Merz,[103] O. Meshkov,[110,108] J. K. R. Meshreki,[147] J. Metcalfe,[5] A. S. Mete,[5] C. Meyer,[63] J-P. Meyer,[140] M. Michetti,[17] R. P. Middleton,[139] L. Mijović,[48] G. Mikenberg,[175] M. Mikestikova,[136] M. Mikuž,[89] H. Mildner,[145] A. Milic,[162] C. D. Milke,[40] D. W. Miller,[35] L. S. Miller,[32] A. Milov,[175] D. A. Milstead,[43a,43b] T. Min,[13c] A. A. Minaenko,[119] I. A. Minashvili,[155b] L. Mince,[55] A. I. Mincer,[121] B. Mindur,[81a] M. Mineev,[77] Y. Minegishi,[159] Y. Mino,[83] L. M. Mir,[12] M. Miralles Lopez,[169] M. Mironova,[130] T. Mitani,[174] V. A. Mitsou,[169] M. Mittal,[58c] O. Miu,[162] P. S. Miyagawa,[90] Y. Miyazaki,[85] A. Mizukami,[79] J. U. Mjörnmark,[94] T. Mkrtchyan,[59a] M. Mlynarikova,[117] T. Moa,[43a,43b] S. Mobius,[51] K. Mochizuki,[107] P. Moder,[44] P. Mogg,[111] A. F. Mohammed,[13a] S. Mohapatra,[37] G. Mokgatitswane,[31f] B. Mondal,[147] S. Mondal,[137] K. Mönig,[44] E. Monnier,[99] A. Montalbano,[148] J. Montejo Berlingen,[34] M. Montella,[123] F. Monticelli,[86] N. Morange,[62] A. L. Moreira De Carvalho,[135a] M. Moreno Llácer,[169] C. Moreno Martinez,[12] P. Morettini,[53b] M. Morgenstern,[156] S. Morgenstern,[173] D. Mori,[148] M. Morii,[57] M. Morinaga,[159] V. Morisbak,[129] A. K. Morley,[34] A. P. Morris,[92] L. Morvaj,[34] P. Moschovakos,[34] B. Moser,[116] M. Mosidze,[155b] T. Moskalets,[50] P. Moskvitina,[115] J. Moss,[29,gg] E. J. W. Moyse,[100] S. Muanza,[99] J. Mueller,[134] R. Mueller,[18] D. Muenstermann,[87] G. A. Mullier,[94] J. J. Mullin,[132] D. P. Mungo,[66a,66b] J. L. Munoz Martinez,[12] F. J. Munoz Sanchez,[98] M. Murin,[98] P. Murin,[26b] W. J. Murray,[173,139] A. Murrone,[66a,66b] J. M. Muse,[124] M. Muškinja,[16] C. Mwewa,[27] A. G. Myagkov,[119,i] A. J. Myers,[7] A. A. Myers,[134] G. Myers,[63] M. Myska,[137] B. P. Nachman,[16] O. Nackenhorst,[45] A. Nag Nag,[46] K. Nagai,[130] K. Nagano,[79] J. L. Nagle,[27] E. Nagy,[99] A. M. Nairz,[34] Y. Nakahama,[113] K. Nakamura,[79] H. Nanjo,[128] F. Napolitano,[59a] R. Narayan,[40] I. Naryshkin,[133] M. Naseri,[32] C. Nass,[22] T. Naumann,[44] G. Navarro,[20a] J. Navarro-Gonzalez,[169] R. Nayak,[157] P. Y. Nechaeva,[108] F. Nechansky,[44] T. J. Neep,[19] A. Negri,[68a,68b] M. Negrini,[21b] C. Nellist,[115] C. Nelson,[101] K. Nelson,[103] S. Nemecek,[136] M. Nessi,[34,hh] M. S. Neubauer,[168] F. Neuhaus,[97] J. Neundorf,[44] R. Newhouse,[170] P. R. Newman,[19] C. W. Ng,[134] Y. S. Ng,[17] Y. W. Y. Ng,[166] B. Ngair,[33e] H. D. N. Nguyen,[99] R. B. Nickerson,[130] R. Nicolaidou,[140] D. S. Nielsen,[38] J. Nielsen,[141] M. Niemeyer,[51] N. Nikiforou,[10] V. Nikolaenko,[119,i] I. Nikolic-Audit,[131] K. Nikolopoulos,[19] P. Nilsson,[27] H. R. Nindhito,[52] A. Nisati,[70a] N. Nishu,[2] R. Nisius,[112] T. Nitta,[174] T. Nobe,[159] D. L. Noel,[30] Y. Noguchi,[83] I. Nomidis,[131] M. A. Nomura,[27] M. B. Norfolk,[145] R. R. B. Norisam,[92] J. Novak,[89] T. Novak,[44] O. Novgorodova,[46] L. Novotny,[137] R. Novotny,[114] L. Nozka,[126] K. Ntekas,[166] E. Nurse,[92] F. G. Oakham,[32,e] J. Ocariz,[131] A. Ochi,[80] I. Ochoa,[135a] J. P. Ochoa-Ricoux,[142a] S. Oda,[85] S. Odaka,[79] S. Oerdek,[167] A. Ogrodnik,[81a] A. Oh,[98] C. C. Ohm,[150] H. Oide,[160] R. Oishi,[159] M. L. Ojeda,[162] Y. Okazaki,[83] M. W. O'Keefe,[88] Y. Okumura,[159] A. Olariu,[25b] L. F. Oleiro Seabra,[135a] S. A. Olivares Pino,[142c] D. Oliveira Damazio,[27] D. Oliveira Goncalves,[78a] J. L. Oliver,[166] M. J. R. Olsson,[166] A. Olszewski,[82] J. Olszowska,[82] Ö. O. Öncel,[22] D. C. O'Neil,[148] A. P. O'neill,[130] A. Onofre,[135a,135e] P. U. E. Onyisi,[10] R. G. Oreamuno Madriz,[117] M. J. Oreglia,[35] G. E. Orellana,[86] D. Orestano,[72a,72b] N. Orlando,[12] R. S. Orr,[162] V. O'Shea,[55] R. Ospanov,[58a] G. Otero y Garzon,[28] H. Otono,[85] P. S. Ott,[59a] G. J. Ottino,[16] M. Ouchrif,[33d] J. Ouellette,[27] F. Ould-Saada,[129] A. Ouraou,[140,a] Q. Ouyang,[13a] M. Owen,[55] R. E. Owen,[139] K. Y. Oyulmaz,[11c] V. E. Ozcan,[11c] N. Ozturk,[7] S. Ozturk,[11c] J. Pacalt,[126] H. A. Pacey,[30] K. Pachal,[47] A. Pacheco Pages,[12] C. Padilla Aranda,[12] S. Pagan Griso,[16] G. Palacino,[63] S. Palazzo,[48]

S. Palestini,[34] M. Palka,[81b] P. Palni,[81a] D. K. Panchal,[10] C. E. Pandini,[52] J. G. Panduro Vazquez,[91] P. Pani,[44] G. Panizzo,[64a,64c] L. Paolozzi,[52] C. Papadatos,[107] S. Parajuli,[40] A. Paramonov,[5] C. Paraskevopoulos,[9] D. Paredes Hernandez,[60b] S. R. Paredes Saenz,[130] B. Parida,[175] T. H. Park,[162] A. J. Parker,[29] M. A. Parker,[30] F. Parodi,[53b,53a] E. W. Parrish,[117] J. A. Parsons,[37] U. Parzefall,[50] L. Pascual Dominguez,[157] V. R. Pascuzzi,[16] F. Pasquali,[116] E. Pasqualucci,[70a] S. Passaggio,[53b] F. Pastore,[91] P. Pasuwan,[43a,43b] J. R. Pater,[98] A. Pathak,[176] J. Patton,[88] T. Pauly,[34] J. Pearkes,[149] M. Pedersen,[129] L. Pedraza Diaz,[115] R. Pedro,[135a] T. Peiffer,[51] S. V. Peleganchuk,[118b,118a] O. Penc,[136] C. Peng,[60b] H. Peng,[58a] M. Penzin,[161] B. S. Peralva,[78a] M. M. Perego,[62] A. P. Pereira Peixoto,[135a] L. Pereira Sanchez,[43a,43b] D. V. Perepelitsa,[27] E. Perez Codina,[163a] M. Perganti,[9] L. Perini,[66a,66b] H. Pernegger,[34] S. Perrella,[34] A. Perrevoort,[116] K. Peters,[44] R. F. Y. Peters,[98] B. A. Petersen,[34] T. C. Petersen,[38] E. Petit,[99] V. Petousis,[137] C. Petridou,[158] P. Petroff,[62] F. Petrucci,[72a,72b] M. Pettee,[178] N. E. Pettersson,[34] K. Petukhova,[138] A. Peyaud,[140] R. Pezoa,[142d] L. Pezzotti,[34] G. Pezzullo,[178] T. Pham,[102] P. W. Phillips,[139] M. W. Phipps,[168] G. Piacquadio,[151] E. Pianori,[16] F. Piazza,[66a,66b] A. Picazio,[100] R. Piegaia,[28] D. Pietreanu,[25b] J. E. Pilcher,[35] A. D. Pilkington,[98] M. Pinamonti,[64a,64c] J. L. Pinfold,[2] C. Pitman Donaldson,[92] D. A. Pizzi,[32] L. Pizzimento,[71a,71b] A. Pizzini,[116] M.-A. Pleier,[27] V. Plesanovs,[50] V. Pleskot,[138] E. Plotnikova,[77] P. Podberezko,[118b,118a] R. Poettgen,[94] R. Poggi,[52] L. Poggioli,[131] I. Pogrebnyak,[104] D. Pohl,[22] I. Pokharel,[51] G. Polesello,[68a] A. Poley,[148,163a] A. Policicchio,[70a,70b] R. Polifka,[138] A. Polini,[21b] C. S. Pollard,[130] Z. B. Pollock,[123] V. Polychronakos,[27] D. Ponomarenko,[109] L. Pontecorvo,[34] S. Popa,[25a] G. A. Popeneciu,[25d] L. Portales,[4] D. M. Portillo Quintero,[163a] S. Pospisil,[137] P. Postolache,[25c] K. Potamianos,[130] I. N. Potrap,[77] C. J. Potter,[30] H. Potti,[1] T. Poulsen,[44] J. Poveda,[169] T. D. Powell,[145] G. Pownall,[44] M. E. Pozo Astigarraga,[34] A. Prades Ibanez,[169] P. Pralavorio,[99] M. M. Prapa,[42] S. Prell,[76] D. Price,[98] M. Primavera,[65a] M. A. Principe Martin,[96] M. L. Proffitt,[144] N. Proklova,[109] K. Prokofiev,[60c] F. Prokoshin,[77] S. Protopopescu,[27] J. Proudfoot,[5] M. Przybycien,[81a] D. Pudzha,[133] P. Puzo,[62] D. Pyatiizbyantseva,[109] J. Qian,[103] Y. Qin,[98] T. Qiu,[90] A. Quadt,[51] M. Queitsch-Maitland,[34] G. Rabanal Bolanos,[57] F. Ragusa,[66a,66b] G. Rahal,[95] J. A. Raine,[52] S. Rajagopalan,[27] K. Ran,[13a,13d] D. F. Rassloff,[59a] D. M. Rauch,[44] S. Rave,[97] B. Ravina,[55] I. Ravinovich,[175] M. Raymond,[34] A. L. Read,[129] N. P. Readioff,[145] D. M. Rebuzzi,[68a,68b] G. Redlinger,[27] K. Reeves,[41] D. Reikher,[157] A. Reiss,[97] A. Rej,[147] C. Rembser,[34] A. Renardi,[44] M. Renda,[25b] M. B. Rendel,[112] A. G. Rennie,[55] S. Resconi,[66a] E. D. Resseguie,[16] S. Rettie,[92] B. Reynolds,[123] E. Reynolds,[19] M. Rezaei Estabragh,[177] O. L. Rezanova,[118b,118a] P. Reznicek,[138] E. Ricci,[73a,73b] R. Richter,[112] S. Richter,[44] E. Richter-Was,[81b] M. Ridel,[131] P. Rieck,[112] P. Riedler,[34] O. Rifki,[44] M. Rijssenbeek,[151] A. Rimoldi,[68a,68b] M. Rimoldi,[44] L. Rinaldi,[21b,21a] T. T. Rinn,[168] M. P. Rinnagel,[111] G. Ripellino,[150] I. Riu,[12] P. Rivadeneira,[44] J. C. Rivera Vergara,[171] F. Rizatdinova,[125] E. Rizvi,[90] C. Rizzi,[52] B. A. Roberts,[173] S. H. Robertson,[101,m] M. Robin,[44] D. Robinson,[30] C. M. Robles Gajardo,[142d] M. Robles Manzano,[97] A. Robson,[55] A. Rocchi,[71a,71b] C. Roda,[69a,69b] S. Rodriguez Bosca,[59a] A. Rodriguez Rodriguez,[50] A. M. Rodríguez Vera,[163b] S. Roe,[34] A. R. Roepe,[124] J. Roggel,[177] O. Røhne,[129] R. A. Rojas,[142d] B. Roland,[50] C. P. A. Roland,[63] J. Roloff,[27] A. Romaniouk,[109] M. Romano,[21b] A. C. Romero Hernandez,[168] N. Rompotis,[88] M. Ronzani,[121] L. Roos,[131] S. Rosati,[70a] B. J. Rosser,[132] E. Rossi,[162] E. Rossi,[4] E. Rossi,[67a,67b] L. P. Rossi,[53b] L. Rossini,[44] R. Rosten,[123] M. Rotaru,[25b] B. Rottler,[50] D. Rousseau,[62] D. Rousso,[30] G. Rovelli,[68a,68b] A. Roy,[10] A. Rozanov,[99] Y. Rozen,[156] X. Ruan,[31f] A. J. Ruby,[88] T. A. Ruggeri,[1] F. Rühr,[50] A. Ruiz-Martinez,[169] A. Rummler,[34] Z. Rurikova,[50] N. A. Rusakovich,[77] H. L. Russell,[34] L. Rustige,[36] J. P. Rutherfoord,[6] E. M. Rüttinger,[145] M. Rybar,[138] E. B. Rye,[129] A. Ryzhov,[119] J. A. Sabater Iglesias,[44] P. Sabatini,[169] L. Sabetta,[70a,70b] H. F-W. Sadrozinski,[141] R. Sadykov,[77] F. Safai Tehrani,[70a] B. Safarzadeh Samani,[152] M. Safdari,[149] P. Saha,[117] S. Saha,[101] M. Sahinsoy,[112] A. Sahu,[177] M. Saimpert,[140] M. Saito,[159] T. Saito,[159] D. Salamani,[34] G. Salamanna,[72a,72b] A. Salnikov,[149] J. Salt,[169] A. Salvador Salas,[12] D. Salvatore,[39b,39a] F. Salvatore,[152] A. Salzburger,[34] D. Sammel,[50] D. Sampsonidis,[158] D. Sampsonidou,[58d,58c] J. Sánchez,[169] A. Sanchez Pineda,[4] V. Sanchez Sebastian,[169] H. Sandaker,[129] C. O. Sander,[44] I. G. Sanderswood,[87] J. A. Sandesara,[100] M. Sandhoff,[177] C. Sandoval,[20b] D. P. C. Sankey,[139] M. Sannino,[53b,53a] Y. Sano,[113] A. Sansoni,[49] C. Santoni,[36] H. Santos,[135a,135b] S. N. Santpur,[16] A. Santra,[175] K. A. Saoucha,[145] A. Sapronov,[77] J. G. Saraiva,[135a,135d] O. Sasaki,[79] K. Sato,[164] C. Sauer,[59b] F. Sauerburger,[50] E. Sauvan,[4] P. Savard,[162,e] R. Sawada,[159] C. Sawyer,[139] L. Sawyer,[93] I. Sayago Galvan,[169] C. Sbarra,[21b] A. Sbrizzi,[64a,64c] T. Scanlon,[92] J. Schaarschmidt,[144] P. Schacht,[112] D. Schaefer,[35] U. Schäfer,[97] A. C. Schaffer,[62] D. Schaile,[111] R. D. Schamberger,[151] E. Schanet,[111] C. Scharf,[17] N. Scharmberg,[98] V. A. Schegelsky,[133] D. Scheirich,[138] F. Schenck,[17] M. Schernau,[166] C. Schiavi,[53b,53a] L. K. Schildgen,[22] Z. M. Schillaci,[24] E. J. Schioppa,[65a,65b] M. Schioppa,[39b,39a] B. Schlag,[97] K. E. Schleicher,[50] S. Schlenker,[34] K. Schmieden,[97] C. Schmitt,[97] S. Schmitt,[44] L. Schoeffel,[140] A. Schoening,[59b] P. G. Scholer,[50] E. Schopf,[130] M. Schott,[97] J. Schovancova,[34] S. Schramm,[52] F. Schroeder,[177] H-C. Schultz-Coulon,[59a] M. Schumacher,[50] B. A. Schumm,[141] Ph. Schune,[140] A. Schwartzman,[149]

T. A. Schwarz,[103] Ph. Schwemling,[140] R. Schwienhorst,[104] A. Sciandra,[141] G. Sciolla,[24] F. Scuri,[69a] F. Scutti,[102] C. D. Sebastiani,[88] K. Sedlaczek,[45] P. Seema,[17] S. C. Seidel,[114] A. Seiden,[141] B. D. Seidlitz,[27] T. Seiss,[35] C. Seitz,[44] J. M. Seixas,[78b] G. Sekhniaidze,[67a] S. J. Sekula,[40] L. P. Selem,[4] N. Semprini-Cesari,[21b,21a] S. Sen,[47] C. Serfon,[27] L. Serin,[62] L. Serkin,[64a,64b] M. Sessa,[72a,72b] H. Severini,[124] S. Sevova,[149] F. Sforza,[53b,53a] A. Sfyrla,[52] E. Shabalina,[51] R. Shaheen,[150] J. D. Shahinian,[132] N. W. Shaikh,[43a,43b] D. Shaked Renous,[175] L. Y. Shan,[13a] M. Shapiro,[16] A. Sharma,[34] A. S. Sharma,[1] S. Sharma,[44] P. B. Shatalov,[120] K. Shaw,[152] S. M. Shaw,[98] P. Sherwood,[92] L. Shi,[92] C. O. Shimmin,[178] Y. Shimogama,[174] J. D. Shinner,[91] I. P. J. Shipsey,[130] S. Shirabe,[52] M. Shiyakova,[77] J. Shlomi,[175] M. J. Shochet,[35] J. Shojaii,[102] D. R. Shope,[150] S. Shrestha,[123] E. M. Shrif,[31f] M. J. Shroff,[171] E. Shulga,[175] P. Sicho,[136] A. M. Sickles,[168] E. Sideras Haddad,[31f] O. Sidiropoulou,[34] A. Sidoti,[21b] F. Siegert,[46] Dj. Sijacki,[14] J. M. Silva,[19] M. V. Silva Oliveira,[34] S. B. Silverstein,[43a] S. Simion,[62] R. Simoniello,[34] S. Simsek,[11b] P. Sinervo,[162] V. Sinetckii,[110] S. Singh,[148] S. Singh,[162] S. Sinha,[44] S. Sinha,[31f] M. Sioli,[21b,21a] I. Siral,[127] S. Yu. Sivoklokov,[110] J. Sjölin,[43a,43b] A. Skaf,[51] E. Skorda,[94] P. Skubic,[124] M. Slawinska,[82] K. Sliwa,[165] V. Smakhtin,[175] B. H. Smart,[139] J. Smiesko,[138] S. Yu. Smirnov,[109] Y. Smirnov,[109] L. N. Smirnova,[110,ii] O. Smirnova,[94] E. A. Smith,[35] H. A. Smith,[130] M. Smizanska,[87] K. Smolek,[137] A. Smykiewicz,[82] A. A. Snesarev,[108] H. L. Snoek,[116] S. Snyder,[27] R. Sobie,[171,m] A. Soffer,[157] F. Sohns,[51] C. A. Solans Sanchez,[34] E. Yu. Soldatov,[109] U. Soldevila,[169] A. A. Solodkov,[119] S. Solomon,[50] A. Soloshenko,[77] O. V. Solovyanov,[119] V. Solovyev,[133] P. Sommer,[145] H. Son,[165] A. Sonay,[12] W. Y. Song,[163b] A. Sopczak,[137] A. L. Sopio,[92] F. Sopkova,[26b] S. Sottocornola,[68a,68b] R. Soualah,[64a,64c] A. M. Soukharev,[118b,118a] Z. Soumaimi,[33e] D. South,[44] S. Spagnolo,[65a,65b] M. Spalla,[112] M. Spangenberg,[173] F. Spanò,[91] D. Sperlich,[50] T. M. Spieker,[59a] G. Spigo,[34] M. Spina,[152] D. P. Spiteri,[55] M. Spousta,[138] A. Stabile,[66a,66b] B. L. Stamas,[117] R. Stamen,[59a] M. Stamenkovic,[116] A. Stampekis,[19] M. Standke,[22] E. Stanecka,[82] B. Stanislaus,[34] M. M. Stanitzki,[44] M. Stankaityte,[130] B. Stapf,[44] E. A. Starchenko,[119] G. H. Stark,[141] J. Stark,[99] D. M. Starko,[163b] P. Staroba,[136] P. Starovoitov,[59a] S. Stärz,[101] R. Staszewski,[82] G. Stavropoulos,[42] P. Steinberg,[27] A. L. Steinhebel,[127] B. Stelzer,[148,163a] H. J. Stelzer,[134] O. Stelzer-Chilton,[163a] H. Stenzel,[54] T. J. Stevenson,[152] G. A. Stewart,[34] M. C. Stockton,[34] G. Stoicea,[25b] M. Stolarski,[135a] S. Stonjek,[112] A. Straessner,[46] J. Strandberg,[150] S. Strandberg,[43a,43b] M. Strauss,[124] T. Strebler,[99] P. Strizenec,[26b] R. Ströhmer,[172] D. M. Strom,[127] L. R. Strom,[44] R. Stroynowski,[40] A. Strubig,[43a,43b] S. A. Stucci,[27] B. Stugu,[15] J. Stupak,[124] N. A. Styles,[44] D. Su,[149] S. Su,[58a] W. Su,[58d,144,58c] X. Su,[58a] N. B. Suarez,[134] K. Sugizaki,[159] V. V. Sulin,[108] M. J. Sullivan,[88] D. M. S. Sultan,[52] S. Sultansoy,[3c] T. Sumida,[83] S. Sun,[103] S. Sun,[176] X. Sun,[98] O. Sunneborn Gudnadottir,[167] C. J. E. Suster,[153] M. R. Sutton,[152] M. Svatos,[136] M. Swiatlowski,[163a] T. Swirski,[172] I. Sykora,[26a] M. Sykora,[138] T. Sykora,[138] D. Ta,[97] K. Tackmann,[44,jj] A. Taffard,[166] R. Tafirout,[163a] E. Tagiev,[119] R. H. M. Taibah,[131] R. Takashima,[84] K. Takeda,[80] T. Takeshita,[146] E. P. Takeva,[48] Y. Takubo,[79] M. Talby,[99] A. A. Talyshev,[118b,118a] K. C. Tam,[60b] N. M. Tamir,[157] A. Tanaka,[159] J. Tanaka,[159] R. Tanaka,[62] Z. Tao,[170] S. Tapia Araya,[76] S. Tapprogge,[97] A. Tarek Abouelfadl Mohamed,[104] S. Tarem,[156] K. Tariq,[58b] G. Tarna,[25b,kk] G. F. Tartarelli,[66a] P. Tas,[138] M. Tasevsky,[136] E. Tassi,[39b,39a] G. Tateno,[159] Y. Tayalati,[33e] G. N. Taylor,[102] W. Taylor,[163b] H. Teagle,[88] A. S. Tee,[176] R. Teixeira De Lima,[149] P. Teixeira-Dias,[91] H. Ten Kate,[34] J. J. Teoh,[116] K. Terashi,[159] J. Terron,[96] S. Terzo,[12] M. Testa,[49] R. J. Teuscher,[162,m] N. Themistokleous,[48] T. Theveneaux-Pelzer,[17] O. Thielmann,[177] D. W. Thomas,[91] J. P. Thomas,[19] E. A. Thompson,[44] P. D. Thompson,[19] E. Thomson,[132] E. J. Thorpe,[90] Y. Tian,[51] V. O. Tikhomirov,[108,ll] Yu. A. Tikhonov,[118b,118a] S. Timoshenko,[109] P. Tipton,[178] S. Tisserant,[99] S. H. Tlou,[31f] A. Tnourji,[36] K. Todome,[21b,21a] S. Todorova-Nova,[138] S. Todt,[46] M. Togawa,[79] J. Tojo,[85] S. Tokár,[26a] K. Tokushuku,[79] E. Tolley,[123] R. Tombs,[30] M. Tomoto,[79,113] L. Tompkins,[149] P. Tornambe,[100] E. Torrence,[127] H. Torres,[46] E. Torró Pastor,[169] M. Toscani,[28] C. Tosciri,[35] J. Toth,[99,mm] D. R. Tovey,[145] A. Traeet,[15] C. J. Treado,[121] T. Trefzger,[172] A. Tricoli,[27] I. M. Trigger,[163a] S. Trincaz-Duvoid,[131] D. A. Trischuk,[170] W. Trischuk,[162] B. Trocmé,[56] A. Trofymov,[62] C. Troncon,[66a] F. Trovato,[152] L. Truong,[31c] M. Trzebinski,[82] A. Trzupek,[82] F. Tsai,[151] A. Tsiamis,[158] P. V. Tsiareshka,[105,cc] A. Tsirigotis,[158,dd] V. Tsiskaridze,[151] E. G. Tskhadadze,[155a] M. Tsopoulou,[158] I. I. Tsukerman,[120] V. Tsulaia,[16] S. Tsuno,[79] O. Tsur,[156] D. Tsybychev,[151] Y. Tu,[60b] A. Tudorache,[25b] V. Tudorache,[25b] A. N. Tuna,[34] S. Turchikhin,[77] I. Turk Cakir,[3b,nn] R. J. Turner,[19] R. Turra,[66a] P. M. Tuts,[37] S. Tzamarias,[158] P. Tzanis,[9] E. Tzovara,[97] K. Uchida,[159] F. Ukegawa,[164] G. Unal,[34] M. Unal,[10] A. Undrus,[27] G. Unel,[166] F. C. Ungaro,[102] K. Uno,[159] J. Urban,[26b] P. Urquijo,[102] G. Usai,[7] R. Ushioda,[160] M. Usman,[107] Z. Uysal,[11d] V. Vacek,[137] B. Vachon,[101] K. O. H. Vadla,[129] T. Vafeiadis,[34] C. Valderanis,[111] E. Valdes Santurio,[43a,43b] M. Valente,[163a] S. Valentinetti,[21b,21a] A. Valero,[169] L. Valéry,[44] R. A. Vallance,[19] A. Vallier,[99] J. A. Valls Ferrer,[169] T. R. Van Daalen,[144] P. Van Gemmeren,[5] S. Van Stroud,[92] I. Van Vulpen,[116] M. Vanadia,[71a,71b] W. Vandelli,[34] M. Vandenbroucke,[140] E. R. Vandewall,[125] D. Vannicola,[157] L. Vannoli,[53b,53a] R. Vari,[70a] E. W. Varnes,[6] C. Varni,[16] T. Varol,[154] D. Varouchas,[62] K. E. Varvell,[153] M. E. Vasile,[25b]

L. Vaslin,[36] G. A. Vasquez,[171] F. Vazeille,[36] D. Vazquez Furelos,[12] T. Vazquez Schroeder,[34] J. Veatch,[51] V. Vecchio,[98] M. J. Veen,[116] I. Veliscek,[130] L. M. Veloce,[162] F. Veloso,[135a,135c] S. Veneziano,[70a] A. Ventura,[65a,65b] A. Verbytskyi,[112] M. Verducci,[69a,69b] C. Vergis,[22] M. Verissimo De Araujo,[78b] W. Verkerke,[116] A. T. Vermeulen,[116] J. C. Vermeulen,[116] C. Vernieri,[149] P. J. Verschuuren,[91] M. L. Vesterbacka,[121] M. C. Vetterli,[148,e] A. Vgenopoulos,[158] N. Viaux Maira,[142d] T. Vickey,[145] O. E. Vickey Boeriu,[145] G. H. A. Viehhauser,[130] L. Vigani,[59b] M. Villa,[21b,21a] M. Villaplana Perez,[169] E. M. Villhauer,[48] E. Vilucchi,[49] M. G. Vincter,[32] G. S. Virdee,[19] A. Vishwakarma,[48] C. Vittori,[21b,21a] I. Vivarelli,[152] V. Vladimirov,[173] E. Voevodina,[112] M. Vogel,[177] P. Vokac,[137] J. Von Ahnen,[44] S. E. von Buddenbrock,[31f] E. Von Toerne,[22] V. Vorobel,[138] K. Vorobev,[109] M. Vos,[169] J. H. Vossebeld,[88] M. Vozak,[98] L. Vozdecky,[90] N. Vranjes,[14] M. Vranjes Milosavljevic,[14] V. Vrba,[137,a] M. Vreeswijk,[116] N. K. Vu,[99] R. Vuillermet,[34] O. V. Vujinovic,[97] I. Vukotic,[35] S. Wada,[164] C. Wagner,[100] W. Wagner,[177] S. Wahdan,[177] H. Wahlberg,[86] R. Wakasa,[164] M. Wakida,[113] V. M. Walbrecht,[112] J. Walder,[139] R. Walker,[111] S. D. Walker,[91] W. Walkowiak,[147] A. M. Wang,[57] A. Z. Wang,[176] C. Wang,[58a] C. Wang,[58c] H. Wang,[16] J. Wang,[60a] P. Wang,[40] R.-J. Wang,[97] R. Wang,[57] R. Wang,[117] S. M. Wang,[154] S. Wang,[58b] T. Wang,[58a] W. T. Wang,[58a] W. X. Wang,[58a] X. Wang,[13c] X. Wang,[168] Y. Wang,[58a] Z. Wang,[103] C. Wanotayaroj,[34] A. Warburton,[101] C. P. Ward,[30] R. J. Ward,[19] N. Warrack,[55] A. T. Watson,[19] M. F. Watson,[19] G. Watts,[144] B. M. Waugh,[92] A. F. Webb,[10] C. Weber,[27] M. S. Weber,[18] S. A. Weber,[32] S. M. Weber,[59a] C. Wei,[58a] Y. Wei,[130] A. R. Weidberg,[130] J. Weingarten,[45] M. Weirich,[97] C. Weiser,[50] T. Wenaus,[27] B. Wendland,[45] T. Wengler,[34] S. Wenig,[34] N. Wermes,[22] M. Wessels,[59a] K. Whalen,[127] A. M. Wharton,[87] A. S. White,[57] A. White,[7] M. J. White,[1] D. Whiteson,[166] L. Wickremasinghe,[128] W. Wiedenmann,[176] C. Wiel,[46] M. Wielers,[139] N. Wieseotte,[97] C. Wiglesworth,[38] L. A. M. Wiik-Fuchs,[50] D. J. Wilbern,[124] H. G. Wilkens,[34] L. J. Wilkins,[91] D. M. Williams,[37] H. H. Williams,[132] S. Williams,[30] S. Willocq,[100] P. J. Windischhofer,[130] I. Wingerter-Seez,[4] F. Winklmeier,[127] B. T. Winter,[50] M. Wittgen,[149] M. Wobisch,[93] A. Wolf,[97] R. Wölker,[130] J. Wollrath,[166] M. W. Wolter,[82] H. Wolters,[135a,135c] V. W. S. Wong,[170] A. F. Wongel,[44] S. D. Worm,[44] B. K. Wosiek,[82] K. W. Woźniak,[82] K. Wraight,[55] J. Wu,[13a,13d] S. L. Wu,[176] X. Wu,[52] Y. Wu,[58a] Z. Wu,[140,58a] J. Wuerzinger,[130] T. R. Wyatt,[98] B. M. Wynne,[48] S. Xella,[38] M. Xia,[13b] J. Xiang,[60c] X. Xiao,[103] M. Xie,[58a] X. Xie,[58a] I. Xiotidis,[152] D. Xu,[13a] H. Xu,[58a] H. Xu,[58a] L. Xu,[58a] R. Xu,[132] W. Xu,[103] Y. Xu,[13b] Z. Xu,[58b] Z. Xu,[149] B. Yabsley,[153] S. Yacoob,[31a] N. Yamaguchi,[85] Y. Yamaguchi,[160] M. Yamatani,[159] H. Yamauchi,[164] T. Yamazaki,[16] Y. Yamazaki,[80] J. Yan,[58c] S. Yan,[130] Z. Yan,[23] H. J. Yang,[58c,58d] H. T. Yang,[16] S. Yang,[58a] T. Yang,[60c] X. Yang,[58a] X. Yang,[13a] Y. Yang,[159] Z. Yang,[103,58a] W-M. Yao,[16] Y. C. Yap,[44] H. Ye,[13c] J. Ye,[40] S. Ye,[27] I. Yeletskikh,[77] M. R. Yexley,[87] P. Yin,[37] K. Yorita,[174] K. Yoshihara,[76] C. J. S. Young,[50] C. Young,[149] R. Yuan,[58b,oo] X. Yue,[59a] M. Zaazoua,[33e] B. Zabinski,[82] G. Zacharis,[9] J. Zahreddine,[99] E. Zaid,[48] A. M. Zaitsev,[119,i] T. Zakareishvili,[155b] N. Zakharchuk,[32] S. Zambito,[34] D. Zanzi,[50] S. V. Zeißner,[45] C. Zeitnitz,[177] J. C. Zeng,[168] O. Zenin,[119] T. Ženiš,[26a] S. Zenz,[90] S. Zerradi,[33a] D. Zerwas,[62] M. Zgubič,[130] B. Zhang,[13c] D. F. Zhang,[13b] G. Zhang,[13b] J. Zhang,[5] K. Zhang,[13a] L. Zhang,[13c] M. Zhang,[168] R. Zhang,[176] S. Zhang,[103] X. Zhang,[58c] X. Zhang,[58b] Z. Zhang,[62] P. Zhao,[47] Y. Zhao,[141] Z. Zhao,[58a] A. Zhemchugov,[77] Z. Zheng,[149] D. Zhong,[168] B. Zhou,[103] C. Zhou,[176] H. Zhou,[6] N. Zhou,[58c] Y. Zhou,[6] C. G. Zhu,[58b] C. Zhu,[13a,13d] H. L. Zhu,[58a] H. Zhu,[13a] J. Zhu,[103] Y. Zhu,[58a] X. Zhuang,[13a] K. Zhukov,[108] V. Zhulanov,[118b,118a] D. Zieminska,[63] N. I. Zimine,[77] S. Zimmermann,[50,a] J. Zinsser,[59b] M. Ziolkowski,[147] L. Živković,[14] A. Zoccoli,[21b,21a] K. Zoch,[52] T. G. Zorbas,[145] O. Zormpa,[42] W. Zou,[37] and L. Zwalinski[34]

(ATLAS Collaboration)

[1]*Department of Physics, University of Adelaide, Adelaide, Australia*
[2]*Department of Physics, University of Alberta, Edmonton AB, Canada*
[3a]*Department of Physics, Ankara University, Ankara, Turkey*
[3b]*Istanbul Aydin University, Application and Research Center for Advanced Studies, Istanbul, Turkey*
[3c]*Division of Physics, TOBB University of Economics and Technology, Ankara, Turkey*
[4]*LAPP, Univ. Savoie Mont Blanc, CNRS/IN2P3, Annecy, France*
[5]*High Energy Physics Division, Argonne National Laboratory, Argonne, Illinois, USA*
[6]*Department of Physics, University of Arizona, Tucson, Arizona, USA*
[7]*Department of Physics, University of Texas at Arlington, Arlington, Texas, USA*
[8]*Physics Department, National and Kapodistrian University of Athens, Athens, Greece*
[9]*Physics Department, National Technical University of Athens, Zografou, Greece*
[10]*Department of Physics, University of Texas at Austin, Austin, Texas, USA*

[11a]*Bahcesehir University, Faculty of Engineering and Natural Sciences, Istanbul, Turkey*
[11b]*Istanbul Bilgi University, Faculty of Engineering and Natural Sciences, Istanbul, Turkey*
[11c]*Department of Physics, Bogazici University, Istanbul, Turkey*
[11d]*Department of Physics Engineering, Gaziantep University, Gaziantep, Turkey*
[12]*Institut de Física d'Altes Energies (IFAE), Barcelona Institute of Science and Technology, Barcelona, Spain*
[13a]*Institute of High Energy Physics, Chinese Academy of Sciences, Beijing, China*
[13b]*Physics Department, Tsinghua University, Beijing, China*
[13c]*Department of Physics, Nanjing University, Nanjing, China*
[13d]*University of Chinese Academy of Science (UCAS), Beijing, China*
[14]*Institute of Physics, University of Belgrade, Belgrade, Serbia*
[15]*Department for Physics and Technology, University of Bergen, Bergen, Norway*
[16]*Physics Division, Lawrence Berkeley National Laboratory and University of California, Berkeley, California, USA*
[17]*Institut für Physik, Humboldt Universität zu Berlin, Berlin, Germany*
[18]*Albert Einstein Center for Fundamental Physics and Laboratory for High Energy Physics, University of Bern, Bern, Switzerland*
[19]*School of Physics and Astronomy, University of Birmingham, Birmingham, United Kingdom*
[20a]*Facultad de Ciencias y Centro de Investigaciónes, Universidad Antonio Nariño, Bogotá, Colombia*
[20b]*Departamento de Física, Universidad Nacional de Colombia, Bogotá, Colombia, Colombia*
[21a]*Dipartimento di Fisica e Astronomia A. Righi, Università di Bologna, Bologna, Italy*
[21b]*INFN Sezione di Bologna, Italy*
[22]*Physikalisches Institut, Universität Bonn, Bonn, Germany*
[23]*Department of Physics, Boston University, Boston, Massachusetts, USA*
[24]*Department of Physics, Brandeis University, Waltham, Massachusetts, USA*
[25a]*Transilvania University of Brasov, Brasov, Romania*
[25b]*Horia Hulubei National Institute of Physics and Nuclear Engineering, Bucharest, Romania*
[25c]*Department of Physics, Alexandru Ioan Cuza University of Iasi, Iasi, Romania*
[25d]*National Institute for Research and Development of Isotopic and Molecular Technologies, Physics Department, Cluj-Napoca, Romania*
[25e]*University Politehnica Bucharest, Bucharest, Romania*
[25f]*West University in Timisoara, Timisoara, Romania*
[26a]*Faculty of Mathematics, Physics and Informatics, Comenius University, Bratislava, Slovak Republic*
[26b]*Department of Subnuclear Physics, Institute of Experimental Physics of the Slovak Academy of Sciences, Kosice, Slovak Republic*
[27]*Physics Department, Brookhaven National Laboratory, Upton, New York, USA*
[28]*Departamento de Física, Universidad de Buenos Aires, Buenos Aires, Argentina*
[29]*California State University, California, USA*
[30]*Cavendish Laboratory, University of Cambridge, Cambridge, United Kingdom*
[31a]*Department of Physics, University of Cape Town, Cape Town, South Africa*
[31b]*iThemba Labs, Western Cape, South Africa*
[31c]*Department of Mechanical Engineering Science, University of Johannesburg, Johannesburg, South Africa*
[31d]*National Institute of Physics, University of the Philippines Diliman (Philippines), Philippines*
[31e]*University of South Africa, Department of Physics, Pretoria, South Africa*
[31f]*School of Physics, University of the Witwatersrand, Johannesburg, South Africa*
[32]*Department of Physics, Carleton University, Ottawa, Ontario, Canada*
[33a]*Faculté des Sciences Ain Chock, Réseau Universitaire de Physique des Hautes Energies—Université Hassan II, Casablanca, Morocco*
[33b]*Faculté des Sciences, Université Ibn-Tofail, Kénitra, Morocco*
[33c]*Faculté des Sciences Semlalia, Université Cadi Ayyad, LPHEA-Marrakech, Morocco*
[33d]*LPMR, Faculté des Sciences, Université Mohamed Premier, Oujda, Morocco*
[33e]*Faculté des sciences, Université Mohammed V, Rabat, Morocco*
[33f]*Mohammed VI Polytechnic University, Ben Guerir, Morocco*
[34]*CERN, Geneva, Switzerland*
[35]*Enrico Fermi Institute, University of Chicago, Chicago, Illinois, USA*
[36]*LPC, Université Clermont Auvergne, CNRS/IN2P3, Clermont-Ferrand, France*
[37]*Nevis Laboratory, Columbia University, Irvington, New York, USA*
[38]*Niels Bohr Institute, University of Copenhagen, Copenhagen, Denmark*
[39a]*Dipartimento di Fisica, Università della Calabria, Rende, Italy*

[39b]INFN Gruppo Collegato di Cosenza, Laboratori Nazionali di Frascati, Italy
[40]Physics Department, Southern Methodist University, Dallas, Texas, USA
[41]Physics Department, University of Texas at Dallas, Richardson, Texas, USA
[42]National Centre for Scientific Research "Demokritos", Agia Paraskevi, Greece
[43a]Department of Physics, Stockholm University, Sweden
[43b]Oskar Klein Centre, Stockholm, Sweden
[44]Deutsches Elektronen-Synchrotron DESY, Hamburg and Zeuthen, Germany
[45]Lehrstuhl für Experimentelle Physik IV, Technische Universität Dortmund, Dortmund, Germany
[46]Institut für Kern- und Teilchenphysik, Technische Universität Dresden, Dresden, Germany
[47]Department of Physics, Duke University, Durham, North Carolina, USA
[48]SUPA—School of Physics and Astronomy, University of Edinburgh, Edinburgh, United Kingdom
[49]INFN e Laboratori Nazionali di Frascati, Frascati, Italy
[50]Physikalisches Institut, Albert-Ludwigs-Universität Freiburg, Freiburg, Germany
[51]II. Physikalisches Institut, Georg-August-Universität Göttingen, Göttingen, Germany
[52]Département de Physique Nucléaire et Corpusculaire, Université de Genève, Genève, Switzerland
[53a]Dipartimento di Fisica, Università di Genova, Genova, Italy
[53b]INFN Sezione di Genova, Italy
[54]II. Physikalisches Institut, Justus-Liebig-Universität Giessen, Giessen, Germany
[55]SUPA—School of Physics and Astronomy, University of Glasgow, Glasgow, United Kingdom
[56]LPSC, Université Grenoble Alpes, CNRS/IN2P3, Grenoble INP, Grenoble, France
[57]Laboratory for Particle Physics and Cosmology, Harvard University, Cambridge, Massachusetts, USA
[58a]Department of Modern Physics and State Key Laboratory of Particle Detection and Electronics, University of Science and Technology of China, Hefei, China
[58b]Institute of Frontier and Interdisciplinary Science and Key Laboratory of Particle Physics and Particle Irradiation (MOE), Shandong University, Qingdao, China
[58c]School of Physics and Astronomy, Shanghai Jiao Tong University, Key Laboratory for Particle Astrophysics and Cosmology (MOE), SKLPPC, Shanghai, China
[58d]Tsung-Dao Lee Institute, Shanghai, China
[59a]Kirchhoff-Institut für Physik, Ruprecht-Karls-Universität Heidelberg, Heidelberg, Germany
[59b]Physikalisches Institut, Ruprecht-Karls-Universität Heidelberg, Heidelberg, Germany
[60a]Department of Physics, Chinese University of Hong Kong, Shatin, N.T., Hong Kong, China
[60b]Department of Physics, University of Hong Kong, Hong Kong, China
[60c]Department of Physics and Institute for Advanced Study, Hong Kong University of Science and Technology, Clear Water Bay, Kowloon, Hong Kong, China
[61]Department of Physics, National Tsing Hua University, Hsinchu, Taiwan
[62]IJCLab, Université Paris-Saclay, CNRS/IN2P3, 91405 Orsay, France
[63]Department of Physics, Indiana University, Bloomington, Indiana, USA
[64a]INFN Gruppo Collegato di Udine, Sezione di Trieste, Udine, Italy
[64b]ICTP, Trieste, Italy
[64c]Dipartimento Politecnico di Ingegneria e Architettura, Università di Udine, Udine, Italy
[65a]INFN Sezione di Lecce, Italy
[65b]Dipartimento di Matematica e Fisica, Università del Salento, Lecce, Italy
[66a]INFN Sezione di Milano, Italy
[66b]Dipartimento di Fisica, Università di Milano, Milano, Italy
[67a]INFN Sezione di Napoli, Italy
[67b]Dipartimento di Fisica, Università di Napoli, Napoli, Italy
[68a]INFN Sezione di Pavia, Italy
[68b]Dipartimento di Fisica, Università di Pavia, Pavia, Italy
[69a]INFN Sezione di Pisa, Italy
[69b]Dipartimento di Fisica E. Fermi, Università di Pisa, Pisa, Italy
[70a]INFN Sezione di Roma, Italy
[70b]Dipartimento di Fisica, Sapienza Università di Roma, Roma, Italy
[71a]INFN Sezione di Roma Tor Vergata, Italy
[71b]Dipartimento di Fisica, Università di Roma Tor Vergata, Roma, Italy
[72a]INFN Sezione di Roma Tre, Italy
[72b]Dipartimento di Matematica e Fisica, Università Roma Tre, Roma, Italy
[73a]INFN-TIFPA, Italy
[73b]Università degli Studi di Trento, Trento, Italy
[74]Institut für Astro- und Teilchenphysik, Leopold-Franzens-Universität, Innsbruck, Austria
[75]University of Iowa, Iowa City, Iowa, USA

[76]*Department of Physics and Astronomy, Iowa State University, Ames, Iowa, USA*
[77]*Joint Institute for Nuclear Research, Dubna, Russia*
[78a]*Departamento de Engenharia Elétrica, Universidade Federal de Juiz de Fora (UFJF), Juiz de Fora, Brazil*
[78b]*Universidade Federal do Rio De Janeiro COPPE/EE/IF, Rio de Janeiro, Brazil*
[78c]*Instituto de Física, Universidade de São Paulo, São Paulo, Brazil*
[79]*KEK, High Energy Accelerator Research Organization, Tsukuba, Japan*
[80]*Graduate School of Science, Kobe University, Kobe, Japan*
[81a]*AGH University of Science and Technology, Faculty of Physics and Applied Computer Science, Krakow, Poland*
[81b]*Marian Smoluchowski Institute of Physics, Jagiellonian University, Krakow, Poland*
[82]*Institute of Nuclear Physics Polish Academy of Sciences, Krakow, Poland*
[83]*Faculty of Science, Kyoto University, Kyoto, Japan*
[84]*Kyoto University of Education, Kyoto, Japan*
[85]*Research Center for Advanced Particle Physics and Department of Physics, Kyushu University, Fukuoka, Japan*
[86]*Instituto de Física La Plata, Universidad Nacional de La Plata and CONICET, La Plata, Argentina*
[87]*Physics Department, Lancaster University, Lancaster, United Kingdom*
[88]*Oliver Lodge Laboratory, University of Liverpool, Liverpool, United Kingdom*
[89]*Department of Experimental Particle Physics, Jožef Stefan Institute and Department of Physics, University of Ljubljana, Ljubljana, Slovenia*
[90]*School of Physics and Astronomy, Queen Mary University of London, London, United Kingdom*
[91]*Department of Physics, Royal Holloway University of London, Egham, United Kingdom*
[92]*Department of Physics and Astronomy, University College London, London, United Kingdom*
[93]*Louisiana Tech University, Ruston, Los Angeles, USA*
[94]*Fysiska institutionen, Lunds universitet, Lund, Sweden*
[95]*Centre de Calcul de l'Institut National de Physique Nucléaire et de Physique des Particules (IN2P3), Villeurbanne, France*
[96]*Departamento de Física Teorica C-15 and CIAFF, Universidad Autónoma de Madrid, Madrid, Spain*
[97]*Institut für Physik, Universität Mainz, Mainz, Germany*
[98]*School of Physics and Astronomy, University of Manchester, Manchester, United Kingdom*
[99]*CPPM, Aix-Marseille Université, CNRS/IN2P3, Marseille, France*
[100]*Department of Physics, University of Massachusetts, Amherst, Massachusetts, USA*
[101]*Department of Physics, McGill University, Montreal QC, Canada*
[102]*School of Physics, University of Melbourne, Victoria, Australia*
[103]*Department of Physics, University of Michigan, Ann Arbor, Michigan, USA*
[104]*Department of Physics and Astronomy, Michigan State University, East Lansing, Michigan, USA*
[105]*B.I. Stepanov Institute of Physics, National Academy of Sciences of Belarus, Minsk, Belarus*
[106]*Research Institute for Nuclear Problems of Byelorussian State University, Minsk, Belarus*
[107]*Group of Particle Physics, University of Montreal, Montreal QC, Canada*
[108]*P.N. Lebedev Physical Institute of the Russian Academy of Sciences, Moscow, Russia*
[109]*National Research Nuclear University MEPhI, Moscow, Russia*
[110]*D.V. Skobeltsyn Institute of Nuclear Physics, M.V. Lomonosov Moscow State University, Moscow, Russia*
[111]*Fakultät für Physik, Ludwig-Maximilians-Universität München, München, Germany*
[112]*Max-Planck-Institut für Physik (Werner-Heisenberg-Institut), München, Germany*
[113]*Graduate School of Science and Kobayashi-Maskawa Institute, Nagoya University, Nagoya, Japan*
[114]*Department of Physics and Astronomy, University of New Mexico, Albuquerque, New Mexico, USA*
[115]*Institute for Mathematics, Astrophysics and Particle Physics, Radboud University/Nikhef, Nijmegen, Netherlands*
[116]*Nikhef National Institute for Subatomic Physics and University of Amsterdam, Amsterdam, Netherlands*
[117]*Department of Physics, Northern Illinois University, DeKalb, Illinois, USA*
[118a]*Budker Institute of Nuclear Physics and NSU, SB RAS, Novosibirsk, Russia*
[118b]*Novosibirsk State University Novosibirsk, Russia*
[119]*Institute for High Energy Physics of the National Research Centre Kurchatov Institute, Protvino, Russia*
[120]*Institute for Theoretical and Experimental Physics named by A.I. Alikhanov of National Research Centre "Kurchatov Institute", Moscow, Russia*
[121]*Department of Physics, New York University, New York, New York, USA*
[122]*Ochanomizu University, Otsuka, Bunkyo-ku, Tokyo, Japan*
[123]*Ohio State University, Columbus, Ohio, USA*

[124]Homer L. Dodge Department of Physics and Astronomy, University of Oklahoma, Norman, Oklahoma, USA
[125]Department of Physics, Oklahoma State University, Stillwater, Oklahoma, USA
[126]Palacký University, Joint Laboratory of Optics, Olomouc, Czech Republic
[127]Institute for Fundamental Science, University of Oregon, Eugene, Oregon, USA
[128]Graduate School of Science, Osaka University, Osaka, Japan
[129]Department of Physics, University of Oslo, Oslo, Norway
[130]Department of Physics, Oxford University, Oxford, United Kingdom
[131]LPNHE, Sorbonne Université, Université de Paris, CNRS/IN2P3, Paris, France
[132]Department of Physics, University of Pennsylvania, Philadelphia, Pennsylvania, USA
[133]Konstantinov Nuclear Physics Institute of National Research Centre "Kurchatov Institute", PNPI, St. Petersburg, Russia
[134]Department of Physics and Astronomy, University of Pittsburgh, Pittsburgh, Pennsylvania, USA
[135a]Laboratório de Instrumentação e Física Experimental de Partículas—LIP, Lisboa, Portugal
[135b]Departamento de Física, Faculdade de Ciências, Universidade de Lisboa, Lisboa, Portugal
[135c]Departamento de Física, Universidade de Coimbra, Coimbra, Portugal
[135d]Centro de Física Nuclear da Universidade de Lisboa, Lisboa, Portugal
[135e]Departamento de Física, Universidade do Minho, Braga, Portugal
[135f]Departamento de Física Teórica y del Cosmos, Universidad de Granada, Granada (Spain), Spain
[135g]Dep Física and CEFITEC of Faculdade de Ciências e Tecnologia, Universidade Nova de Lisboa, Caparica, Portugal
[135h]Instituto Superior Técnico, Universidade de Lisboa, Lisboa, Portugal
[136]Institute of Physics of the Czech Academy of Sciences, Prague, Czech Republic
[137]Czech Technical University in Prague, Prague, Czech Republic
[138]Charles University, Faculty of Mathematics and Physics, Prague, Czech Republic
[139]Particle Physics Department, Rutherford Appleton Laboratory, Didcot, United Kingdom
[140]IRFU, CEA, Université Paris-Saclay, Gif-sur-Yvette, France
[141]Santa Cruz Institute for Particle Physics, University of California Santa Cruz, Santa Cruz, California, USA
[142a]Departamento de Física, Pontificia Universidad Católica de Chile, Santiago, Chile
[142b]Universidad Andres Bello, Department of Physics, Santiago, Chile
[142c]Instituto de Alta Investigación, Universidad de Tarapacá, Arica, Chile
[142d]Departamento de Física, Universidad Técnica Federico Santa María, Valparaíso, Chile
[143]Universidade Federal de São João del Rei (UFSJ), São João del Rei, Brazil
[144]Department of Physics, University of Washington, Seattle, Washington, USA
[145]Department of Physics and Astronomy, University of Sheffield, Sheffield, United Kingdom
[146]Department of Physics, Shinshu University, Nagano, Japan
[147]Department Physik, Universität Siegen, Siegen, Germany
[148]Department of Physics, Simon Fraser University, Burnaby BC, Canada
[149]SLAC National Accelerator Laboratory, Stanford, California, USA
[150]Department of Physics, Royal Institute of Technology, Stockholm, Sweden
[151]Departments of Physics and Astronomy, Stony Brook University, Stony Brook, New York, USA
[152]Department of Physics and Astronomy, University of Sussex, Brighton, United Kingdom
[153]School of Physics, University of Sydney, Sydney, Australia
[154]Institute of Physics, Academia Sinica, Taipei, Taiwan
[155a]E. Andronikashvili Institute of Physics, Iv. Javakhishvili Tbilisi State University, Tbilisi, Georgia
[155b]High Energy Physics Institute, Tbilisi State University, Tbilisi, Georgia
[156]Department of Physics, Technion, Israel Institute of Technology, Haifa, Israel
[157]Raymond and Beverly Sackler School of Physics and Astronomy, Tel Aviv University, Tel Aviv, Israel
[158]Department of Physics, Aristotle University of Thessaloniki, Thessaloniki, Greece
[159]International Center for Elementary Particle Physics and Department of Physics, University of Tokyo, Tokyo, Japan
[160]Department of Physics, Tokyo Institute of Technology, Tokyo, Japan
[161]Tomsk State University, Tomsk, Russia
[162]Department of Physics, University of Toronto, Toronto ON, Canada
[163a]TRIUMF, Vancouver BC, Canada
[163b]Department of Physics and Astronomy, York University, Toronto ON, Canada
[164]Division of Physics and Tomonaga Center for the History of the Universe, Faculty of Pure and Applied Sciences, University of Tsukuba, Tsukuba, Japan
[165]Department of Physics and Astronomy, Tufts University, Medford, Massachusetts, USA

[166]*Department of Physics and Astronomy, University of California Irvine, Irvine, California, USA*
[167]*Department of Physics and Astronomy, University of Uppsala, Uppsala, Sweden*
[168]*Department of Physics, University of Illinois, Urbana, Illinois, USA*
[169]*Instituto de Física Corpuscular (IFIC), Centro Mixto Universidad de Valencia—CSIC, Valencia, Spain*
[170]*Department of Physics, University of British Columbia, Vancouver BC, Canada*
[171]*Department of Physics and Astronomy, University of Victoria, Victoria BC, Canada*
[172]*Fakultät für Physik und Astronomie, Julius-Maximilians-Universität Würzburg, Würzburg, Germany*
[173]*Department of Physics, University of Warwick, Coventry, United Kingdom*
[174]*Waseda University, Tokyo, Japan*
[175]*Department of Particle Physics and Astrophysics, Weizmann Institute of Science, Rehovot, Israel*
[176]*Department of Physics, University of Wisconsin, Madison, Wisconsin, USA*
[177]*Fakultät für Mathematik und Naturwissenschaften, Fachgruppe Physik, Bergische Universität Wuppertal, Wuppertal, Germany*
[178]*Department of Physics, Yale University, New Haven, Connecticut, USA*

[a]Deceased.
[b]Also at Department of Physics, King's College London, London, United Kingdom.
[c]Also at Istanbul University, Department of Physics, Istanbul, Turkey.
[d]Also at Instituto de Fisica Teorica, IFT-UAM/CSIC, Madrid, Spain.
[e]Also at TRIUMF, Vancouver BC, Canada.
[f]Also at Department of Physics, University of Fribourg, Fribourg, Switzerland.
[g]Also at Department of Physics and Astronomy, University of Louisville, Louisville, Kentucky, USA.
[h]Also at Departament de Fisica de la Universitat Autonoma de Barcelona, Barcelona, Spain.
[i]Also at Moscow Institute of Physics and Technology State University, Dolgoprudny, Russia.
[j]Also at Faculty of Physics, Sofia University, 'St. Kliment Ohridski', Sofia, Bulgaria.
[k]Also at Department of Physics, Ben Gurion University of the Negev, Beer Sheva, Israel.
[l]Also at Università di Napoli Parthenope, Napoli, Italy.
[m]Also at Institute of Particle Physics (IPP), Canada.
[n]Also at Bruno Kessler Foundation, Trento, Italy.
[o]Also at Department of Physics, St. Petersburg State Polytechnical University, St. Petersburg, Russia.
[p]Also at Borough of Manhattan Community College, City University of New York, New York, New York, USA.
[q]Also at Department of Physics, California State University, Fresno, USA.
[r]Also at Department of Financial and Management Engineering, University of the Aegean, Chios, Greece.
[s]Also at Centro Studi e Ricerche Enrico Fermi, Italy.
[t]Also at Department of Physics, California State University, East Bay, USA.
[u]Also at Institucio Catalana de Recerca i Estudis Avancats, ICREA, Barcelona, Spain.
[v]Also at Graduate School of Science, Osaka University, Osaka, Japan.
[w]Also at Physikalisches Institut, Albert-Ludwigs-Universität Freiburg, Freiburg, Germany.
[x]Also at University of Chinese Academy of Sciences (UCAS), Beijing, China.
[y]Also at Institute of Physics, Azerbaijan Academy of Sciences, Baku, Azerbaijan.
[z]Also at Yeditepe University, Physics Department, Istanbul, Turkey.
[aa]Also at Institute of Theoretical Physics, Ilia State University, Tbilisi, Georgia.
[bb]Also at CERN, Geneva, Switzerland.
[cc]Also at Joint Institute for Nuclear Research, Dubna, Russia.
[dd]Also at Hellenic Open University, Patras, Greece.
[ee]Also at Center for High Energy Physics, Peking University, China.
[ff]Also at The City College of New York, New York, New York, USA.
[gg]Also at Department of Physics, California State University, Sacramento, USA.
[hh]Also at Département de Physique Nucléaire et Corpusculaire, Université de Genève, Genève, Switzerland.
[ii]Also at Faculty of Physics, M.V. Lomonosov Moscow State University, Moscow, Russia.
[jj]Also at Institut für Experimentalphysik, Universität Hamburg, Hamburg, Germany.
[kk]Also at CPPM, Aix-Marseille Université, CNRS/IN2P3, Marseille, France.
[ll]Also at National Research Nuclear University MEPhI, Moscow, Russia.
[mm]Also at Institute for Particle and Nuclear Physics, Wigner Research Centre for Physics, Budapest, Hungary.
[nn]Also at Giresun University, Faculty of Engineering, Giresun, Turkey.
[oo]Also at Department of Physics and Astronomy, Michigan State University, East Lansing, Michigan, USA.